IJCSI

International Journal of Computer Science Issues

Optimization of Channel Estimation Algorithms for MIMO-OFDM based LTE-Advanced

By Saqib Saleem

Volume 2, 2012
ISSN (Online): 1694-0814

IJCSI proceedings are currently indexed by:

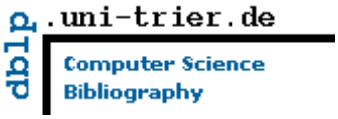

OPTIMIZATION OF CHANNEL ESTIMATION ALGORITHMS FOR MIMO-OFDM BASED LTE-ADVANCED

ISSN(online) 1694-0814

Optimization of Channel Estimation Algorithms for MIMO-OFDM based LTE-Advanced

Submitted by

Saqib Saleem

Supervisor

Dr. Qamar-ul-Islam

A THESIS SUBMITTED IN PARTIAL FULFILLMENT
OF THE REQUIREMENTS FOR THE DEGREE OF
MASTER OF SCIENCE
IN
COMMUNICATION ENGINEERING

Department of Communication System Engineering
Institute of Space Technology, Islamabad
Pakistan

2011

Institute of Space Technology

Department of Communication System Engineering

"Optimization of Channel Estimation Algorithms for MIMO-OFDM based LTE-Advanced"

By

Saqib Saleem

APPROVAL BY BOARD OF EXAMINERS

Head of Department	Signature
Advisor	Signature
Internal Examiner	Signature
External Examiner	Signature

Abstract

For high data rate communication with the required Quality of Service (QoS) in 3G and 4G systems, Orthogonal Frequency Division Multiplexing (OFDM) is proposed, which is capable to resist the channel impairments caused by high mobility conditions, by dividing the frequency-selective fading channel into narrowband flat fading channels. For increased data rate and reduced latency for 4G radio communication standards, ITU made proposals for LTE-Advanced in 2009. To achieve Release-10 targets, made by 3rd Generation Partnership Project (3GPP), channel state information at the transmitter is a pre-requisite. This thesis focuses on channel estimation algorithms in three domains: Frequency Domain Channel Estimation, Time Domain Channel Estimation and Adaptive Filtering Based Channel Estimation. This thesis focuses on the use of time domain channel statistics, mainly concentrating on two schemes: Linear Minimum Mean Square Estimation (LMMSE), Least Square Estimation (LSE) and their variants. LMMSE performs better than LSE but at the cost of more computational complexity. The performance of LSE can be improved by increasing CIR samples and channel taps. To avoid the matrix inversion lemma, the channel matrix can be Down-Sampled or regularized. In this thesis three time-domain channel estimation techniques, Discrete Fourier Transform (DFT), Discrete Cosine Transform (DCT) and Windowed-DFT, are compared based on the time-domain channel impulse response (CIR) energy characteristics and they have less complexity and efficient performance than Linear Minimum Mean Square Error (LMMSE) and Least Square Error (LSE). In this thesis, three adaptive channel estimation techniques: Least Mean Square (LMS), Recursive Least Square (RLS) and Kalman-Filtering Based, are also compared. The comparison of all these algorithms is evaluated in terms of complexity and performance. The performance is evaluated for different number of channel filter lengths, in terms of CIR Samples, and multi-path channel taps. The performance is given in terms of Mean Square Error (MSE), Symbol Error Rate (SER), Packet Error Rate (PER) and Frame Error Rate (FER). The complexity is given in terms of computational time. MATLAB Monte Carlo Simulations are performed for the optimization of the above discussed channel estimation algorithms, first for OFDM system and then for MIMO-OFDM system, according to the physical layer parameters of LTE-Advanced.

Preface

This thesis is submitted in partial fulfillment of the requirements for the degree of Master of Science in Communication Engineering at Department of Communication System Engineering at Institute of Space Technology (IST), Islamabad, Pakistan. My advisor has been Professor Dr. Qamar-ul-Islam at Department of Communication System Engineering at IST, Islamabad, Pakistan.

The studies have been carried out in the period from July 2010 to July 2011. The work includes the equivalent of a year of full-time course studies and 2 semesters of being a Lab Demonstrator in Digital Signal Processing and Digital Communication Labs. Most of the time I spent at IST in Communication Laboratory , but I have also spent shorter and longer periods in close collaboration with Dr Adnan A.Khan at CASE, Islamabad—for assistant in Advanced Digital Communication course at IST, Islamabad and Space-Time Communication course at CASE, Islamabad. From May 2011 I have been engaged in test bed design of MIMO-OFDM Wireless Communication System at the Department of Communication System Engineering at Institute of Space Technology, Islamabad under the supervision of Dr. Qamar-ul-Islam.

The funding for publications was provided by IST, Islamabad.

Declaration of Originality

I hereby declare that the research recorded in this thesis and the thesis itself was developed entirely by myself at Department of Communication System Engineering at Institute of Space Technology, Islamabad, Pakistan.

The MATLAB software programs used to perform the simulations and all corresponding results were developed entirely by myself, with the following exception: Literature Review performed in Chapter 1 and Chapter 2 has been properly cited.

_____

Saqib Saleem
Department of Communication System Engineering
Institute of Space Technology
Islamabad, Pakistan
July, 2011

Acknowledgments

I would like to thank my supervisor, Professor Dr. Qamar-ul-Islam, without his encouragement I would probably not have started on the MS thesis. The first part of the thesis, dealing with Physical Layer of LTE-Advanced and MIMO-OFDM System, was at large done in cooperation under guidance of Dr. Adnan A.Khan. Dr. Usman Riaz and Dr. Akmal Butt has also been a great help for me, especially for encouraging me for publications. Their enthusiasm and knowledge, both in wireless communications and in mathematics and stochastic processes are invaluable. During the stay at IST their ideas, tips, pointers and suggestions enabled me to carry out the work that ended up as the second part of the thesis, dealing with statistical methods relevant to channel estimation algorithms for wireless communications.

I am also in debt to other researchers at IST, most notably Dr. Muhammad Faisal Khan and Dr. Khurram Khurshid. They have guided me in research methodology that was probably trivial to them, however far from obvious to me.

MS studies should not only be dry course work; a living and vital work environment is also essential. My class fellows, Khurram Shahzad (Doctor Sahb) and Adil Ali Raja (Bhai Sahb) at IST have provided that environment for me. I will miss the elevated discussions during class days, combined assignments- especially MATLAB assignments of Simulation and Modeling by Dr.Akmal Butt-. During the last year in IST, I also conducted two undergraduate Labs that was a great chance of sharing my experiences with undergraduate students- special thanks to Abdul Basit, Ghulam Abbas and Waqar Aziz for helping me in publications. Also special thanks to my room-mate and junior, Abdul Waheed Khandhro – his forever blame that my (Saqib's) services are always available for others but never for him- but I always learnt from his long professional experience. Lastly, I would like to thank my parents- Muhammad Mansha Saleem and Shahnaz Saleem, my sisters- Misbah Saleem and Tayyaba Saleem, my brother- Amir Saleem and littles- Saleha, Hadia and Mariam- for their support and encouragement during my stay in hostel- far away from my home town, at distance of 8 hours.

My deepest gratitude goes to my love Amna for her understanding, patience – for not sparing time for chat with her - and permanent encouragement, as well as for the wonderful moments spent together –for which I have to travel for 10 hours each month on regular basis-.

In end, but most importantly, Thanks to ALMIGHTY ALLAH for giving me strength for pursuing this thesis. Without HIS blessing I would not have been able to finish this thesis.

Saqib Saleem
Institute of Space Technology, Islamabad
Pakistan
Email: saqibsaleem2002@hotmail.com

Contents

List of Publications

[1] Saqib Saleem, Qamar-ul-Islam, "Optimization of LSE and LMMSE Channel Estimation Algorithms based on CIR Samples and Channel Taps ", IJCSI International Journal of Computer Science Issues, Vol.8, Issue.1, pp.437-443,January 2011

[2] Saqib Saleem, Qamar-ul-Islam, "Performance and Complexity Comparison of Channel Estimation Algorithms for OFDM System", IJECS International Journal of Electrical & Computer Sciences, Vol.11, Issue.02, pp.6-12, April 2011

[3] Saqib Saleem, Qamar-ul-Islam, "LMS and RLS Channel Estimation Algorithms for LTE-Advanced ", Journal of Computing, Vol.3, Issue.4, pp.155-163, April 2011

[4] Saqib Saleem, Qamar-ul-Islam, "Transform-Based Channel Estimation Techniques for LTE-Advanced ", Journal of Computing, Vol.3, Issue.4, pp.164-169, April 2011

[5] Saqib Saleem, Qamar-ul-Islam, "On Comparison of DFT-based and DCT-based Channel Estimation for OFDM System ", IJCSI International Journal of Computer Science Issues, Vol.8, Issue.3, No.2, pp.353-358, May 2011

[6] Saqib Saleem, Qamar-ul-Islam, "Channel Estimation using Adaptive Filters for LTE-Advanced ", IJCSI International Journal of Computer Science Issues, Vol.8, Issue.3, No.2, pp.344-352,May 2011

[7] Saqib Saleem, Qamar-ul-Islam, Waqar Aziz, Abdul Basit, "Performance Evaluation of Linear Channel Estimation Algorithms for MIMO-OFDM in LTE-Advanced " IJECS International Journal of Electrical and Computer Sciences, Vol.11, No.3, pp.64-69, May 2011

[8] Saqib Saleem, Qamar-ul-Islam, "CIR Samples and Channel Taps Based Windowed-DFT Channel Estimation for MIMO-OFDM System " Submitted for publication in IJCA International Journal of Computer Applications, Vol.28, August 2011

[9] Saqib Saleem, Qamar-ul-Islam, "Time-Domain Channel Estimation for MIMO-OFDM Systems " Accepted for publication in 3rd IEEE International Conference of Signal Processing Systems (ICSPS), Yantai, China, August 2011

[10] Saqib Saleem, Qamar-ul-Islam, "MIMO-OFDM Channel Estimation using Least Mean Square (LMS) Algorithm " Submitted for publication in 2th International Conference on Aerospace Science and Engineering (ICASE), Islamabad, Pakistan, September 2011

[11] Saqib Saleem, Qamar-ul-Islam, " Channel Estimation using Least Mean Square (LMS) Algorithm for LTE-Advanced ", Submitted for publication in Signal Processing: An International Journal (SPIJ), Vol.5, Issue.04, October 2011

[12] Saqib Saleem, Qamar-ul-Islam, " Evaluation of Kalman Filtering Based Channel Estimation for LTE-Advanced ", Submitted for publication in IJCST International Journal of Computer Science and Telecommunication, Vol.2, Issue.05, August 2011

[13] Saqib Saleem, Qamar-ul-Islam, " RLS-Based Channel Estimation for MIMO-OFDM System ", to be submitted for publication in IJACSA International Journal of Advanced Computer Science and Applications, Vol.2, Issue.08, August 2011

[14] Saqib Saleem, Qamar-ul-Islam, ” Optimization of Time-Domain Based Channel Estimation Algorithms for MIMO-OFDM based LTE-Advanced System ”, to be submitted for publication in IJCSI International Journal of Computer Science Issues, Vol.8, Issue.05, September 2011

[15] Saqib Saleem, Qamar-ul-Islam, ” Comparison of Time-Domain and Frequency-Domain Channel Estimation Techniques for MIMO-OFDM System ”, to be submitted for publication in IJCA International Journal of Computer Applications, Vol.23, August 2011

[16] Saqib Saleem, Qamar-ul-Islam, ” Performance Analysis of LMS, RLS and Kalman Filtering Channel Estimation Techniques for LTE-Advanced ”, to be submitted for publication in Journal of Emerging Trends in Computing and Information Sciences, Vol.2, No.8, August 2011

[17] Saqib Saleem, Qamar-ul-Islam, ” Optimization of Channel Estimation Algorithms for MIMO-OFDM based LTE-Advanced System ”, IJCSI International Journal of Computer Science Issues, Thesis Publication

List of Figures

List of Tables

List of Abbreviations

CCPCH	Control Channel and Common Control Physical Channel
CIR	Channel Impulse Response
CoMP	Co-ordinated Multiple Point
CSI	Channel State Information
DCT	Discrete Cosine Transform
DFT	Discrete Fourier Transform
DL	Down Link
DwPTS	Downlink Pilot Timeslot
FDD	Frequency Division Duplexing
GP	Guard Period
IMT	International Mobile Telecommunication
ITU	International Telecommunication Union
LMMSE	Linear Minimum Mean Square Error
LMS	Least Mean Square
LSE	Least Square Error
LTE	Long Term Evaluation
MSE	Mean Square Error
PDP	Power Delay Profile
PDSCH	Physical Downlink Shared Channel
RAP	Random Access Preamble
RLS	Recursive Least Square
RN-UE	Radio Network-User Equipment
RS	Reference Signal
SC-FDMA	Single Carrier Frequency Division Multiple Access
TDD	Time Division Duplexing
UL	Uplink
UpPTS	Uplink Pilot Timeslot

Chapter No. 1

Physical Layer of LTE-Advanced

For further enhancements in performance and capability of existing 3G cellular systems like GSM and UMTS [1], ITU proposed a new radio-access technology in Release-10, beyond IMT-Advanced, termed as LTE-Advanced, which is supposed to provide compatibility with the existing IMT networks and interworking with other radio-access systems. LTE-Advanced provide high data rate services of 100 Mbps for high mobility and 1Gbps for low mobility conditions [2].

1.1 Frame Structure

In Downlink and Uplink, the data is transmitted in form of radio frames having duration $T_f = 307200 \times T_s$. In LTE-Advanced, two types of radio frames are [1]

1- Generic Frame Structure
2- Alternative Frame Structure

1-Generic Frame Structure

Data can be transmitted by using the generic frame structure for both FDD and TDD modes. Each Generic radio frame is made of 20 sub-frames and length of each sub-frame is $T_{sf} = 15360 \times T_s$, numbered from 0 to 19 and of duration 10 ms [1]. Sub-frames are paired such that sub-frame 0 and 1 form the first sub-frame pair and so on. For FDD mode, all sub-frames can be used for both DL and UL. But for TDD mode, a sub-frame pair can be either used for DL or UL where the first sub-frame is always used for DL data transmission.

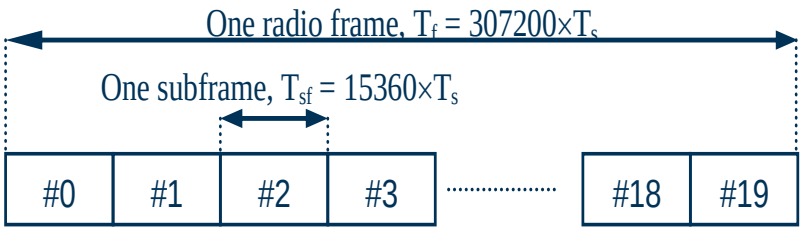

Figure 1.1: Generic Frame Structure [1]

2- Alternative Frame Structure

The alternative frame structure can be used only for TDD mode. Two half-frames of length $T_f = 153600 \times T_s$ make a radio frame where each half-frame is of duration 5 ms [1]. All half-frames in any radio frame are of same structure. Each half-frame is made of seven sub-frames which are numbered from 0 to 6, and three special purpose sub-frames: Downlink Pilot Timeslot (DwPTS), Guard Period (GP) and Uplink Pilot Timeslot (UpPTS).

In alternative frame structure, sub-frame 0 and DwPTS are always used for DL and sub-frame 1 and UpPTS are used only for UL.

1.2 Support for Wider Bandwidth

To support wider transmission bandwidth up to 100MHz, two or more Component Carriers can be aggregated in LTE-advanced. This process is called Carrier Aggregation [2].

A terminal can be made capable of receiving and transmitting one or many component carriers simultaneously, so a LTE-A terminal having capability for carrier aggregation can perform transmission and reception simultaneously of multiple component carriers while the earlier LTE Rel-8 terminal is capable of performing transmission and reception of a single component carrier only, when the component carrier is according to Rel-8 specifications.

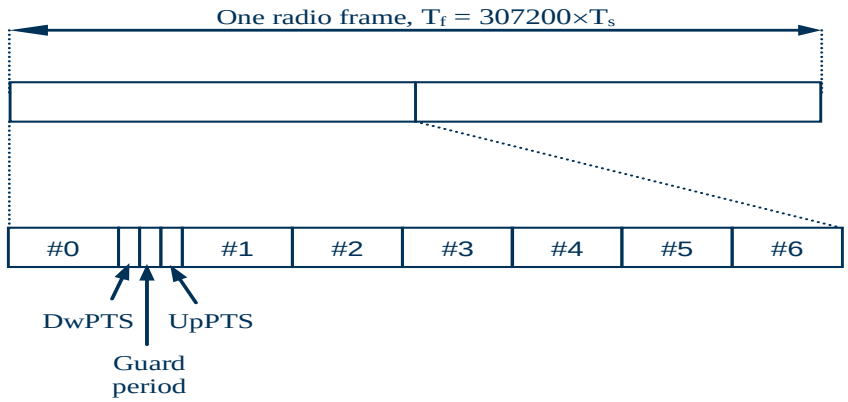

Figure 1.2: Alternative Frame Structure [1]

1.3 Downlink Transmission

The following three physical channels are used in LTE-A: Physical Downlink Shared Channel (PDSCH), Control Channel and Common Control Physical Channel (CCPCH). To transmit data for DL by using any one of the physical channels, the following three steps are carried out

i. The data bits are modulated which results in complex-valued symbols
ii. The modulated symbols are mapped to the available resource atoms
iii. Transmission of time-domain OFDM signal by physical antennas

i-Modulation

For PDSCH, the modulation technique can be Quadrature Phase Shift Keying (QPSK), 16-QAM or 64-QAM but for CCPCH only QPSK is used [1].

ii-Resource Mapping

The mapping of complex-valued symbols to the resource atoms $a_{k,l}$ for PDSCH is done such that first we go in increasing order of index k and then along with the index l. But for CCPCH the mapping of symbols follow the following relation [1]

$$a_{k,l} = \begin{cases} d(72l + k + 36) & k = -36, \dots -1 \\ d(72l + k + 35) & k = 1, \dots, 36 \end{cases} \quad (1.1)$$

iii-OFDM Signal Generation

In a sub-frame, OFDM symbols are indexed in increasing order of l. The continuous time signal $s_l(t)$ in l^{th} OFDM DL sub-frame is defined by

$$s_l(t) = \sum_{\left\lfloor \frac{N_{BW}{}^{DL}}{2} \right\rfloor}^{\left\lceil \frac{N_{BW}{}^{DL}}{2} \right\rceil} a_{k,l} e^{\frac{2j\pi k\,(t - N_{CP}\,T_s)}{NT_s}} \quad (1.2)$$

For $0 \leq t < (N_{CP} + N)T_s$. Tables 1.1 and 1.2 provide the values of N_{CP} used for the generic and alternative frame structures.

TABLE 1.1: OFDM PARAMETERS FOR GENERIC FRAME STRUCTURE [1]

	Cyclic prefix length $N_{\mathrm{CP},l}$
Normal cyclic prefix	160 for $l = 0$ 144 for $l = 1,\dots,6$
Extended cyclic prefix	512 for $l = 0,\dots,5$

TABLE 1.2: OFDM PARAMETERS FOR ALTERNATIVE FRAME STRUCTURE [1]

	Cyclic prefix length $N_{\mathrm{CP},l}$
Normal cyclic prefix	224 for $l = 0,...,8$
Extended cyclic prefix	512 for $l = 0,...,7$

In LTE-A, up to eight layers can be multiplexed spatially which is not possible in LTE Rel-8.

1.3.1 Physical Signals

A DL physical signal which does not have any information from the upper layers is used by the physical layer of LTE-A. LTE-A supports two DL physical signals: Reference Signal (RS) and Synchronization Signal (SS) [1].

In each sub-frame, a resource grid is used to represent the transmitted signal. A resource grid is made of $N_{\mathrm{BW}}^{\mathrm{DL}}$ subcarriers and OFDM symbols are N_{symb} . Figure.3 shows the structure of a resource grid.

The length of cyclic prefix defines N_{symb}, the number of OFDM symbols, used in a sub-frame, as given in Table 1.3.

TABLE 1.3: N_{symb} IN A SUB-FRAME [1]

Configuration	N_{symb}	
	Generic frame structure	**Alternative frame structure**
Normal cyclic prefix	7	9
Extended cyclic prefix	6	8

1.3.1.1 Reference Signal

Each DL transmit antenna sends one reference signal. In LTE-A, DL transmit antennas can be 1, 2 or 4 [1]. LTE-A supports two types of reference signals [2]

- Reference signals used for PDSCH demodulation
- Reference signals used for estimation of Channel State Information (CSI)

1.3.1.1.1 Generation of Reference Signal

The reference signals of two dimensional, $r_{m,n}$, can be generated from orthogonal sequence, $r_{m,n}^{OS}$, and pseudo-random sequence, $r_{m,n}^{PRS}$, by the symbol-by-symbol product

of these sequences. In LTE-A, the available orthogonal sequences are 3 and pseudo-random sequences are 170. A unique pair of orthogonal sequence entity and pseudo-random sequence entity forms a cell identity, so in LTE-A, different 510 cell identities can be made [1].

Figure 1.4 shows the resource atoms that will be used for reference symbol transmission. In case of one transmit antenna only R1 will be transmitted, for two transmit antennas R1 and R2 will be transmitted, for 3 transmit antennas R1, R2 and R3 will be and for four transmit antennas all four symbols will be transmitted.

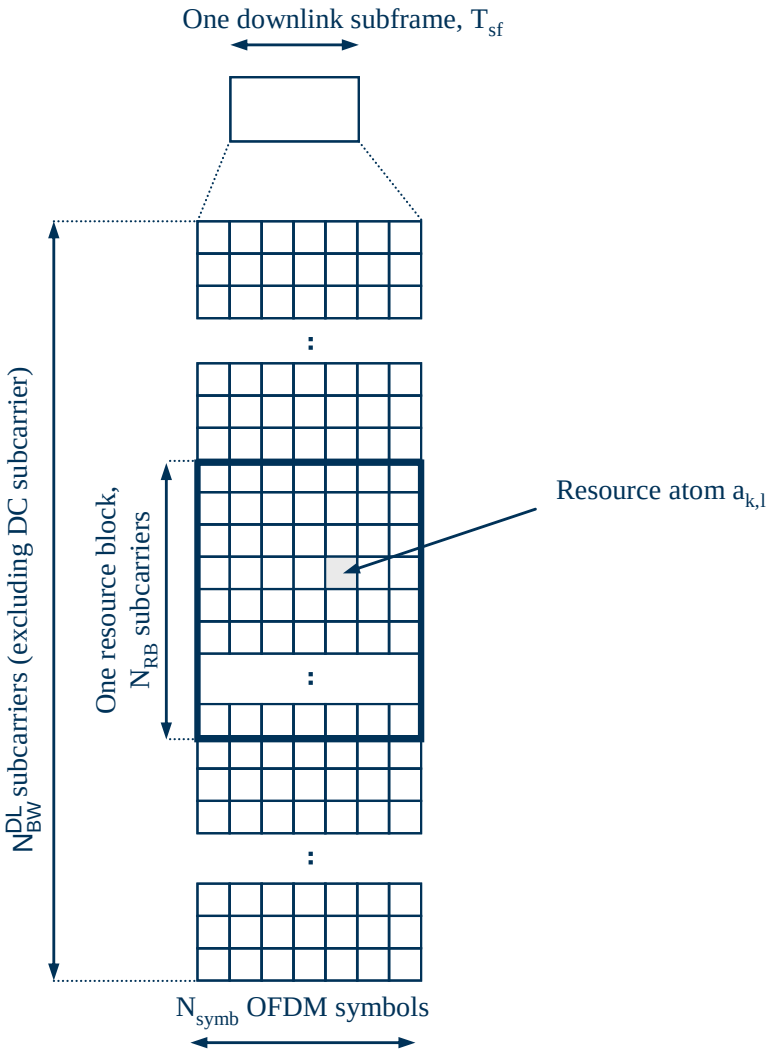

Figure 1.3: Downlink Resource Grid [1]

1.4 Uplink Transmission

In LTE-A, for UL data transmission two UL physical channels are used: Physical Uplink Shared Channel (PUSCH) and Physical Uplink Control Channel (PUCCH). To transmit data in UL, the following steps are taken by any of the physical channel

i- The data bits are converted into complex-valued symbols by any modulation technique

ii- Modulated symbols are then mapped to the available resource atoms

iii- To transmit by each antenna, complex-valued time-domain SC-FDMA signal is generated.

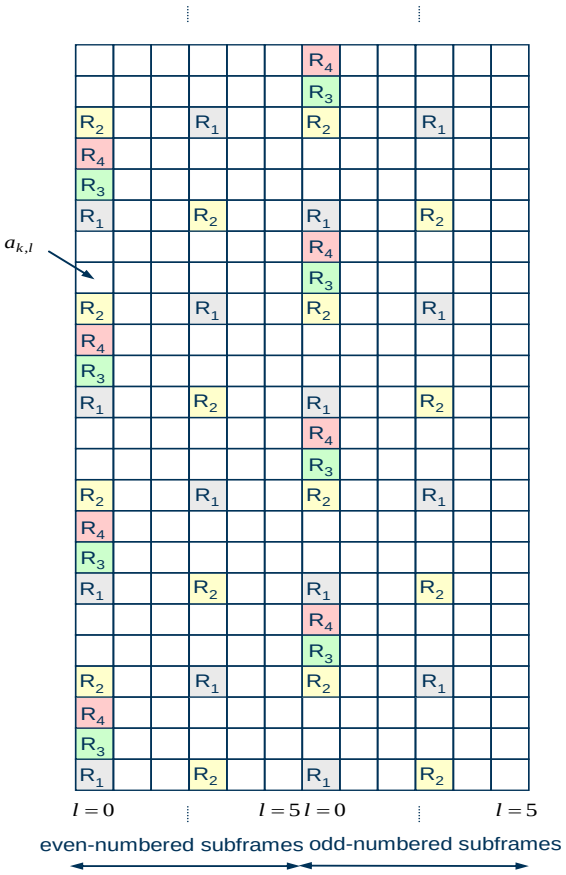

Figure 1.4: DL Reference Signals for Generic Frame Structure with Normal Cyclic Prefix [1]

i-Modulation

For PUSCH the modulation can be either QPSK or 16 QAM but PUCCH will be transmitted on a reserved frequency region.

ii- Mapping of Resource Atoms

In SC-FDMA signal, l, the mapping of complex-valued modulated symbols to the resource atoms $a_{u,l}$ is done according to

$$a_{u,l} = \begin{cases} d(l' \times N_{TX} + u) & in\ the\ first\ subframe\ of\ a\ subframe\ pair \\ d([l' + N_{block} - 2] \times N_{TX} + u) & in\ the\ second\ subframe\ of\ a\ subframe\ pair \end{cases}$$

where

$$l' = \begin{cases} l & if\ l = 0 \\ l-1 & if\ 2 \le l < N_{block} - 2 \\ l-2 & if\ l = N_{block} - 1 \end{cases} \qquad (1.3)$$

iii- Generation of SC-FDMA Signal

For UL transmission, in any sub-frame the continuous time signal $s_l(t)$ in SC-FDMA symbol, l, is given by

$$s_l(t) = \sum_{k=\left\lfloor \frac{N_{TX}}{2} \right\rfloor}^{\lceil N_{TX} \rceil} \sum_{u=0}^{N_{TX}-1} a_{u,l}\, e^{\frac{-j2\pi uk}{N_{TX}}}\, e^{\frac{2j\pi (k+N_{symbl})}{N_d T_s}(t - N_{CP} T_s} \qquad (1.4)$$

For $0 \le t < (N_{CP} + N_d) \times T_s$

Tables 1.4 and 1.5 shows different values of N_{CPl} and N_d that are used for generic and alternative frame structures, respectively.

TABLE 1.4: SC-FDMA PARAMETERS FOR GENERIC FRAME STRUCTURE [1]

l	Normal cyclic prefix						Extended cyclic prefix	
	$N_{BW}^{UL} \le 72$		$72 < N_{BW}^{UL} \le 144$		$144 < N_{BW}^{UL}$			
	$N_{CP,l}$	N_d	$N_{CP,l}$	N_d	$N_{CP,l}$	N_d	$N_{CP,l}$	N_d
0	240	2048	184	2048	156	2048	432	2048
1	112	1024	120	1024	124	1024	440	1024
2		2048		2048		2048		2048
3								
4								
5								1024
6		1024		1024		1024		2048
7		2048		2048		2048		

In LTE-Advanced, the spatial multiplexing can be done up to four layers [3].

TABLE 1.5: SC-FDMA PARAMETERS FOR ALTERNATIVE FRAME STRUCTURE [1]

l	Normal cyclic prefix				Extended cyclic prefix			
	$N_{BW}^{UL} \le 300$		$300 < N_{BW}^{UL}$		$N_{BW}^{UL} \le 300$		$300 < N_{BW}^{UL}$	
	$N_{CP,l}$	N_d	$N_{CP,l}$	N_d	$N_{CP,l}$	N_d	$N_{CP,l}$	N_d
0	320	2048	224	2048	560	2048	472	2048
1	192	1024	204	1024	423	1024	456	1024
2		2048		2048		2048		2048
3								
4								
5								
6								
7						1024		1024
8		1024		1024		2048		2048
9		2048		2048				

1.4.1 Physical Signals

An UL physical signal also does not carry the upper layer's information. In LTE-A, the supported physical signals are [1]

- Reference Signal (RS)
- Random Access Preamble (RAP)

In each sub-frame, the structure of the transmitting signal is given by the information contained in N_{block} SC-FDMA complex-valued modulated symbols. UL reference signals are only carried in SC-FDMA symbol 1 and N_{block}-2. The UL sub-frame structure is shown in Figure 1.5.

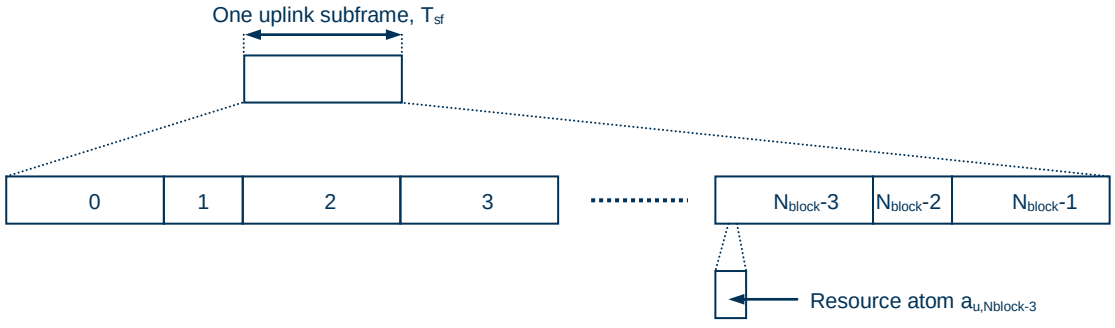

Figure 1.5: UL Sub-Frame Structure [1]

In each sub-frame, the supported number of SC-FDMA symbols also depends on the cyclic prefix length and is given in Table 1.6.

TABLE 1.6: NUMBER OF SC-FDMA SYMBOLS PER SUB-FRAME [1]

Configuration	N_{block}	
	Generic frame structure	Alternative frame structure
Normal cyclic prefix	8	10
Extended cyclic prefix	7	9

1.4.1.1 Reference Signal

The structure of reference signal of LTE-Advanced is same to that of structure of LTE Rel-8. In LTE-A, the reference signals are [3]

- Reference Signal used for Demodulation
- Reference Signal used for Sounding

1.5 Coordinated Multiple Point (CoMP) Transmission and Reception

For support of high data rate and cell-edge throughput, co-ordinated multi-point (CoMP) transmission/reception technique is used for LTE-A [3]. The CoMP can be done for both UL and DL data transmission. In CoMP different geographically separated points are performing different types of co-ordination. The co-ordination can be in the form scheduling, which can be performed by beam-forming. The data is available at the serving cell only but by using scheduling and beam-forming, the decisions are made by all cells involved in the co-ordination, which form a CoMP co-operating set. [2].

1.6 Relaying Functionality

Co-operation through relaying can be carried in LTE-A for the following purposes e.g. to increase the supported data rates, to enhance the mobility, deployment of a user in any temporary network, the cell-edge throughput and/or to enlarge the coverage areas [2]. Un interface is used to connect a relay node (RN) of a donor eNB to a donor cell and UEs get connected with RN through Uu interface, as demonstrated in Figure 1.6.

RN can operate in two modes: Inband and Outband. The same carrier frequency is used for eNB-RN link and RN-UE links in inband mode while in outband mode the eNB-RN link operates on a different carrier frequency to that of RN-UE links [3]. Relays can be transparent and non-transparent with respect to UE. UE does not know about any kind of communication with the network while using transparent relay but non-transparent relay informs the UE about the communication being carried in the network [2]. A RN can be a part of a donor cell only and it can also have the capability to control different cells.

Figure 1.6: Relay in LTE-Advanced [3]

LTE-A supports two types of RNs: Type-1 and Type-1a [3]. Type-1 RN operates only in inband mode and it controls cells, which have their own Physical Cell IDs. The scheduling knowledge and HARQ feedback can be sent to UE through RN to control the channels. A "Type 1a" relay node has same characteristics as "Type 1", except that it is outband relay.

1.7 Radio Transmission and Reception

Radio requirements are given according to the required carrier aggregation. Each component carrier for carrier aggregation can be of following bandwidths: 1.4MHz, 3.0MHz, 5MHz, 10MHz, 15MHz and 20 MHz [3] and the spacing between adjacent CCs can be integer multiple of 300 KHz. LTE-A can operate in all bands specified by E-UTRA and IMT bands described by ITU-R.

1.8 Capability-Related Requirements

1.8.1 Peak Data Rate

The peak data rate supported by LTE-A depends on the allowable spectrum allocation. The number of transmit and receive antennas have proportional effect on the data rate. The DL and UL data rates are given in terms of the following configurations of UE

a) For DL peak data rate, there should be at least 2 receive antennas at UE
b) For UL peak data rate, there should be at least 1 transmit antenna at UE

Under these configurations, a peak data rate of 100Mb/s can be achieved for 20 MHz DL bandwidth which results in spectrum efficiency of 5 bps/Hz, while for UL a peak data rate of 50 Mb/s can be achieved for same bandwidth resulting in spectrum efficiency of 2.5 bps/Hz [4].

1.8.2 Latency

Control Plane Latency

In LTE-A, less than 50 ms are required to transit from idle mode to connected mode and during this time user plane should also be established. While only 10 ms are given for transition to connected mode from dormant mode [3]. According to the targets described by 3GPP to reduce this latency, RRC connection request can be combined with NAS service request, which results in reduced processing delays and reduced RACH scheduling period.

Control Plane Capacity

In LTE-A, for bandwidth up to 5 MHz, at least 200 users should be supported per cell. But as the bandwidth increases, the capacity should increase to at least 400 users [4].

User Plane Latency

In Rel-8, the U-Plane latency is already below 10 ms for synchronized UEs. But when the UEs are not synchronized then the latency can be improved by any of the following techniques: RACH scheduling period should be shorter PUCCH cycle, UL transmission can be contention based or processing delays should be reduced [3].

1.9 System Performance Requirements

1.9.1 Spectrum Efficiency

In LTE-A, average spectrum efficiency and the cell-edge user throughput are given a higher priority than the peak spectrum efficiency and Voice over IP (VoIP) capacity.

Peak Spectrum Efficiency

When all available radio resources are used only for a single UE then the highest data rate per cell bandwidth is defined as peak spectrum efficiency. In LTE-A, the DL peak spectrum efficiency is targeted up to 30 bps/Hz while for UL peak spectrum efficiency should be up to 15 bps/Hz for a system employing 8×8 or less antenna configurations for DL and 4×4 or less antenna configurations for UL [4].

Average Spectrum Efficiency

The unit of average spectrum efficiency is b/s/Hz/cell. For LTE-A, in UL case it should be 1.2 for 1×2 configuration and for 2×4 it should be 2.0. For DL case, 2×2 configuration should have 2.4, 4×2 should have 2.6 and 4×4 should have 3.7 [4].

Cell Edge user throughput

The cell edge user throughput should be improved to make a homogenous distribution of the cell resources for the whole coverage area. If we consider 10 users which are uniformly placed in a cell, then for LTE-A, the targets given in the following table for different antenna configurations should be achieved [4]

Antenna Configuration	Bps/Hz/cell/10 users
UL 1×2	0.04
UL 2×4	0.07
DL 2×2	0.07
DL 4×2	0.09
DL 4×4	0.12

Chapter No.2

MIMO- OFDM System

For high data rate widespread communication systems -- DSL, WLAN, DVB, WiMAX, Flash-OFDM and LTE-- a multi-carrier modulation known as OFDM is used [5].

2.1 Multicarrier Modulation

In OFDM system, a large data stream is divided into many small sub streams and different sub-channels are used to transmit each small data stream. To avoid inter-symbol interference (ISI), these sub channels are made orthogonal to each other when the propagation conditions are ideal. Multicarrier technique can be implemented in many ways, like vector coding and OFDM [6].

Suppose a communication system of bandwidth B is transmitting data at rate of R bps. If we assume that the coherence bandwidth B_c of the channel is less than the overall system bandwidth B, then the data passing through channel will experience frequency selective fading. A transmitter transmitting data over multi-carriers is shown in Figure 2.1. Here a serial to parallel converter (S/P) divides a large incoming bit stream into N sub-streams. The data of n^{th} sub-stream is modulated by using QAM or PSK modulation technique for sub carrier frequency f_n occupying bandwidth B_N. The transmitted signal is sum of all the modulated signals of all sub-channels and it can be written as

$$s(t) = \sum_{i=0}^{N-1} s_i(t) \cos(2\pi f_i t + \emptyset_i) \qquad (2.1)$$

where s_i is the modulated complex symbol being transmitted on the i^{th} subcarrier and the added phase offset to the i^{th} sub-carrier is $\emptyset_i$. To make all sub-channel orthogonal to each other we have $f_i = f_o + i(B_N),\ i = 0, \ldots, N-1$.

Figure 2.2 demonstrates the receiver structure for the above described multi-carrier system. In order to remove the interference caused by the data passing through other sub-streams, a narrow-band filter is used. After performing demodulation, a parallel to serial converter is used to get the original data sequence.

In spite of simplicity, this transmission scheme has some drawbacks. First, in real-time signal processing systems, a large bandwidth would be required as all sub-carriers cannot have

sharp filters for generating rectangular waveforms but we have time-limited signals. Moreover, to avoid ISI and to make all sub-carriers orthogonal to each other, low pass filters of high quality are required at the receiving side. And for transmitting using this system, we require as many RF antennas as many sub-carriers are used for data transmission [5].

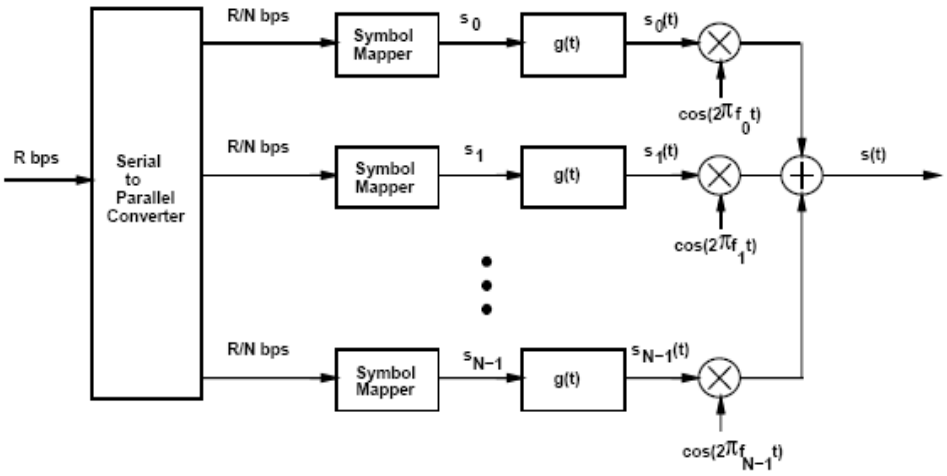

Figure 2.1: Multicarrier Transmitter [6]

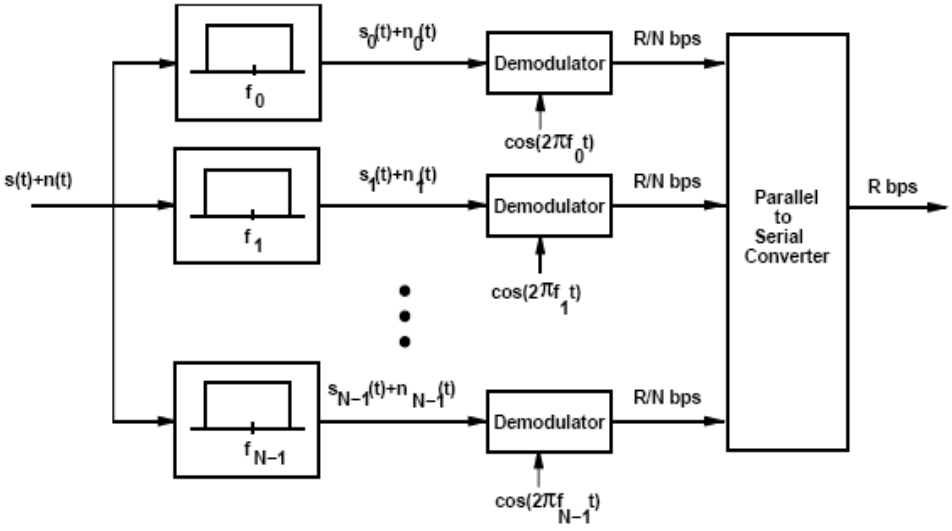

Figure 2.2: Multicarrier Receiver [6]

2.2 OFDM Basics

To reduce the equipment cost and to require less number of RF radios at the transceiver ends, Discrete Fourier Transform (DFT) is used as a efficient computational tool.

2.2.1 Guard Interval Insertion for Block Transmission

In one OFDM symbol, L data symbols are combined. The duration of OFDM symbol $T = LT_s$. To avoid inter-symbol interference between OFDM symbols, guard intervals are added as shown in figure below.

2.2.2 Circular Convolution

Let x[n], $0 \leq n \leq N-1$ is input data stream to a channel whose behavior is linear and time invariant having Finite Impulse Response (FIR), after passing through such channel the output will be linear convolution of the input data and the channel impulse response: y[n]=x[n]*h[n].

The circular convolution between x[n] and h[n] can be computed as [5]

$$y[n]= x[n] \otimes h[n] = h[n] \otimes x[n] \qquad (2.2)$$

where

$$x[n] \otimes h[n] = h[n] \otimes x[n] = \sum_{k=0}^{L-1} h[k]\, x[n-k]_N \qquad (2.3)$$

where $[n-k]_N$ denotes [n-k] module N and here x[n-k] is repeated periodically after N interval [6].

If the output of the channel is due to the circular convolution of the input and channel impulse response, then for frequency domain representation, we can take DFT of the output

$$DFT\{y[n]\} = DFT\{ h[n] \otimes x[n]\} \qquad (2.4)$$

As a result we get the following

$$Y[m] = H[m]X[m] \qquad (2.5)$$

For case of circular convolution, if the channel impulse response is estimated at the receiver, then the data being transmitted can be recovered by employing IDFT operation on $Y[m]/H[m]$. Because in real time channel output is not due to circular convolution but we can make linear convolution as circular convolution due to addition of cyclic prefix.

2.2.3 Cyclic Prefix

In order to avoid ISI between OFDM symbols, if the maximum delay spread of the channel is $v + 1$ samples, then at least v samples are required to be added before and after of the transmitting signals [5]. In time-domain, an OFDM symbol of length N sample values can be represented as

$$\boldsymbol{X} = [x_1\ x_2\ x_3\ \ldots\ x_N]$$

And discrete time channel with FIR as

$$\boldsymbol{h} = [h_o\ h_1\ \ldots\ h_v]$$

The transmitted signal after adding a cyclic prefix of length v is represented as

$$\boldsymbol{X_{CP}} = [x_{N-v}\ x_{N-v+1}\ \ldots\ x_{N-1}\ x_0\ x_1 \ldots\ x_{N-1}]$$

After passing through channel, the output becomes

$$\boldsymbol{y_{CP}} = \boldsymbol{h} * \boldsymbol{x_{CP}}$$

where $\boldsymbol{h}$ denotes the impulse response of the channel and has $v + 1$ samples during transmitting one OFDM symbol. The output $\boldsymbol{y_{CP}}$ will contain $(N + v) + (v + 1) = N + 2v$ samples. The interference will effect only on the first v samples of $\boldsymbol{y_{CP}}$ due to the preceding OFDM symbol and that is why these samples are neglected. The last v samples of the output will also interfere with the next OFDM symbol that is why these are also discarded. After removing these interference affected samples, in the end we get only N samples of the output, that is our desired output.

The output of the channel can be made simple multiplication of the channel frequency response $\boldsymbol{H} = DFT\{\boldsymbol{h}\}$ and the frequency response of the input data to the channel, $\boldsymbol{X} = DFT\{\boldsymbol{x}\}$. Instead of the advantageous behavior of adding the cyclic prefix, we have to pay for extra bandwidth and more power consumption [5].

2.3 OFDM Block Diagram

The key steps carried out in an OFDM communication system are shown in Figure 2.3(a) and Figure 2.3(b). A QAM modulator is used to convert the incoming data into complex valued symbols $X[0], X[1], \dots, X[N-1]$. These symbols are then converted into N parallel QAM symbols and each symbol is transmitted over different sub-carriers. These N parallel symbols are called discrete frequency components of the modulator output. IDFT operation is performed over these N symbols to get back time domain samples from these frequency domain components and in order to reduce the complexity IFFT operation is performed for IDFT operation. Time domain OFDM symbol having N samples is given by the following IDFT relation

$$IDFT\{X[i]\} = x[n] = \frac{1}{\sqrt{N}} \sum_{n=0}^{N-1} X[i] e^{j\frac{2\pi ni}{N}} \qquad (2.6)$$

This sequence contains the samples of the multicarrier signal and each QAM symbol X[i] is transmitted over different carrier frequency, given as $e^{j2\pi i \frac{t}{T_N}}$, $i = 0, \dots, N-1$. After modulating over carrier frequency, CP is added to each OFDM symbol. At receiver side the incoming parallel data is passed through parallel to serial converter and then these digital samples are converted into analog data sequence, which gives a baseband OFDM signal $\tilde{x}(t)$ which is again up-converted to the passband frequency f_0.

After passing through AWGN channel having *h(t)* impulse response, the received signal will be

$$y(t) = \tilde{x}(t) * h(t) + n(t) \qquad (2.7)$$

At the receiver end, the received signal is down-converted to get back the baseband signal and is passed through a low pass filter. The continuous signal is again converted back into digital samples after passing A/D converter. After removing CP from the output signal, we have only N samples. Neglecting the effect of noise, the DFT of the output is given as $Y[i] = H[i]X[i]$. Then these frequency domain samples are converted into N parallel streams and each stream is demodulated using QAM demodulator to get back the original transmitted data.

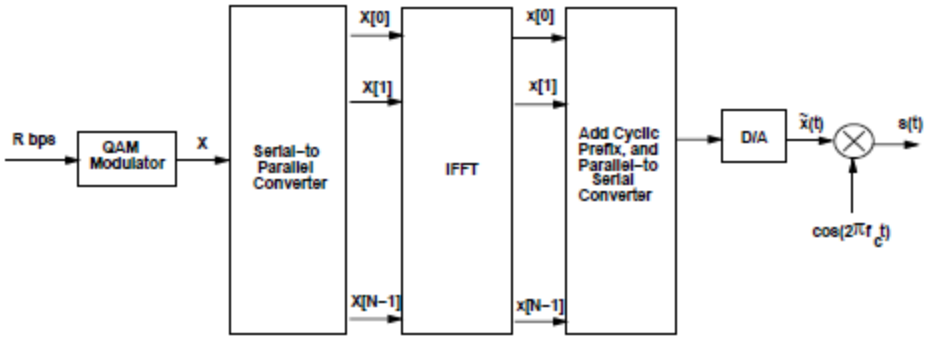

Figure 2.3(a): Transmitter Structure of OFDM [8]

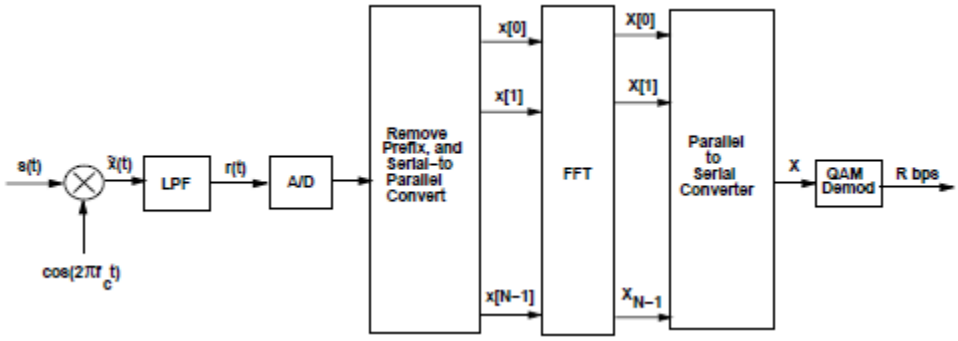

Figure 2.3(b): Receiver Structure of OFDM [8]

2.4 DFT

N samples of output $\boldsymbol{y_{CP}}$ are equivalent to $\boldsymbol{y_{CP}} = h * \boldsymbol{x_{CP}}$. Consider y_0 is the first element in $\boldsymbol{y_{CP}}$. According to Figure 2.4, y_0 depends on x_0 and the circularly wrapped values $x_{N-v}, \dots x_{N-1}$ and can be written as

$$\begin{aligned} y_0 &= h_0x_0 + h_1x_{N-1} + \dots + h_vx_{N-v} \\ y_1 &= h_0x_1 + h_1x_0 + \dots + h_vx_{N-v+1} \\ &\vdots \\ y_{N-1} &= h_0x_{N-1} + h_1x_{N-2} + \dots + h_vx_{N-v-1} \end{aligned} \qquad (2.8)$$

In matrix form this can be written as

$$\begin{bmatrix} y_{N-1} \\ y_{N-2} \\ \vdots \\ y_0 \end{bmatrix} = \begin{bmatrix} h_0 & h_1 & \dots & h_\mu & 0 & \dots & 0 \\ 0 & h_0 & \dots & h_{\mu-1} & h_\mu & \dots & 0 \\ \vdots & \vdots & \ddots & \ddots & \ddots & \ddots & \vdots \\ 0 & \dots & 0 & h_0 & \dots & h_{\mu-1} & h_\mu \end{bmatrix} \begin{bmatrix} x_{N-1} \\ \vdots \\ x_0 \\ x_{-1} \\ \vdots \\ x_{-\mu} \end{bmatrix} + \begin{bmatrix} v_{N-1} \\ v_{N-2} \\ \vdots \\ v_0 \end{bmatrix} \qquad (2.9)$$

and we can represent it as

$$y = Hx + v \qquad (2.10)$$

The symbols $y_{-1} \dots y_{-V}$ are discarded because they are affected by ISI. The last v symbols of $x[n]$ correspond to the cyclic prefix: $x_{-1}=x_{N-1}, x_{-2}=x_{N-2}, \dots, x_{-v}=v_{N-v}$

So we can write

$$\begin{bmatrix} y_{N-1} \\ y_{N-2} \\ \vdots \\ \vdots \\ \vdots \\ y_0 \end{bmatrix} = \begin{bmatrix} h_0 & h_1 & \dots & h_\mu & 0 & \dots & 0 \\ 0 & h_0 & \dots & h_{\mu-1} & h_\mu & \dots & 0 \\ \vdots & \vdots & \ddots & \ddots & \ddots & \ddots & \vdots \\ 0 & \dots & 0 & h_0 & \dots & h_{\mu-1} & h_\mu \\ \vdots & \vdots & \ddots & \ddots & \ddots & \ddots & \vdots \\ h_2 & h_3 & \dots & h_{\mu-2} & \dots & h_0 & h_1 \\ h_1 & h_2 & \dots & h_{\mu-1} & \dots & 0 & h_0 \end{bmatrix} \begin{bmatrix} x_{N-1} \\ x_{N-2} \\ \vdots \\ \vdots \\ x_0 \end{bmatrix} + \begin{bmatrix} v_{N-1} \\ v_{N-2} \\ \vdots \\ \vdots \\ \vdots \\ v_0 \end{bmatrix} \qquad (2.11)$$

Alternatively we can write it as

$$y=\tilde{H}x + v \qquad (2.12)$$

where $\tilde{H}$ is a N ×N circulant matrix over N samples.

The expression for N-point DFT of a data sequence x[n] is given by [3]

$$DFT\{x[n]\} = X[i] = \frac{1}{\sqrt{N}} \sum_{n=0}^{N-1} x[n] e^{-j\frac{2\pi ni}{N}} \qquad (2.13)$$

$$0 \le i \le N-1$$

In matrix multiplication it can be written as

$$X = Qx \tag{2.14}$$

Where Q is an $N \times N$ matrix and is given by

$$Q = \frac{1}{\sqrt{N}}\begin{bmatrix} 1 & 1 & 1 & \dots & 1 \\ 1 & W_N & W_N^2 & \dots & W_N^{N-1} \\ \vdots & \vdots & \ddots & \vdots & \vdots \\ 1 & W_N^{N-1} & W_N^{2(N-1)} & \dots & W_N^{(N-1)^2} \end{bmatrix} \tag{2.15}$$

For $w_N = e^{-j\frac{2\pi}{N}}$

The rows of the DFT matrix Q are eigenvectors of $\widetilde{H}$ [6].

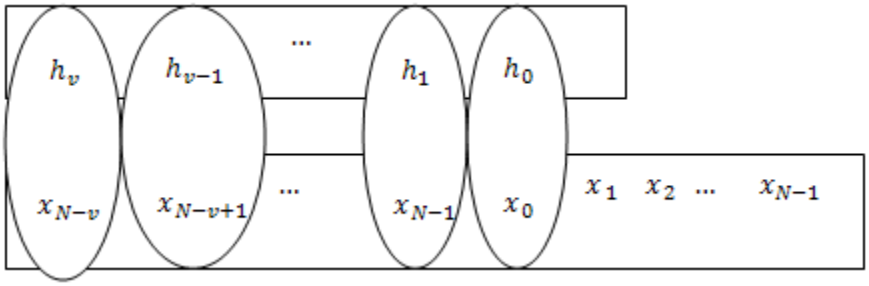

Figure 2.4: Circular Convolution created by OFDM CP [5]

Discrete Fourier Transform (DFT) is equivalent representation of the continuous time Fourier transform in discrete time, as $X[i]$ is used to represent the frequency content of the time-domain sample of the data sample $x[n]$, which is discrete time sample of signal $x(t)$. The time domain sample $x[n]$ can be obtained by using IDFT, given as [7]:

$$IDFT\{X[i]\} = x[n] = \frac{1}{\sqrt{N}}\sum_{n=0}^{N-1} X[i]^{e^{j\frac{2\pi ni}{N}}} \tag{2.16}$$

In hardware, DFT and IDFT are performed by FFT and IFFT, respectively.

2.5 DCT

In DFT, the basis sequences are the complex periodic sequences $e^{j2\pi\frac{kn}{N}}$ and the resulting sequence will be, in general, complex even sequence. It is natural to inquire whether there exist a set of real-valued basis sequences that will yield a real-valued transform sequence [7]. This orthogonal transform for real sequences is Discrete Cosine Transform (DCT). DCT is closely related to DFT and has become useful in a number of signal processing applications, speech and image compression.

In DCT, the basis sequences are cosines. Since the cosines are both periodic and have even symmetry, the DCT of any sequence will also be periodic and symmetric. There are many definitions of DCT e.g. DCT-1, DCT-2, DCT-3 and DCT-4.

For example DCT-1 is defined by the following transform pair [7]

$$X^{c1}[k] = 2\sum_{n=0}^{N-1} \alpha[n]x[n]\cos\left(\frac{\pi kn}{N-1}\right) \qquad (2.17)$$

$$0 \leq k \leq N-1$$

$$x[n] = \frac{1}{N-1}\sum_{k=0}^{N-1} \alpha[k]X^{c1}[k]\cos\left(\frac{\pi kn}{N-1}\right) \qquad (2.18)$$

$$0 \leq n \leq N-1$$

Where $\alpha[n]$ is defined by

$$\alpha[n] = \begin{cases} \frac{1}{2}, & n = 0 \text{ and } N-1 \\ 1, & 1 \leq n \leq N-2 \end{cases} \qquad (2.19)$$

Consider Figure 2.5 where the finite-length sequence x[n] is plotted with solid dots. Figure 2.5(a) shows DCT-1 and Figure 2.5(b) is DCT-2 representation.

The major application of DCT is in signal compression, where the blocks of the signal are represented by their cosine transforms. The main reason of using DCT is due to its energy concentration [7].

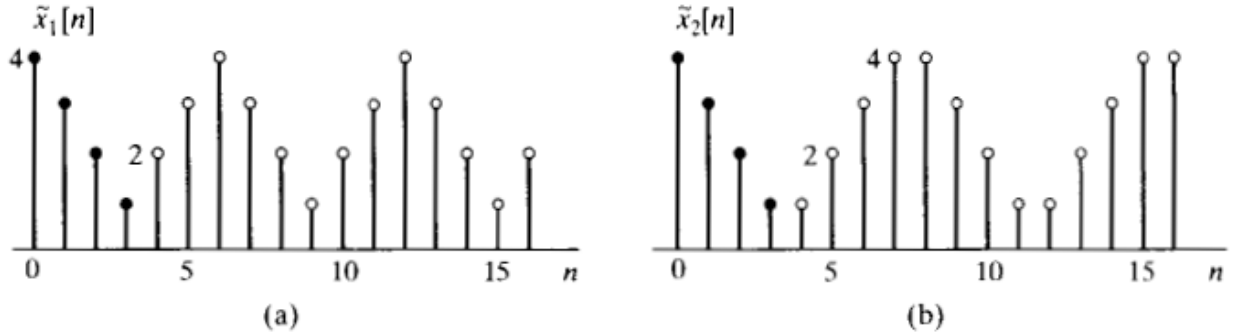

Figure 2.5: (a) Representation of DCT-1 (b) Representation of DCT-2 [7]

2.6 MIMO

For increased data rate and throughput, Multi Input Multi Output (MIMO) has been proposed for wireless networks and for these improved performances no extra bandwidth and more power consumption is required.

2.6.1 MIMO Channel

Suppose a communication system having *T* transmit antennas and *R* receive antennas, the system description is shown in Figure 2.6.

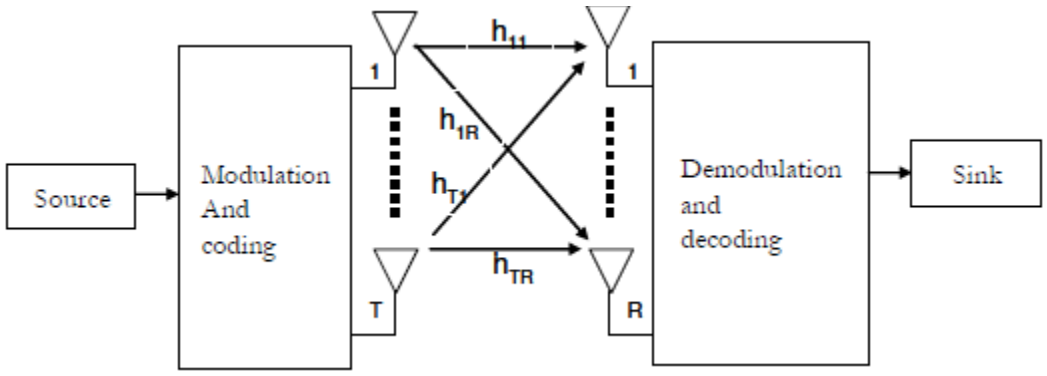

Figure 2.6: MIMO Channel [9]

Let h_{tr} denotes the channel co-efficient between the t^{th} transmit antenna and r^{th} receive antenna. The transmitted data is represented by $x=[x_1 \ x_2 \ \dots \ x_T]^T$ and received data after passing through channel is given *as* $y=[y_1 \ y_2 \ \dots \ y_R]^T$. Then in matrix form we can write

$$\begin{bmatrix} y_1 \\ y_2 \\ \vdots \\ y_R \end{bmatrix} = \begin{bmatrix} h_{11} & h_{21} & \cdots & h_{T1} \\ h_{12} & h_{22} & \cdots & h_{T2} \\ \vdots & \vdots & \vdots & \vdots \\ h_{T1} & h_{T2} & \cdots & h_{TR} \end{bmatrix} \begin{bmatrix} x_1 \\ x_1 \\ \vdots \\ x_T \end{bmatrix} + \begin{bmatrix} \eta_1 \\ \eta_2 \\ \vdots \\ \eta_R \end{bmatrix}$$

Which is equal to

$$y = Hx + \eta \qquad (2.20)$$

Where H is $T \times R$ channel matrix and η is complex AWGN vector.

2.6.2 Time-varying MIMO Channel

Consider the same channel as above described and h_{ij} is used to represent the channel co-efficient between i^{th} transmit antenna and j^{th} receive antenna. To make all fading channels independent of each other, the spacing between antennas is kept large enough. At time instant k, the channel co-efficients $h_{ij}(k)$ are given by zero mean complex Gaussian random variable with variance

$$\sigma_h{}^2 = E\{\left|h_{ij}(k)\right|^2\} \qquad (2.21)$$

and Doppler Spectrum

$$S(\omega) = \sum_{n=\infty}^{\infty} E\{h_{ij}(k) h_{ij}{}^*(k+n\} e^{j\omega n} \qquad (2.22)$$

If at time instant k, the transmitted symbol by antenna i is given by $s_i(k)$ then the whole antenna array will be transmitting energy equal to

$$E_s(k) = \sum_{i=1}^{T} |s_i(k)|^2 \qquad (2.23)$$

At receive antenna j , the signal received at instant k is given by

$$y_j(k) = \sum_{i=1}^{nT} h_{ij}(k) s_i(k) + n_j(k) \qquad (2.24)$$

2.7 MIMO Techniques for Time-varying Channels

In MIMO fading channels, due to the complexity of the equalization process for single carrier communication system, data transmission over multi-carriers is preferred as the equalizer's complexity reduces for such systems. The channel capacity can be utilized at full rate by exploiting space-time coding for MIMO-OFDM systems.

To make multi-antenna transmission easy and less complex, array of antennas can be divided into groups and separate encoders are used for each group and at receiver side MLSE technique can be used as a decoding algorithm. Under high mobility conditions, where the multi-path channels have time-variant effects, advanced signal processing techniques are needed for reliable communication. To lessen the multipath effects in fading channels, Doppler diversity can be combined with Doppler scattering. The performance of MIMO systems can be improved significantly by using multi-path Doppler diversity.

2.7.1 BLAST

Figure 2.7 shows the process followed by BLAST multi input multi output technique. The data to be transmitted is first converted into many parallel data streams and then each stream is coded separately, which is transmitted by a separate antenna. According to Figure 2.8, each coded stream is rotated every few code symbols before being transmitted by antennas, where a group of code symbols is represented by a different labeled block. The signals being transmitted from different antennas are represented by rows. So by using approach, data transmitting on particular antenna face severe fading but code should be capable of neglecting this fading effect. At receiver side, the MMSE algorithm is applied for detection, after which decoder and equalizer are applied to neglect the effect of interference.

2.7.2 Space-Time Trellis Code (STTC)

The trellis used in channel coding like convolutional coding is also based on trellis coded modulation (TCM). In TCM, the vectors used for branch labels are representing the data transmitting by multiple antennas. A simple QPSK modulation scheme on array of two transmit antennas is shown in Figure 2.9. The left side labels of the nodes show the trellis branches originating from that branch, in the descending order. The states of four phases of QPSK are represented by the corresponding numbering sequence from 0 to 3. The data transmitting during one trellis period consists of two bits as each node originates four branches. On each antenna, at

least one different symbol is transmitted by any pair of paths. In Figure 2.9, the symbol pairs 00 00 and 01 10 are shown by dark lines. So if a symbol transmitting from a specific antenna undergoes severe fading then decoder will be still capable of tracking their paths. The overall diversity of the system is of order two

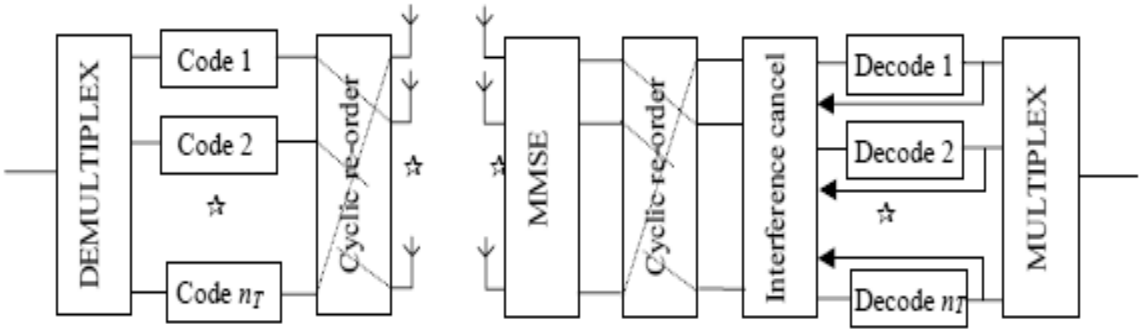

Figure 2.7: Architecture of BLAST System [8]

Time

Antennas												
	1	6	5	4	3	2	1	6	5	4	3	2
	2	1	6	5	4	3	2	1	6	5	4	3
	3	2	1	6	5	4	3	2	1	6	5	4
	4	3	2	1	6	5	4	3	2	1	6	5
	5	4	3	2	1	6	5	4	3	2	1	6
	6	5	4	3	2	1	6	5	4	3	2	1

Figure 2.8: Mapping of coded Data Streams to antennas in BLAST [8]

.

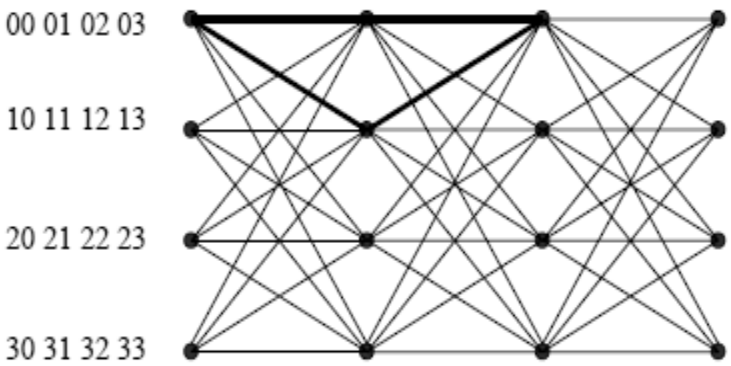

Figure 2.9: Trellis for Space-time Code [8]

2.7. 3 Space-Time Block Codes (STBC)

STBC is used for linear mapping of the data information to the multiple antennas. The main aim of the coding technique is not to increase the system capacity or coding gain, instead it is used to gain maximum diversity order.

An $m \times n$ array of k variables $x_1, x_2, \ldots, x_k$ is shown in the matrix form given below . To make all columns orthogonal to each other, negative complex conjugates of some entries are taken. A simple example of STBC is Alamouti scheme for which transmission scheme is shown in the following matrix form

$$\begin{pmatrix} x_1 & x_2 \\ -x_2^* & x_1^* \end{pmatrix}$$

For high order diversity, the matrix becomes

$$\begin{pmatrix} x_1 & x_2 & x_3 \\ -x_2 & x_1 & -x_4 \\ -x_3 & x_4 & x_1 \\ -x_4 & -x_3 & x_2 \\ x_1^* & x_2^* & x_3^* \\ -x_2^* & x_1^* & -x_4^* \\ -x_3^* & x_4^* & x_1^* \\ -x_4^* & -x_3^* & x_2^* \end{pmatrix}$$

Time representation is along rows and number of antennas are represented by the number of columns.

2.8 MIMO-OFDM

For high data rate requirement for next generation wireless communication systems, as the system bandwidth should be greater than coherence bandwidth, so the channel cannot be assumed having flat fading. To make channel effect flat fading, OFDM can be applied for any MIMO technique. The resulting system is shown in Figure 2.10.

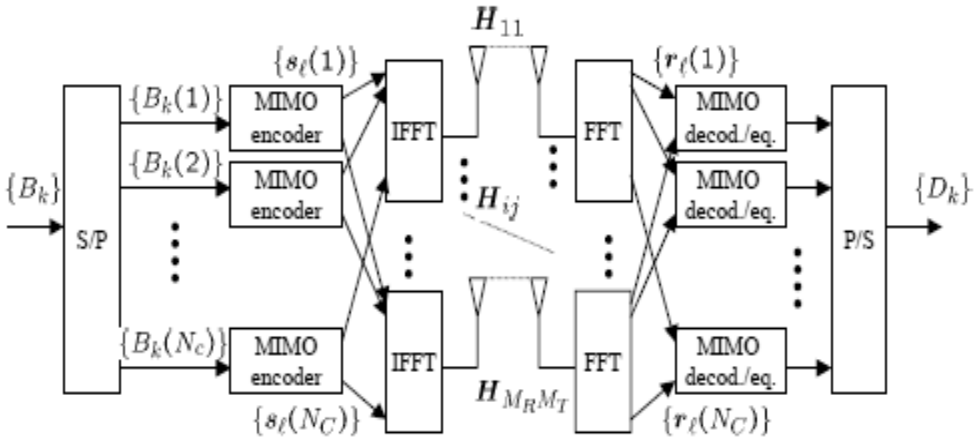

Figure 2.10: MIMO-OFDM System Model [8]

The modulated complex input symbols are encoded by using MIMO encoder to form encoded data bits like STBC is used to generate code-words. For each sub-carrier different encoder is used, so total number of encoders used are N_c. The modulated information according to the constellation is denoted by $\{B_k\}$ where k is time index. The data on the specific sub-carrier can be routed by using serial to parallel converter. So the input sequence $\{B_k(n)\}$ can be converted into T $\times$ 1 vector sequence $\{s_l(n)\}$ by using MIMO encoder. Different antennas are used to transmit each component on the same sub-carrier. For a specific time instant, if we drop the time-subscript then output of all encoders can be written in a long vector of dimension $TN_c \times 1$, so we can write

$$s(n) = (s(1), s(2), \dots, s(N_c))^T$$

Then OFDM system is applied to this vector.

If multi-carrier system is so designed that no ICI and ISI occur, then the transmission path for different antennas can be represented by single complex co-efficient. Suppose the fading co-efficient of the channel transfer function is denoted by $H_{ij}(n)$ for sub-carrier n. The matrix consisting of all the co-efficients of the channel are given in form of the following matrix

$$H(\mathrm{n})=\begin{pmatrix} H_{1,1}(n) & \dots & H_{1,T}(n) \\ \vdots & & \vdots \\ H_{R,1}(n) & \dots & H_{R,T}(n) \end{pmatrix} \qquad (2.25)$$

The received data on sub-carrier n is given by

$$r(n) = H(n)s(n) + \eta(n) \qquad (2.26)$$

where $n(n)$ is zero mean complex Gaussian noise on each antenna.

If the frequency spacing and the pulse shaping filtering results in no ICI and ISI, the channel matrix for complete MIMO system can be written as

$$H = \begin{pmatrix} H_{1,1}(1) & \dots & H_{1,T}(1) & & & & & & & \\ \vdots & & \vdots & & 0 & & \dots & & 0 & \\ H_{R,1}(1) & \dots & H_{R,T}(1) & & & & & & & \\ & & & H_{1,1}(2) & \dots & H_{1,T}(2) & & & & \\ 0 & & & \vdots & & \vdots & & & 0 & \\ & & & H_{R,1}(2) & \dots & H_{R,T}(2) & \ddots & & & \\ \vdots & & & & & & \ddots & H_{1,1}(N_c) & \dots & H_{1,T}(N_c) \\ & & & & & & & \vdots & & \vdots \\ 0 & & \dots & & 0 & & & H_{R,1}(N_c) & \dots & H_{R,T}(N_c) \end{pmatrix} \qquad (2.27)$$

And a single long receiver vector r of dimension $N_C R \times 1$ will be

$$r = (r(1), r(2), \dots, r(N_c))^T \qquad (2.28)$$

So the received signal after passing through MIMO-OFDM system becomes

$$r = Hs + \eta \qquad (2.29)$$

At receiver side, decoder for MIMO system is used for each sub-carrier to get back $\{D_k(n)\}$, which are complex numbers. Before applying the detector to the received data, first parallel to serial converter is applied.

2.9 Simulation Results

2.9.1 OFDM Simulation

The system specifications for this simulation are given in Table 2.1.

TABLE 2.1: OFDM SYSTEM PARAMETERS

Parameters	Values
Data Symbols	1024
FFT Size	256
Frame Length	128
CP Length	16

The representations of OFDM signal in both domains: time and frequency, according to these parameters are shown in Figure 2.11 and Figure 2.12.

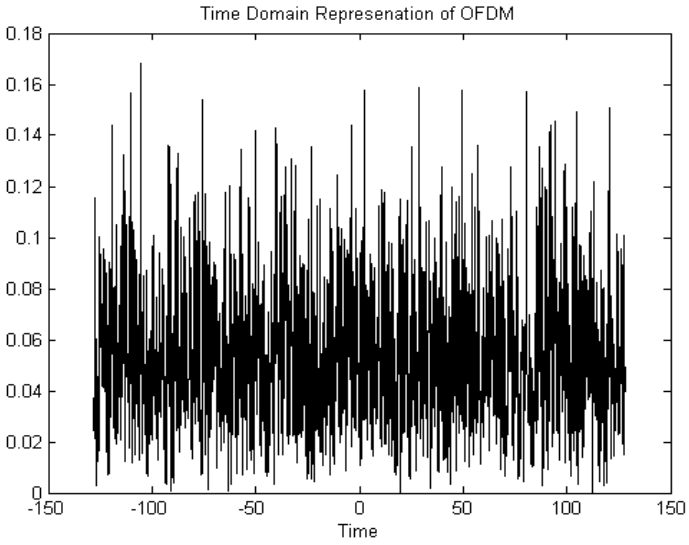

Figure 2.11: Time Domain Representation of OFDM

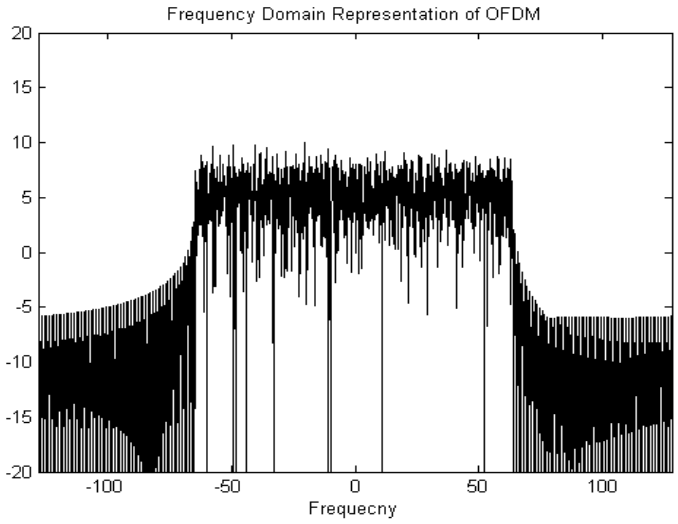

Figure 2.12: Frequency Domain Representation of OFDM

2.9.2 MIMO Simulation

In this simulation the system parameters considered are listed in Table 2.2.

TABLE 2.2: SIMULATION PARAMETERS FOR MIMO

Parameters	Values
Frame Length	130
Modulation	16 QAM
MIMO configuration	2×2 4×4
Number of Packets	100
MIMO Technique	STBC

Figure 2.13 and Figure 2.14 show the comparison between Uncoded and MIMO technique in terms of BER vs SNR.

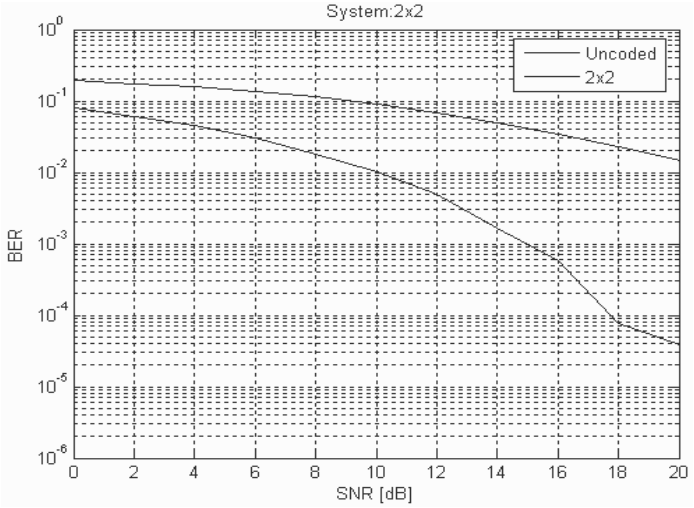

Figure 2.13: BER Comparison for Uncoded and 2 × 2 System

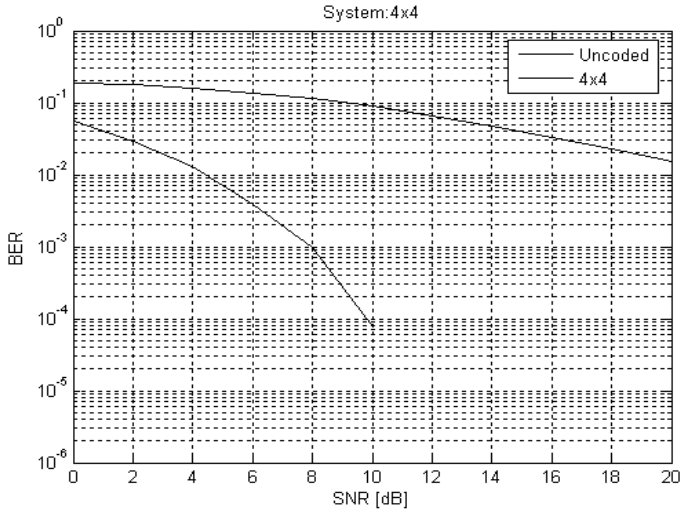

Figure 2.14: BER Comparison between Uncoded and 4 × 4 Systems

2.9.3 MIMO-OFDM Simulation

In MIMO-OFDM system simulation the parameters taken into account are mentioned in Table 2.3.

TABLE 2.3: MIMO-OFDM SYSTEM PARAMETERS

Parameters	Values
FFT Size	16
CP	4
Channel Order	3
MIMO Detection	MMSE
MIMO Configuration	4 × 4

The graph between Probability of error and SNR for the above mentioned shown parameters is shown in Figure 2.15.

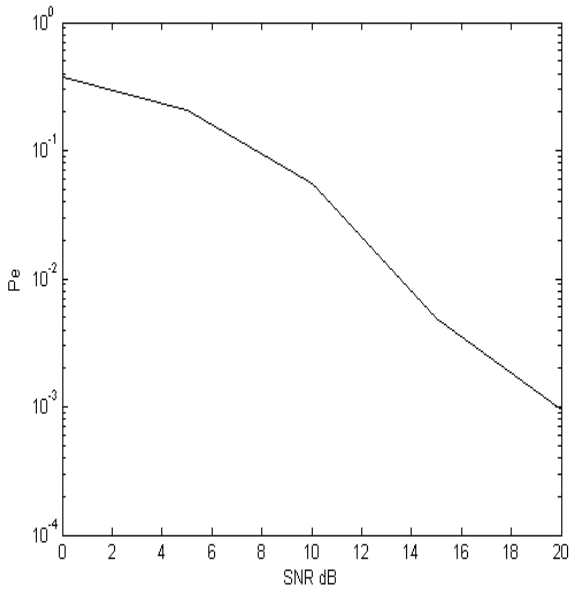

Figure 2.15: P_e vs SNR for MIMO-OFDM System

Chapter No. 3

Channel Estimation of OFDM System

MIMO systems that use coherent OFDM can provide high channel capability if there is precise information of the channel available at the receiver. This performance can even be increased if the Channel State Information (CSI) is also available at the transmitter because it makes our receiver design simpler [15]. The performance of the system usually relies on the channel estimation algorithm. Decision directed channel estimation and pilot- assisted channel estimation are the two basic methods for channel estimation. In decision directed method, there is no need of additional pilots because recovered data is treated as "new pilots" that provides the channel estimation module with that data which keeps track of the state of channel and provides the advantage of less delay as compared to other techniques such as interpolation, Wiener or Kalman Filtering. However this method has some disadvantages: its response to error detection is not suitable that causes error propagation and the need of huge amount of data slows down its convergence rate. In pilot-assisted method, we collect channel information from the pilots that are transmitted with the signal using interpolation filters. There are two modes of pilot-assisted channel estimation method, one in which all subcarriers are used as pilots for a specific period, known as block pilot mode and the other one is comb pilot mode in which some of the subcarriers are used as pilots.

Channel can be estimated in time domain or frequency domain. In frequency domain two algorithms are proposed Least Square Estimation (LSE) and Linear Minimum Mean Square Estimation (LMMSE). LSE algorithm is relatively easy to implement due to its less complexity and it also does not require any channel apriority probability. To achieve better performance LMMSE is proposed. LMMSE is optimum in minimizing Mean Square Error (MSE) as it uses addition information of operating SNR and the channel statistics. But its complexity is higher due to the channel correlation and the matrix inversion lemma. There can be a compromise of complexity and performance by taking the effect of the channel taps and channel impulse response (CIR) samples. By assuming the impulse response of finite length, these two algorithms can be modified having less complexity. In mobile wireless links the channel statistics are not known, in these cases it is robust to consider the uniform Power delay profile (PDP), which also reduces complexity of LMMSE. The complexity of LSE can be reduced by regularizing the Eigen values of the matrix being inverted or by down-sampling the channel vector.

Instead of frequency domain, channel can be estimated in time-domain by DFT-based approach, whose performance is better and complexity is less than LSE and LMMSE. The

performance can be improved further by making a suitable selection of CIR samples and channel taps by using the Most Significant Taps (MST) method. In this method, the estimated channel in frequency-domain is converted to time-domain by using IDFT. Then this estimated CIR is passed through MST to suppress the noise by discarding certain CIR. The remaining significant CIR is transformed back to frequency domain by DFT, thus improving the performance than LMMSE and reduced complexity due to the presence of fast algorithms FFT and IFFT. The performance of DFT-based approach degrades in case of non-integer spaced multipath delays due to the presence of the dispersed CIR. To avoid this problem, new approach has been proposed, named as DCT/EIDCT. In this method, DCT is applied to get the channel response in transform domain, instead of DFT.

In transform-based techniques, the channel samples having less energy than noise can be discarded by employing a windowing function such as Hanning or Hamming window. This windowed based technique shows improved performance and less complexity than other transform-based approaches.

Channel State Information (CSI) can also be achieved through PUCCH and PUSCH for DL transmission. Adaptive equalization is required in case of time-dispersive and multi-path fading channel for reliable communication [16]. For this purpose reference signals are transmitted in place of the unknown transmitted data. Iterative receivers for 4G mobile standards performing joint detection and decoding are proposed for high performance gain [17]. For these iterative receivers, adaptive filtering techniques are most suitable as compared to LSE and LMMSE [18]. LMS, RLS and Kalman Filtering algorithms can be used for wiener-based channel estimation, which may or may not require the second order statistics of the channel and noise [19]. To the best knowledge of the authors, first time adaptive filters using channel statistics are investigated in this thesis. Effect of varying step-size on performance and complexity is also presented. We also show that how these adaptive algorithms can be optimized by taking filter length and multi-path channel taps into consideration.

3.1 Frequency Domain Based Channel Estimation

3.1.1 LMMSE Channel Estimation

After passing through AWGN channel having the noise variance, σ_n^2, the LMMSE estimation of the channel vector , g, is given by [20]

$$\hat{g} = \Gamma_{gy}\Gamma_{yy}^{-1}y \tag{3.1}$$

Where

$$\Gamma_{gy} = \Gamma_{gg}F^H X^H \tag{3.2}$$

$$\Gamma_{yy} = XF\Gamma_{gg}F^H X^H + \sigma_n^2 I_N \tag{3.3}$$

Where Γ_{gy} is the cross co-variance matrix between g and y and Γ_{yy} is the auto-covariance matrix of y. These co-variance matrices should be positive definite to make a unique minimum MSE.

The channel estimate $\hat{h}_{mmse}$, in frequency domain, is obtained by taking DFT of $\hat{g}$, given by

$$\hat{h}_{mmse} = F\hat{g} = FQF^H X^H y \qquad (3.4)$$

Where F is orthonormal DFT-matrix and Q is given by [21]

$$Q = \Gamma_{gg}\left[(F^H X^H XF)^{-1}\sigma_n^2 + \Gamma_{gg}\right]^{-1}(F^H X^H XF)^{-1} \qquad (3.5)$$

3.1.2 Modified LMMSE Channel Estimation

For large N the calculation of Q matrix implies high complexity. To reduce the size of Q, we can take only first L taps having significant energy. Using this approximation, Γ_{gg} is reduced to L × L matrix. So modified LMMSE estimation becomes [20]

$$\hat{h}_{mmse} = TQ^{'}T^H X^H y \qquad (3.6)$$

Where T have only first L columns of DFT matrix and $Q^{'}$ is

$$Q^{'} = \Gamma^{'}_{gg}\left[(T^H X^H XT)^{-1}\sigma_n^2 + \Gamma^{'}_{gg}\right]^{-1}(T^H X^H XT)^{-1} \qquad (3.7)$$

$\Gamma^{'}_{gg}$ denotes the upper left L × L matrix of Γ_{gg}.

3.1.3 Low Complex LMMSE Channel Estimation

Inversion of a large matrix is required in LMMSE channel estimation. The complexity of LMMSE increases especially when the input data X changes and the matrix inversion is needed recursively. If same modulation constellation is considered for each OFDM symbol, then the average of the input data X becomes

$$E(XX^H)^{-1} = E\left|\frac{1}{x_k}\right|^2 \qquad (3.8)$$

And low complex LMMSE estimation is given by [22]

$$\hat{h}_{mmse} = \Gamma_{gg}(\Gamma_{gg} + \frac{\beta}{SNR}I)^{-1}X^{-1}y \qquad (3.9)$$

Where β depends upon the constellation of the modulation technique used for OFDM symbol.

3.1.4 Robust LMMSE Channel Estimation

The behavior of the channel also changes especially for high mobility wireless links due to the time-varying surrounding environment [23]. In such a situation, the channel PDP is difficult to know. If all PDP's are assumed to be having same maximum delay then the channel co-variance matrix with a uniform PDP gives better performance [24].

3.1.5 LSE Channel Estimation

A prior knowledge of second order channel statistics is required for LMMSE estimator, which is not possible in many practical situations. We can design an estimator filter which is a function of available data only [25]. In LSE estimation, we use only signal model, no probabilistic assumptions are required.

LSE estimation of channel is given by

$$\hat{h}_{ls} = FQ_{ls}F^H X^H y \qquad (3.10)$$

where

$$Q_{ls} = (F^H X^H XF)^{-1} \qquad (3.11)$$

$\hat{h}_{ls}$ can also be written as [1]

$$\hat{h}_{ls} = X^{-1} y \qquad (3.12)$$

3.1.6 Modified LSE Channel Estimation

Though no modifications are needed because of less complexity of LSE estimator but performance can be improved by considering only first L high energy channel taps. The modified LSE estimator becomes

$$\hat{h}_{ls} = TQ_{ls}^{'} T^H X^H y \qquad (3.13)$$

where

$$Q_{ls}^{'} = (T^H X^H XT)^{-1} \qquad (3.14)$$

3.1.7 Regularized LSE Channel Estimation

The problem of inversion of $N \times N$ matrix can be solved by regularizing the Eigen values of the matrix by adding a constant term to the diagonal elements. In this case, the matrix Q_{ls} will be [26]

$$Q_{reg,ls} = (\alpha I + F^H X^H XF)^{-1} \qquad (3.15)$$

Where off-line constant α is chosen such that the matrix $Q_{reg,ls}$ is least perturbed.

3.1.8 Down-Sampled Impulse Response LSE Channel Estimation

The inversion of $N \times N$ matrix can be simplified by decreasing the sampling frequency, but ensuring the absence of aliasing. Only 2 out of 3 channel taps are used and the discarded taps are set to zero.

The down-sampled version of channel vector g can be [26]

$$\bar{g} = (g_0 \;\; g_1 \;\; 0 \;\; g_3 \;\; g_4 \;\; 0 \;\; \dots \;\; g_{L-1})^{\boldsymbol{T}} \qquad (3.16)$$

The channel transfer function can be written as

$$H^{DS} = F\bar{g} \qquad (3.17)$$

Which is equivalent to

$$H^{DS} = \begin{bmatrix} 1 & 1 & 1 & 1 & 1 \\ 1 & w^1 & w^3 & \dots & w^{(L-1)} \\ 1 & w^2 & w^6 & \dots & w^{2(L-1)} \\ 1 & w^3 & w^9 & \dots & w^{3(L-1)} \\ 1 & w^4 & w^{12} & \dots & w^{4(L-1)} \\ 1 & w^5 & w^{15} & \dots & w^{5(L-1)} \\ 1 & \dots & \dots & \dots & \dots \\ 1 & w^{N-1} & w^{3(N-1)} & \dots & w^{(N-1)(L-1)} \end{bmatrix} \begin{bmatrix} g_0 \\ g_1 \\ g_3 \\ g_4 \\ \vdots \\ g_{L-1} \end{bmatrix} \qquad (3.18)$$

The estimated channel in this case will be

$$\hat{h}_{DS} = (F^{DS,H} X^H X F^{DS})^{-1} F^{DS,H} X^H y \qquad (3.19)$$

3.2 Time Domain Based Channel Estimation

3.2.1 DFT-Based Channel Estimation

Since the energy of the channel is concentrated in time-domain, so DFT-based method is used to suppress the noise in time-domain to achieve good performance at low SNR [9]. The advantage of this method is that it is less complex than LSE since the complexity of N-point DFT operation is *O(NlogN)*. If number of pilot subcarriers is larger than the number of channel taps and all pilot sub-carriers are equi-distanced, then the performance of DFT-based estimation is also good than LSE estimation [28]. For DFT-based channel estimation, first we perform the LSE channel estimation that is given by

$$\hat{h}_{ls} = X^{-1} y \qquad (3.20)$$

By using the N-point inverse-DFT we can obtain the channel impulse response (CIR) from this channel frequency response (CFR), $\hat{h}_{ls}$.

$$\hat{H}_{ls} = IDFT[\hat{h}_{ls}] \tag{3.21}$$

In multipath wireless channels, many samples of CIR have little energy so we take only first L samples having relatively more energy than noise [16], so we get

$$\hat{H}_{ls} = \begin{cases} IDFT[\hat{h}_{ls}] & 0 \le n \le L-1 \\ 0 & otherwise \end{cases} \tag{3.22}$$

Windowing functions can also be applied for this frequency leakage compensation [29]. After IDFT operation we increase samples by padding zeros

$$\hat{H}_{P,ls} = \begin{cases} \hat{H}_{ls} & 0 \le n \le L-1 \\ 0 & otherswise \\ \hat{H}_{ls} & N-L \le n \le N-1 \end{cases} \tag{3.23}$$

So CIR samples beyond L samples will contain only noise that is why this part will be discarded. We will consider only first L samples for DFT-based channel estimation.

$$\hat{h}_{ls} = \{DFT[\hat{H}_{P,ls}] \quad 0 \le n \le N-1 \tag{3.24}$$

This method can be used to improve the channel estimation accuracy without increasing the complexity because the IDFT/DFT operations can be implemented with the fast algorithms IFFT/FFT. DFT-CE can be used to improve the performance of LMMSE channel estimation as proposed in [30], because from this method both the channel autocorrelation matrix and noise variance can be estimated.

3.2.2 DCT-Based Channel Estimation

When the multipath delays are not integer multiples, then DFT-CE is not suitable due to frequency leakage which causes aliasing. Under this condition the performance can be improved by employing a window-based DFT method [29], but at the cost of more bandwidth utilization. The real time signal has smaller high-frequency components but the DFT approach results in high frequency component. This high frequency component can be reduced by DCT, which is extensively used for voice and picture processing, because DCT employs mirror extension of *N*-point data sequence to *2N*-point data sequence, which removes the discontinuous edge.

First, the channel frequency response of the pilot subcarriers is obtained by using LSE estimation. After that we perform the DCT operation as [31]

$$\hat{H}_{ls} = DCT[\hat{h}_{ls}] \tag{3.25}$$

$$= w_k \sum_{m=0}^{M-1} \hat{h}_{ls} \cos\frac{\pi(2m+1)k}{2M} \quad k = 0, \dots, M-1$$

Where

$$w_k = {}^{1}/_{\sqrt{M}}\ ,\ k = 0\ ;\ w_k = \sqrt{{}^{2}/_{M}}\ ,\ k = 0$$

In next step zeros are inserted in the DCT domain. But different from DFT-based, zeros must be inserted at the end of $\hat{H}_{ls}$.

$$\hat{H}_{P,ls} = \begin{cases} \hat{H}_{ls} & k \le M-1 \\ 0 & otherwise \end{cases} \qquad (3.26)$$

IDCT can't be directly applied to get CFR because DCT cause a shift in time-domain data. To remove this shift effect extendible IDCT is employed, that is given by [32]

$$\hat{h}_{ls} = \sum_{k=0}^{M-1} w_k \hat{H}_{P,ls} \cos\left(\left(\frac{n}{N} + \frac{1}{2M}\right)\pi k\right)\ , n = 0, \dots, N-1 \qquad (3.27)$$

By exchanging the DCT and IDCT processes, the time-shift problem can be avoided but the performance degradation will occur at the spectrum edge [32]. Performance can be further improved by using adaptive filters as proposed in next section [33].

3.2.3 Windowed-DFT Channel Estimation

For finite-duration channel impulse response (CIR), when power delay profile (PDP) is continuous and multi-path delays are non-integer sample-spaced, the performance degrades due to the channel energy ignorance. To avoid this spectral leakage, a windowing function i.e. Hanning or Hamming Window can be applied [30].
Initially the channel is estimated by Least Square Error (LSE) method, given by

$$\hat{h}_{ls} = X^{-1} y$$

Then *N*-point IDFT operation is performed on $\hat{h}_{ls}$ to get CIR.

$$\hat{H}_{ls} = IDFT[\hat{h}_{ls}] \qquad (3.28)$$

The Hanning window is applied to CIR to make less spectral leakage, which is defined by [31].

$$d(i) = (0.5 + 0.5\cos\frac{2\pi i}{N-1})\ , i = 0,1, \dots, N-1 \qquad (3.29)$$

Where N is the length of Hanning window. Now the windowed-estimated channel becomes

$$\hat{H}_{wls} = \hat{H}_{ls}.d(i) \quad (3.30)$$

In next step zeros are padded, as given in Eq. 3.23, to get $\hat{H}_{p,wls}$. For synchronization purposes, before applying FFT operation, window is removed by [32]

$$\hat{H}_{p,ls} = \frac{\hat{H}_{p,wls}}{d'(i)} \quad (3.31)$$

Where

$$d'(i) = (0.5 + 0.5cos\frac{2\pi i}{N-1}) , i = 0,1, \dots, N-1 \quad (3.32)$$

To get CFR again DFT operation is applied to $\hat{H}_{p,ls}$, given in Eq. 3.24.
Hamming window can also be applied for the above described procedure, given by

$$d(i) = (0.54 + 0.46cos\frac{2\pi i}{N-1}) \quad (3.33)$$

3.3 Adaptive Filtering Based Channel Estimation

3.3.1 RLS Based Channel Estimation

To implement LSE as adaptive filtering, the desired output and the past data values are required at each iteration but in RLS algorithm, which is based on LS estimate of co-efficients $\hat{w}(n-1)$ at iteration $n-1$, to estimate the co-efficients at iteration n only new data values are required [34].

At iteration n, the optimal filter co-efficients $\hat{w}[n]$ results in the minimization of the following function

$$E[n] = \sum_{k=0}^{n} \beta[n,k]\left|\hat{w}^T[n]\hat{H}_{RLS}[k]\right|^2 \quad (3.34)$$

Where $0 < \beta[n,k] \leq 1$ is the weighting factor, which is commonly of the following exponential form

$$\beta[n,k] = \lambda^{n-k} \quad (3.35)$$

Where λ is less than but should be close to 1.

The necessary steps carried out in RLS algorithm are

1- Correlation matrix $\widehat{R}_{gg}$ is updated by

$$\hat{R}_{gg}[n] = \lambda \hat{R}_{gg}[n-1] + \hat{H}_{RLS}[n]\hat{H}^{H}{}_{RLS}[n] \quad (3.36)$$

2- Adaptation gain is given by

$$\hat{R}_{gg}[n]k[n] = \hat{H}_{RLS}[n] \quad (3.37)$$

3- A priori error is given by

$$E[n] = \hat{H}_{LS}[n] - \hat{W}^{T}[n-1]\hat{H}_{RLS}[n] \quad (3.38)$$

4- The conversion factor is given by

$$\alpha[n] = 1 - k[n]\hat{H}_{RLS}[n] \quad (3.39)$$

5- A posteriori error becomes

$$\varepsilon[n] = \alpha[n]E[n] \quad (3.40)$$

6- The updated co-efficients are given by

$$\hat{W}^{T}[n-1] = \hat{W}^{T}[n-1] + k[n-1]E^{*}[n] \quad (3.41)$$

After iteration n, the estimated channel is given by

$$\hat{H}_{RLS}[n] = \sum_{m=0}^{M-1} \hat{W}[m]\, \hat{H}_{RLS}[n-m] \quad (3.42)$$

Where M is the length of RLS filter.
The gain vector $k[n]$ is given by

$$k[n] = \frac{Q[n-1]\hat{H}_{LS}[n]}{\lambda + \hat{H}_{RLS}[n]Q[n-1]\hat{H}_{RLS}[n]} \quad (3.43)$$

and

$$Q[n] = \frac{1}{\lambda}\left(I - k[n]\hat{H}_{RLS}[n]P[n-1]\right) \qquad (3.44)$$

The initialization parameters are

$$Q[0] = [\hat{H}_{RLS}[0].\hat{H}_{RLS}[0] + \delta I]^{-1} \qquad (3.45)$$

and

$$k[0] = Q[0]\hat{H}_{RLS}[0] = \frac{1}{\left\|\hat{H}_{RLS}[0]\right\|^2 + \delta}.\hat{H}_{LS}[0] \qquad (3.46)$$

Where $\hat{H}_{RLS}[0]$ is found by LSE.

Where δ is the regularization parameter. In conventional RLS algorithms, the whole reference signals are assigned equal forgetting factor value and the parameters are $\lambda = 0.9$ and $\delta = 0.1$. For comb-pilot mode, two-step forgetting factor value is assigned such that the low forgetting factor value is used for the first few reference signals to make communication more dependent on channel information while high forgetting factor value is assigned to the remaining reference signals to make the communication dependent on the statistical information of the channel response [35].

3.3.2 LMS Based Channel Estimation

To avoid the matrix inversion, involved in LSE and LMMSE [18], LMS algorithm can be used to solve Wiener-Holf equation, which may or may not require a priori statistical information of the channel and data.
A summary of LMS algorithm is given as follows

1- First estimate the channel, $\hat{H}_{LS}$ by using LSE technique.
2- Filtering gives

$$\hat{H}_{LMS}[n] = \hat{W}^H[n]\hat{H}_{LS}[n] \qquad (3.47)$$

Where

$$\hat{H}_{LS}[n] = [\hat{H}_{LS}[n]\ \ \hat{H}_{LS}[n-1] \ldots \hat{H}_{LS}[n-1+M]]$$

Where M is the length of LMS filter.

3- Error Vector

$$E[n] = \hat{H}_{LS}[n] - \hat{H}_{LMS}[n] \qquad (3.48)$$

4- Co-efficient Updating

$$\hat{w}[n+1] = \hat{w}[n] + \mu \hat{H}_{LS}[n] E^*[n] \qquad (3.49)$$

Where μ is the step-size parameter.

5- Weight error vector is given by

$$\epsilon[n] = w[n] - \hat{w}[n] \qquad (3.50)$$

The performance of LMS algorithm is expressed in form of Mean Square Error (MSE), defined as

$$D(n) = Tr[k(n)] \qquad (3.51)$$

Where $k(n) = E[\epsilon(n)\epsilon^*(n)]$
$E[.]$ is the expectation operator.

In wireless communication, the step-size parameter is of small value. It is proved in [36] that for the stability of LMS algorithm, the optimal adaptation constant value is

$$\mu_{opt} = min\{1, \frac{3}{2}\sqrt[3]{\alpha_l}\}$$

Where

$$\alpha_l = (2\pi\xi_l)^2 P \frac{\sigma_h^2}{\sigma_\eta^2}$$

ξ_l is Doppler Spread of l^{th} channel tap, P is number of reference signals and $\frac{\sigma_h^2}{\sigma_\eta^2}$ is SNR value.

$\mu = 0$ results in slow co-efficient updating but better channel estimation while $\mu = 1$ is fast channel tracking algorithm with poor estimation because in this case $\hat{H}_{LMS}[n+1] \cong \hat{H}_{LMS}[n]$[36].

3.3.3 Leaky-LMS Based Channel Estimation

Under fast fading conditions, there may be the possibility of no convergence even for large n which results in the unstabilization of the LMS algorithm. To force this un-damped mode to zero, a leakage co-efficient is introduced which gives the following adaptation [37]

$$\hat{w}[n+1] = (1 - 2\mu\gamma)\hat{w}[n] + 2\mu \hat{H}_{LS}[n] E^*[n] \qquad (3.52)$$

Where $0 < \gamma \ll 1$.

3.3.4 Normalized LMS Based Channel Estimation

For minimum disturbance in adaptation of co-efficients the following technique is employed [37]

$$\hat{w}[n+1] = \hat{w}[n] + \frac{\mu}{\varepsilon + \left\|\hat{H}_{LS}\right\|^2} \hat{H}_{LS}[n]E^*[n] \qquad (3.53)$$

Where ε is only used for the numerical problems. This approach results in time-varying step-size LMS algorithm, whose convergence rate is faster than conventional LMS.

3.3.5 $sign$ −LMS Based Channel Estimation

For less complex hardware implementation, $signum$ function is utilized in LMS such that [37]

$$\hat{w}[n+1] = \hat{w}[n] + \frac{2\mu\, sign(\hat{H}_{LS}[n]E^*[n])}{\varepsilon + \left\|\hat{H}_{LS}\right\|^2} \qquad (3.54)$$

3.3.6 Linearly Constrained LMS Based Channel Estimation

To make estimation technique more optimized, some constraints are taken into consideration, for which we have [37]

$$\hat{w}[n+1] = \hat{w}'[n] + \frac{a - c\hat{w}[n]}{c^T c} c \qquad (3.55)$$

Where

$$\hat{w}'[n] = \hat{w}[n] + 2\mu E[n]\hat{H}_{LS}[n]$$

c is a constant vector.

3.3.7 Self-Correcting LMS Based Channel Estimation

The performance of LMS can be improved by comparing the ideal channel with the estimated channel that is closer and closer to the ideal channel. The estimated channel at i^{th} iteration is [37]

$$\hat{H}_{i+1}[n] = \hat{H}_i[n]\hat{w}_{i+1}[n] \qquad (3.56)$$

This technique can be implemented by employing any LMS algorithm discussed above.

3.3.8 Kalman-Filtering Based Channel Estimation

According to [38], the channel estimation problem can be formulated by the following state space vector

$$h[n+1] = Fh[n] + v[n] \quad (3.57)$$

Where $h[n] = (h_n[0]\ h_n[1]\ \ldots\ h_n[L-1])^T$, F is $L \times L$ channel matrix showing the state transition of $h[n]$ and $v[n]$ is the complex white Gaussian noise.
The received signal is represented by [39]

$$y[n] = h^H[n]x[n] + w_o[n] \quad (3.58)$$

Considering the noise and the channel statistics, the following recursive Kalman-Filtering equations are performed for channel estimation [40].

$$\hat{h}[n/n-1] = F\hat{h}[n-1/n-1] \quad (3.59)$$

$$e[n/n-1] = y[n] - \hat{h}^H[n/n-1]x[n] \quad (3.60)$$

$$q[n] = \sum_{k=0}^{L-1} [R_h[0]]_{k,k}\, \sigma_x^2[n-k] + N_o \quad (3.61)$$

$$k[n] = \frac{P[n/n-1]x[n]}{q[n] + x^H[n]P[n/n-1]x[n]} \quad (3.62)$$

$$\hat{h}[n/n] = \hat{h}[n-1/n-1] + k[n]e^*[n/n-1] \quad (3.63)$$

$$P[n+1/n] = F(I - k[n]x^H[n])P[n/n-1]F^H + Q_v[n] \quad (3.64)$$

The parameters at initialization are

$$\hat{h}[-1/-1] = \mu_h \quad (3.65)$$

$$P[-1/-1] = C_h \quad (3.66)$$

$k[n]$ is the Kalman filter gain.
$Q_v[n]$ is the covariance matrix of the noise $v[n]$ and

$$R_h[0] = E\left[\hat{h}[n/n-1]\hat{h}^H[n/n-1]\right] + P[n/n-1] \quad (3.67)$$

3.4 Simulation Results

The performance and complexity of the proposed algorithms is carried out by using MATLAB Monte-Carlo Simulations in 64-tap Rayleigh fading channel. The remaining system parameters, according to Release-10, are given in Table 3.1.

TABLE 3.1: SYSTEM PARAMETERS FOR OFDM CHANNEL ESTIMATION

Parameters	
Frame Structure	Generic
Reference Signals	CAZAC
Bandwidth	70 MHz
Carrier Frequency	2 GHz
FFT Size	2048
Modulation	QPSK
Power Spectral Density	Jake's Model
Multipath PDP	EVA

The performance of LMMSE with its variants i.e. Modified LMMSE with 10 taps, 40 taps, Robust LMMSE and Low Complex LMMSE is shown in Figure 3.1. The difference between LMMSE and Modified LMMSE estimators is due to the fact that some parts of the channel statistics are not taken into account in the former estimators. For low SNR values, the performance of LMMSE is better than R.LMMSE but for higher SNRs R.LMMSE outperforms LMMSE. The performance of both LMMSE and Low Complex LMMSE is same and the difference lies in the complexity as the computational time of Low Complex LMMSE is less than that of LMMSE. The comparison of computational time of LMMSE estimators is given in Table 3.2. Table 3.2 indicates that there is a wide gap of time between LMMSE while using covariance matrix and correlation matrix.

The performance of LMMSE estimator in terms of CIR samples for different values of SNR is shown in Figure 3.2. As we notice that after a certain number of CIR samples we have the same MSE for all values of SNR. The effect of increasing CIR samples on time is shown in Table 3.3.

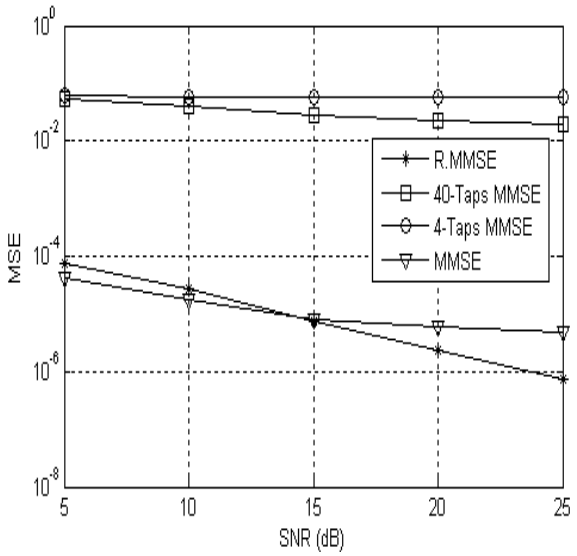

Figure 3.1: MSE v/s SNR for LMMSE Estimators

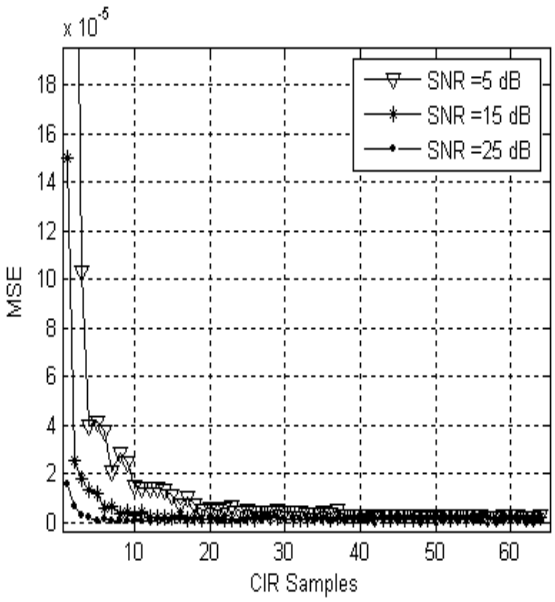

Figure 3.2: MSE v/s CIR Samples for LMMSE Estimator

TABLE 3.2: COMPUTATIONAL TIME FOR LMMSE ESTIMATORS

Estimator	5000 Simulations (sec)	1 OFDM Symbol (mSec)	1 Bit (mSec)
LMMSE Modified-10	208.278	41.656	0.651
Low Complex LMMSE	320.713	64.143	1.003
LMMSE (Corr Mtx)	346.8	69.36	1.084
LMMSE Modified-40	440.945	88.189	1.378
R.LMMSE	528.133	105.627	1.651
LMMSE (Cov Mtx)	529.319	105.864	1.65

TABLE 3.3: TIME V/S CIR SAMPLES FOR LMMSE ESTIMATOR

CIR Samples	Time (mSec)
30	1
40	1.25
50	1.5
60	1.75

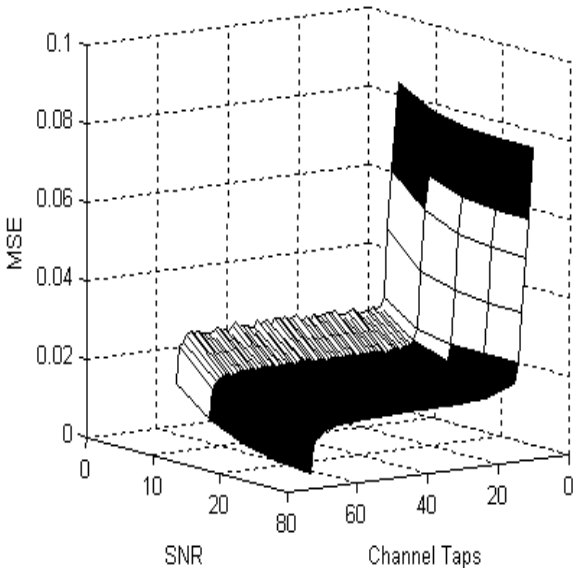

Figure 3.3: MSE v/s SNR v/s Channel Taps for Modified LMMSE Estimator

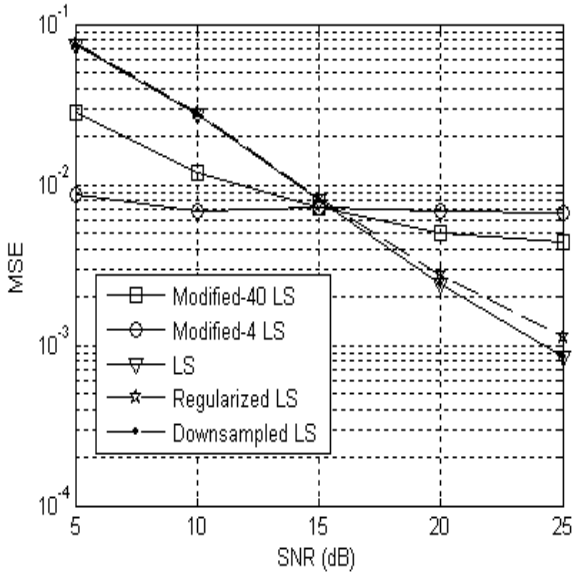

Figure 3.4: MSE v/s SNR for LS Estimators

TABLE 3.4: TIME V/S CHANNEL TAPS FOR MODIFIED LMMSE ESTIMATOR

Channel Taps	Time (mSec)
30	5
40	6
50	10
60	12

The effect of channel taps and SNR on MSE is shown in Figure 3.3. By increasing channel taps up to 10, there is a significant improvement in MSE but from 10 to 60, the MSE behavior remains same and after 60 we get further improvement. Since there is no improvement in MSE by increasing channel taps from 10 up to 60 as the disadvantage only comes in form of more time of computation as shown in Table 3.4.

Figure 3.4 shows the MSE verus SNR for LSE, Modified LS, Regularized LS and Downsampled LS estimators. Contrary to the modification of LMMSE estimator, the modification of LS estimator reduces MSE for a range of SNRs. However the same approximation effect, as in the modified LMMSE estimators, shows up at high SNRs. For every SNR, there exists an estimator which gives the smallest MSE. The effect of regularized LS is same to LSE but at higher SNR the performance of regularized LS degrades. Downsampled LS is exaclty same to that of LSE, advantage of former is only less complexity. The effect of CIR samples on MSE of LS estimator is shown in Figure 3.5. For CIR samples 0 to 10, there is a

rapid improvement in performance specially at low SNRs, but by increasing samples further there is no further improvement in terms of MSE but the cost comes in more computational complexity that is shown in Table 3.5. It is clear from Table 3.5 that by increasing number of samples, there is a gradual increment in computational time, that is a drawback of increasing samples without improving performance. The effect of CIR samples and SNR on MSE is shown in Figure 3.6. The combined effect of channel taps and SNR on MSE is shown in Figure 3.7. For specific channel taps, the effect of CIR samples on MSE is demonstrated in Figure 3.8. By increasing samples from1 to 2, there is a dominant improvement in MSE but beyond this value of samples the performance satuarates. The effect of channel taps for certain values of CIR samples on MSE is shown in Figure 3.9.

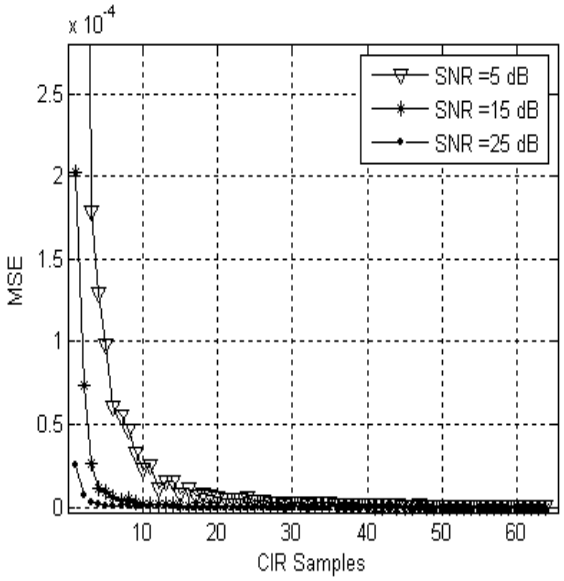

Figure 3.5. MSE v/s CIR Samples for LS Estimator

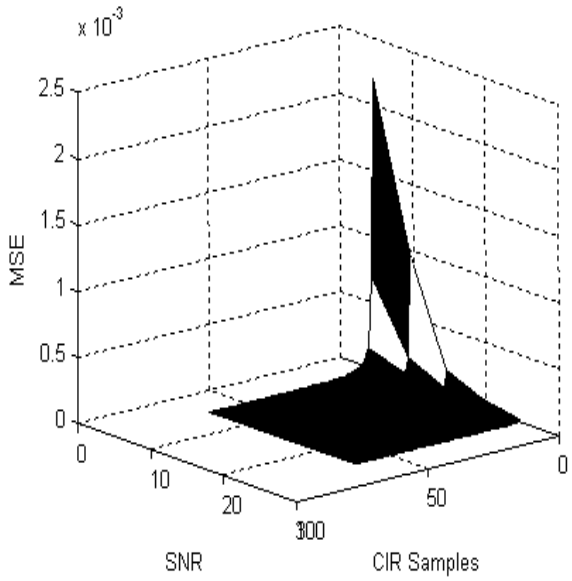

Figure 3.6: MSE v/s SNR v/s CIR Samples for LS Estimator

TABLE 3.5: TIME V/S CIR SAMPLES FOR LS ESTIMATOR

CIR Samples	Time (mSec)
30	0.5
40	1
50	1.25
60	1.5

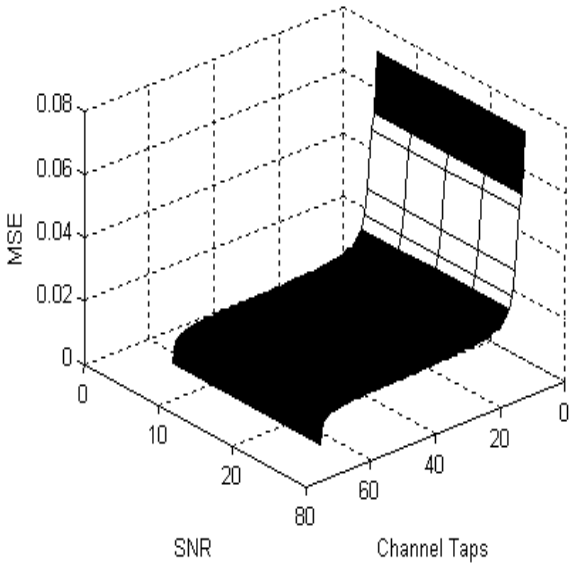

Figure 3.7: MSE v/s SNR v/s Channel Taps for Modified LS Estimator

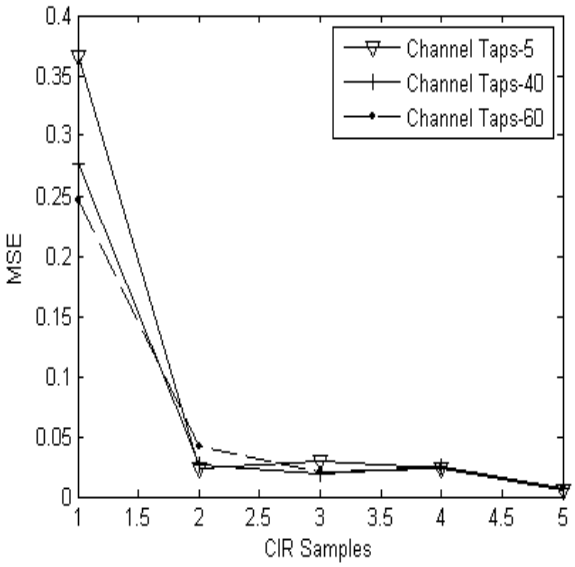

Figure 3.8: MSE v/s CIR Samples for Modified LS Estimator

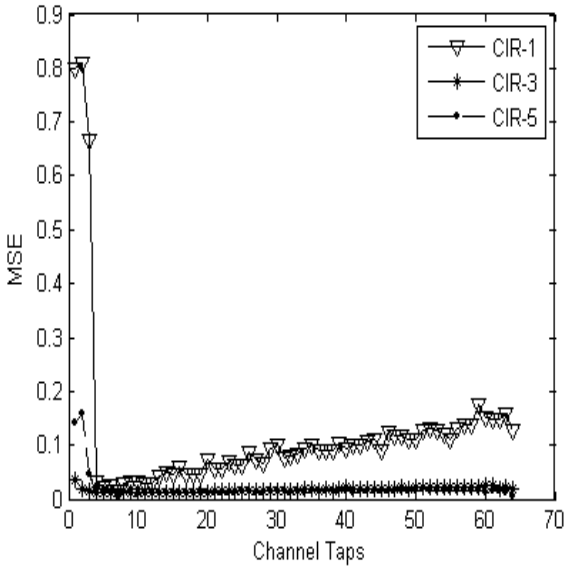

Figure 3.9: MSE v/s Channel Taps for Modified LS Estimator

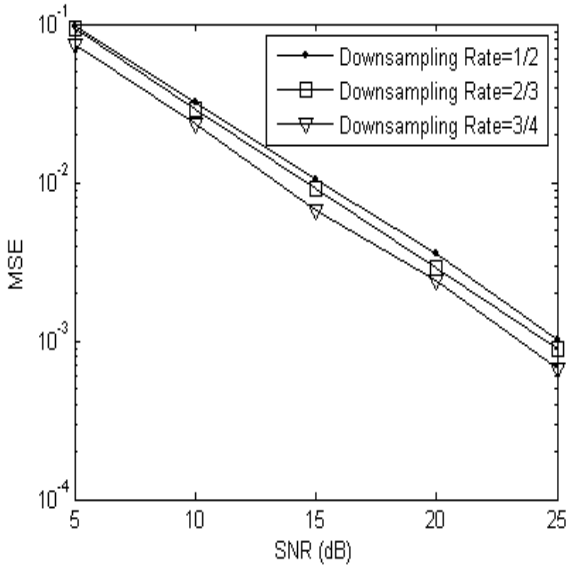

Figure 3.10: MSE v/s SNR for Down-Sampled LS Estimators

The different downsampling rate versus corresponding MSE is shown in Figure 3.10. By increasing the downsampling rate, the performance is degraded while there is no significant effect on complexity.

The performance comparison between LSE and LMMSE estimator is shown in Figure 3.11. When the channel has less number of CIR samples, then LMMSE is better to use than LSE due to less MSE, not in terms of time. But as CIR samples increases, for lower SNR values LMMSE is better in terms of MSE than LSE but for higher SNR values later one is better to use. But if we increase CIR samples further, then after certain number of CIR samples, LSE outperforms LMMSE for whole range of SNR values. The computation of both LSE and LMMSE with the increasing number of CIR samples is shown in Table 3.6. It is evident from Table 3.6 that LSE takes always less time than LMMSE, as it does not account for the channel statistics.

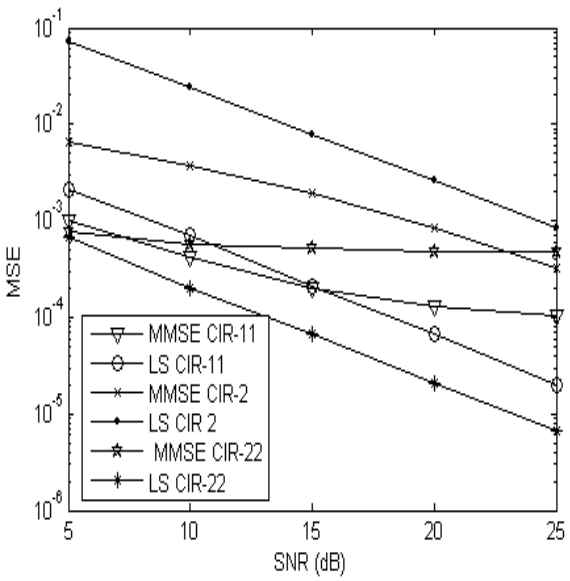

Figure 3.11: MSE v/s SNR for LMMSE and LS Estimators with different CIR Samples

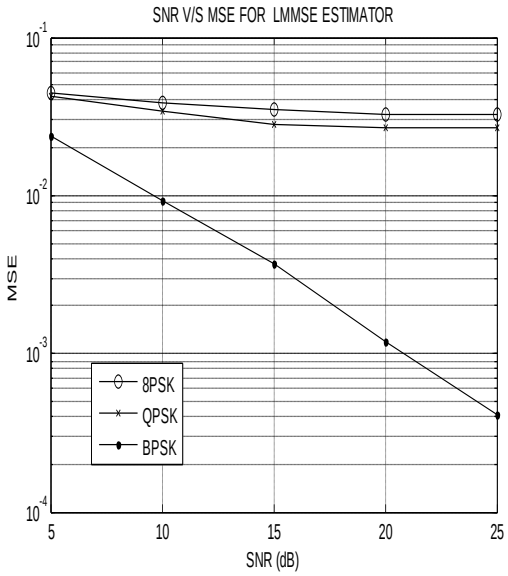

Figure 3.12: MSE v/s SNR for LMMSE Estimators for different Modulations

TABLE 3.6: TIME V/S CIR SAMPLES FOR LMMSE AND LS ESTIMATOR

CIR Samples	Time (mSec)	
	LS	*LMMSE*
30	0.5	1
40	1	1.25
50	1.25	1.5
60	1.5	1.75

The performance of LMMSE Estimator for different modulation schemes is shown in Figure 3.12 as a function of SNR values. For BPSK, the performance is better that for QPSK and 8-PSK, but the later modulations result in high transmission rate. Figure 3.12 shows the performance of LMMSE estimators in terms of Symbol Error Rate (SER). The LMMSE outperforms the modified LMMSE algorithms because in later techniques, some of the channel statistics are ignored.

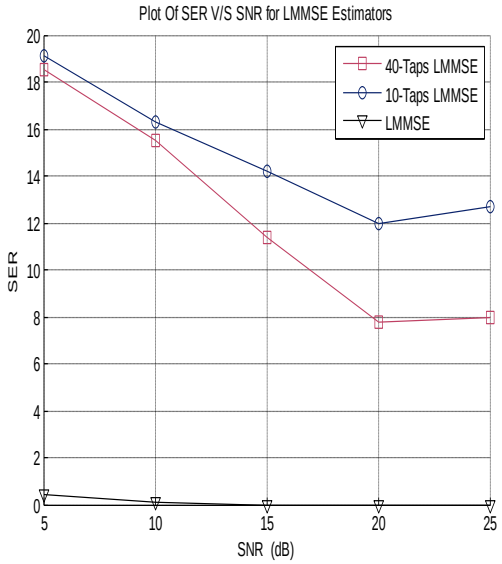

Figure 3.13: SER v/s SNR for LMMSE Estimators

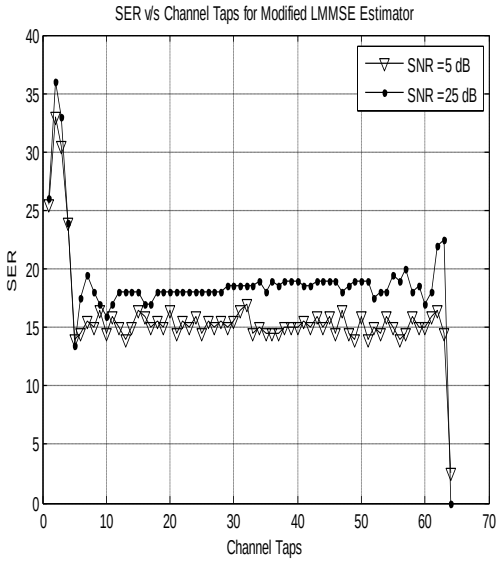

Figure 3.14: SER v/s Channel Taps for Modified LMMSE Estimator

The performance improves significantly as number of channel taps increases to 10, but after that there is no improvement in MSE. So increasing the channel taps after 10, only complexity increases such that as we go from 30 to 50 channel taps, the complexity increases 100%.

Figure 3.14 shows the performance in terms of SER, as a function of channel taps for different SNR values for modified LMMSE Estimators. The performance also remains same for channel taps from 10 to 60 and after 60 channel taps, the performance improves slightly. The performance in terms of SER for different SNR values is shown in Figure 3.15. SER performance comparison of LSE and LMMSE is shown in Figure 3.16. The performance of LMMSE is better as it utilizes the channel statistics.

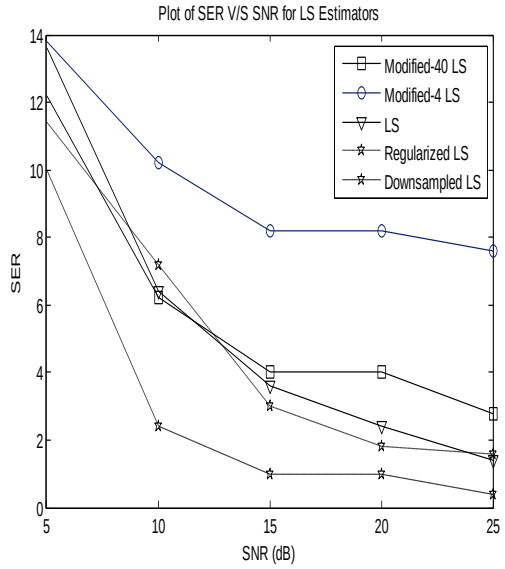

Figure 3.15: SER v/s SNR for LSE Estimators

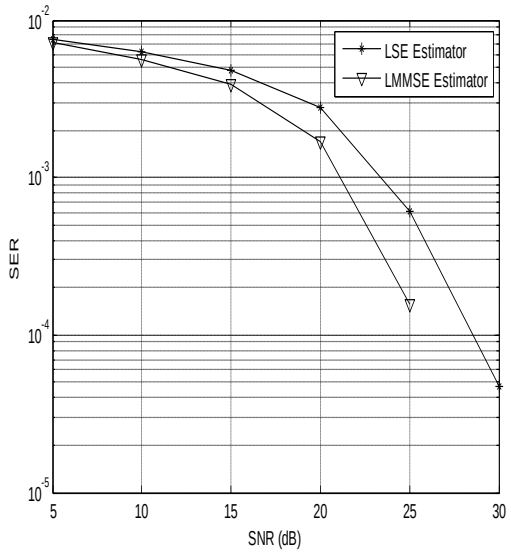

Figure 3.16: SER v/s SNR for LSE and LMMSE Estimators

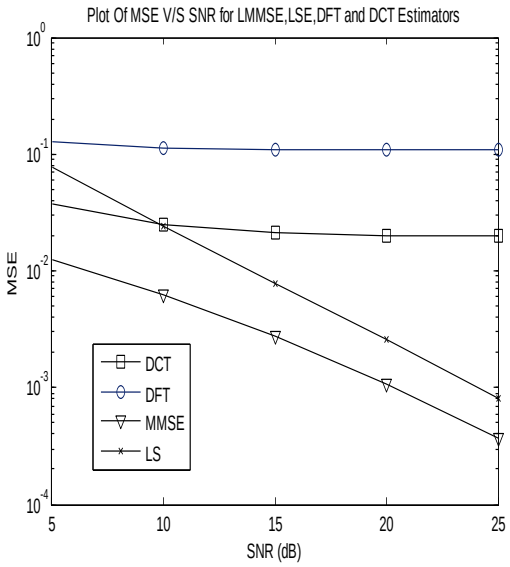

Figure 3.17: MSE v/s SNR for Channel Estimators

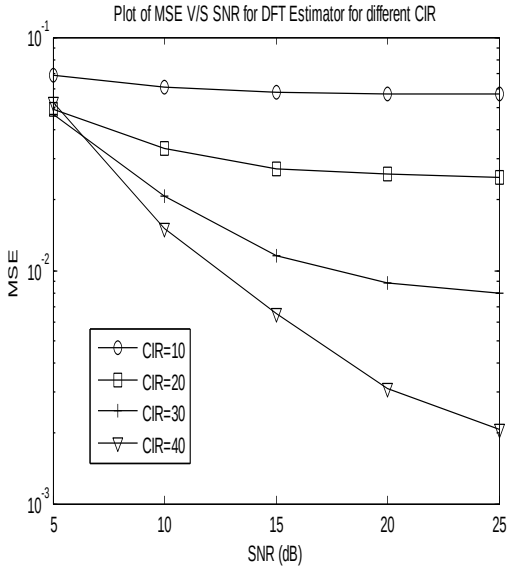

Figure 3.18: MSE v/s SNR for DFT-CE for different CIR Samples

Figure 3.17 shows the performance comparison of DCT-CE and DFT-CE approach with LMMSE and LSE methods. It is clear from Figure 3.17 that LMMSE demonstrates better performance than DFT-CE and DCT-CE but this approach results in more computational time. The complexity can be reduced by using DFT-CE and DCT-CE methods and the performance degradation is not so prominent. Figure 3.17 also shows that DCT approach outperforms DFT approach at all SNR values.

In DFT-based CE method, the effect of discarding certain CIR samples by using MST processor is demonstrated in Figure 3.18. It is clear from Figure 3.18 that as we go on increasing the number of discarded CIR samples, the performance also degrades which is not prominent at low SNR but at high SNR values, the performance degradation is severe.The same performance behavior is also observed for DCT-CE approach, as shown in Figure 3.19. When CIR samples are reduced from 20 to 10, the performance degrades significantly. Under low SNR operating conditions, less CIR samples can be considered for less complexity but for high SNR we have to take more CIR samples having significant energy, otherwise the performance will degrade.

There are two options for DCT-CE, either apply DCT first and then IDCT or exchange these operations. The comparison between these two approaches is shown in Figure 3.20. The performance of DCT/IDCT is better than IDCT/DCT, especially for high SNR values. But both these methods outperform the DFT-CE. As we go on increasing the SNR, the performance of DCT/IDCT also improves than DFT and IDCT/DCT. The comparison between DFT and DCT for different number of CIR samples is shown in Figure 3.21. For DCT, the CIR samples greater than 10 have no effect on performance and only complexity increases. But for DFT, after 20 CIR samples, the performance behavior remains constant. So for DFT we have to consider more CIR samples than DCT approach, to have same performance.

The effect of number of multi-paths channel taps on the performance of DFT and DCT is shown in Figure 3.22. In Figure 3.22, it is demonstrated that for channel taps more than 10, the performance also remains same and further improvement can be achieved by increasing multi-paths channel taps to a value greater than 60. So for less complexity and better performance, approximate 10 to 15 multi-paths can be taken, while more multi-paths will result only in high complexity.

Comparison between DFT and DCT in terms of Symbol Error Rate (SER) is shown in Figure 3.23. Here again the performance of DCT is better than DFT. By increasing SNR, the performance of DCT improves while that of DFT remains constant, so there is no advantage of increasing SNR while using DFT-CE. The effect of CIR samples on SER for DFT-CE is shown in Figure 3.24. For large values of CIR samples, performance improves for high SNR values, while for less CIR samples SNR value has no significant effect on performance. The same behavior is observed for DCT case as shown in Figure 3.25.

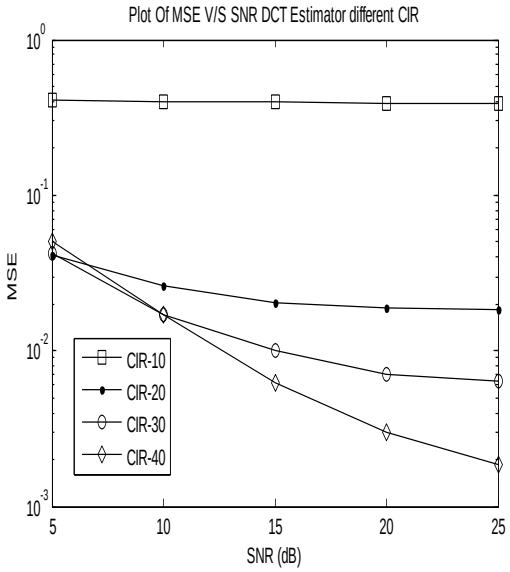

Figure 3.19: MSE v/s SNR for DCT-CE for different CIR Samples

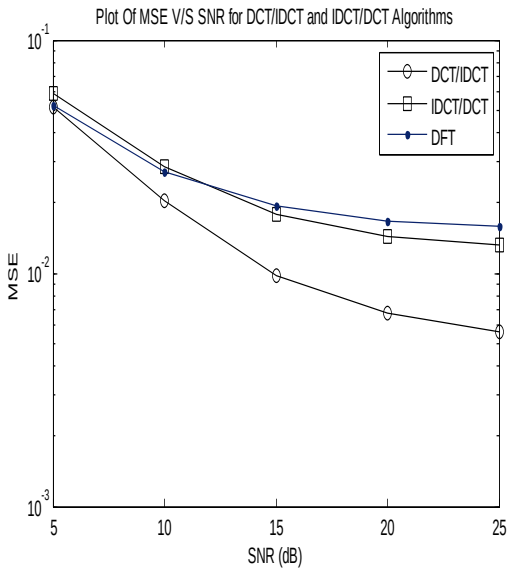

Figure 3.20: MSE v/s SNR for DCT/IDCT and IDCT/DCT

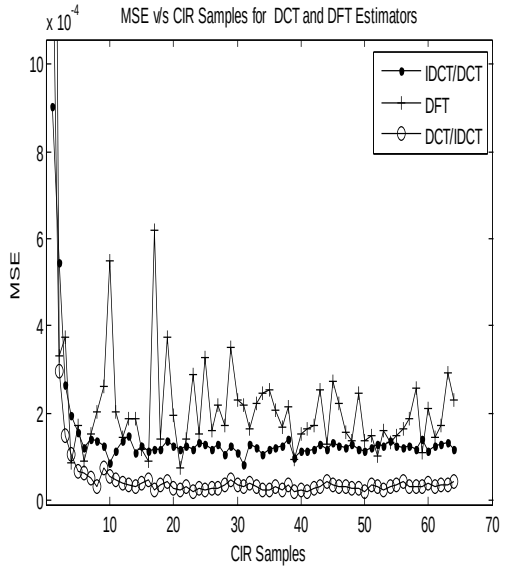

Figure 3.21: MSE v/s CIR Samples for DCT-CE and DFT-CE

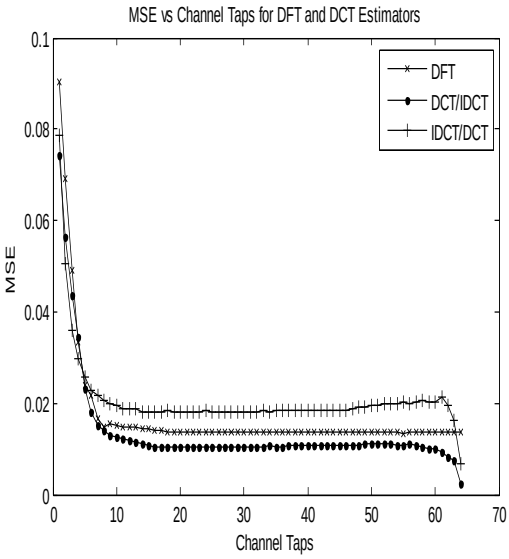

Figure 3.22: MSE v/s Channel Taps for DFT- CE and DCT-CE

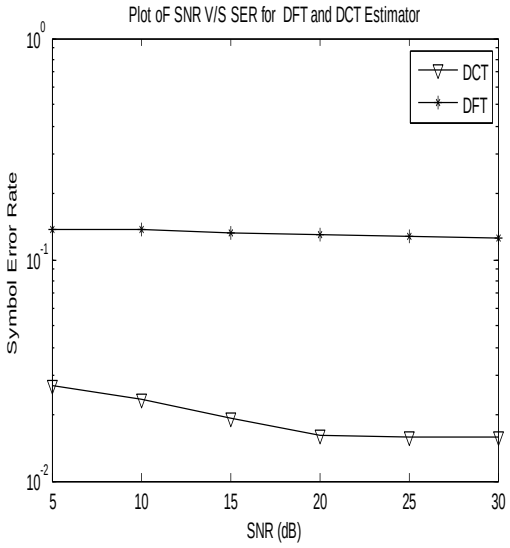

Figure 3.23: Comparison of SER of DFT-CE and DCT-CE

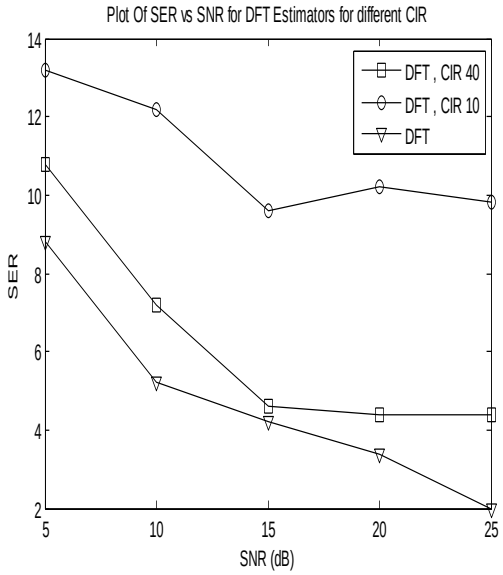

Figure 3.24: SER vs SNR of DFT-CE for different CIR Samples

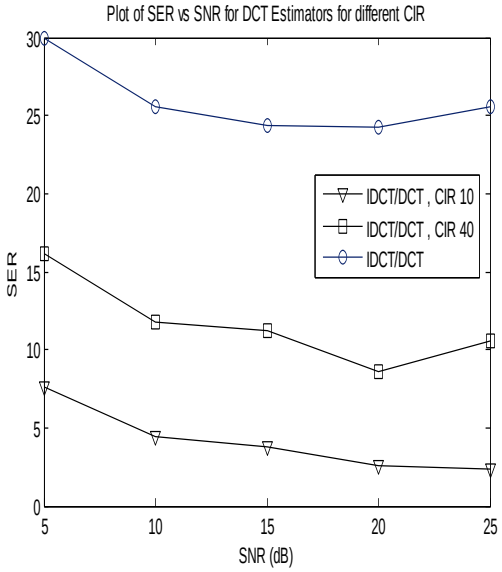

Figure 3.25: SER v/s SNR of DCT-CE for different CIR Samples

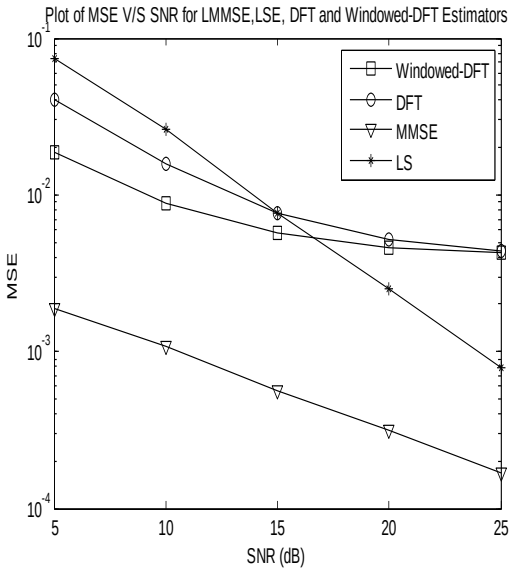

Figure 3.26: MSE vs SNR of Windowed-DFT

The performance comparison of Windowed-DFT with other techniques is shown in Figure 3.26. Windowed-DFT shows significant improvement in performance at low SNR as compared to simple DFT approach but we have to pay for more computational time as given in Table 3.7. Table 3.7 also demonstrates that Windowed-DFT has less complexity than DCT.

The effect of two windowing functions: Hannig and Hamming Windows is shown in Figure 3.27, from which is stated that Hanning window is better to use to avoid leakage effects under any SNR values. Figure 3.28 shows peformance variation for different virtual carriers exploited in Windowed-DFT CE approach. As VC's are increased performance also improves as more less-energy components are discarded and complexity also increases as shown in Table 3.8.

TABLE 3.7: COMPLEXITY COMPARISON OF CHANNEL ESTIMATORS

	1000 Simulations	1 OFDM Symbol	1 Bit
LMMSE	13.2	0.206	0.103
LSE	1.12	0.0175	0.00875
DFT	1.2	0.01875	0.009375
Windowed-DFT	1.26	0.02	0.01
DCT	2.07	.033	0.0165

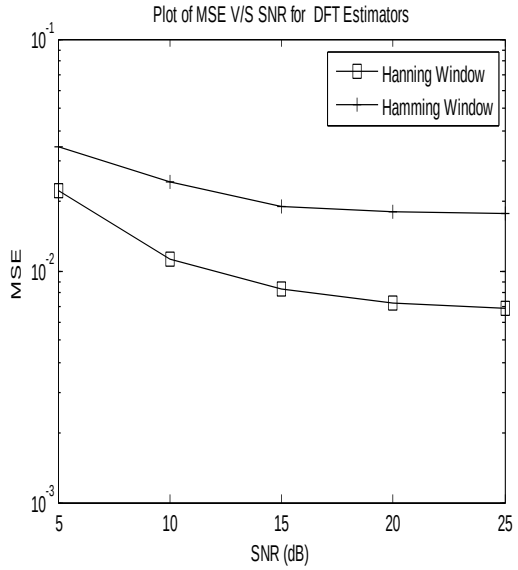

Figure 3.27: MSE vs SNR for different Winowing Functions

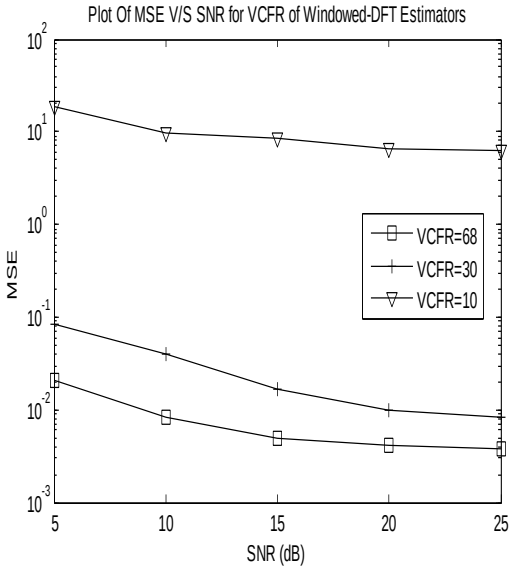

Figure 3.28: MSE vs SNR for VCFR of Windowed-DFT Estimators

TABLE 3.8: COMPLEXITY OF DIFFERENT VCFR FOR WINDOWED-DFT

VCFR	Time
10	0.019
30	0.02725
68	0.0964

TABLE 3.9: COMPLEXITY OF DIFFERENT CIR SAMPLES FOR WINDOWED-DFT

CIR Samples	Time (μsec)
5	0.172
10	0.2
30	0.288

Figure 3.29 gives the MSE value for different CIR samples and shows that CIR samples more than 5 results only in greater complexity as given in Table 3.9. The combined effect of CIR samples and SNR on MSE is shown in Figure 3.30. Figure 3.31 demonstrates the MSE as a function of channel taps which shows that by increasing channel taps from 1 to 10 there is a significant improvement in performance and further increase in channel taps results only in more complexity as shown in Table 3.10. The effect of SNR and Channle Taps on MSE is shown in Figure 3.32.

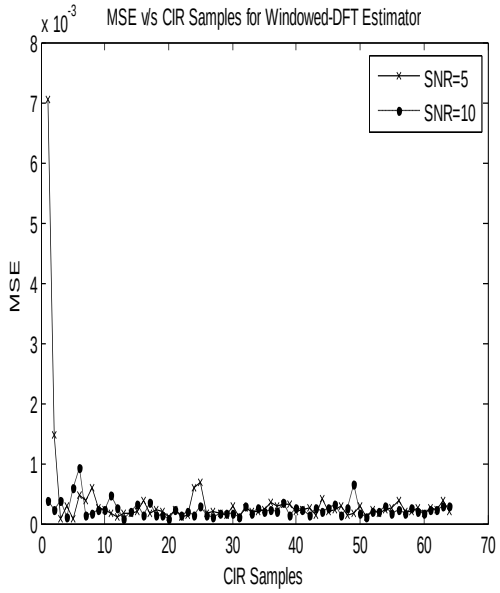

Figure 3.29: MSE vs CIR Samples for Windowed-DFT

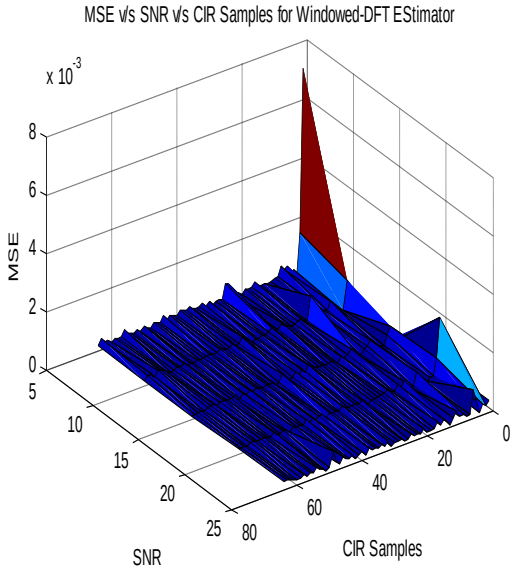

Figure 3.30: MSE vs SNR vs CIR Samples for Windowed-DFT

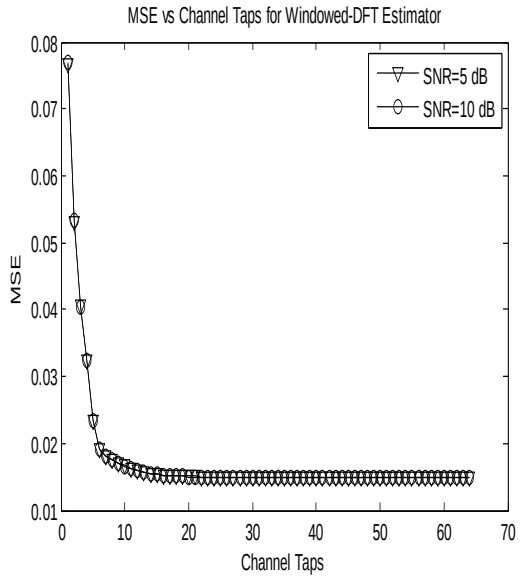

Figure 3.31: MSE vs Channel Taps for Windowed-DFT

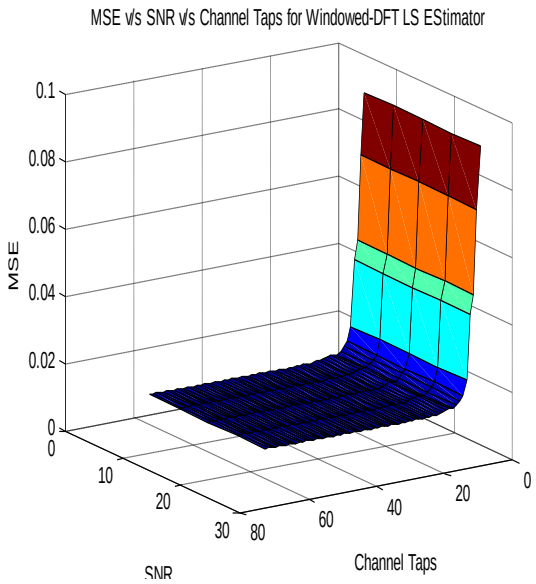

Figure 3.32: MSE vs SNR vs Channel taps for Windowed-DFT

TABLE 3.10: COMPLEXITY OF DIFFERENT CHANNEL TAPS FOR WINDOWED-DFT

Channel Taps	Time (μsec)
10	0.172
20	0.2081
30	0.21

TABLE 3.11: COMPARISON OF LS, LMS AND RLS

	5000 Simulations (mSec)	1 OFDM Symbol (nSec)	1 Bit (nSec)
LS	0.34	5.24	2.62
LMS	1.9	29.68	14.84
RLS	1.8	28.12	14.06

Figure 3.33 shows the performance comparison of LS, LMS and RLS. It is clear from Figure 3.33 that RLS outperforms both LS and LMS for whole range of SNR values. RLS is better than LMS not only in performance but also in complexity as shown in Table 3.11. LMS and RLS take more computational time to converge due to the requirement of the second order channel statistics used in this paper, which are not required for simple LS.

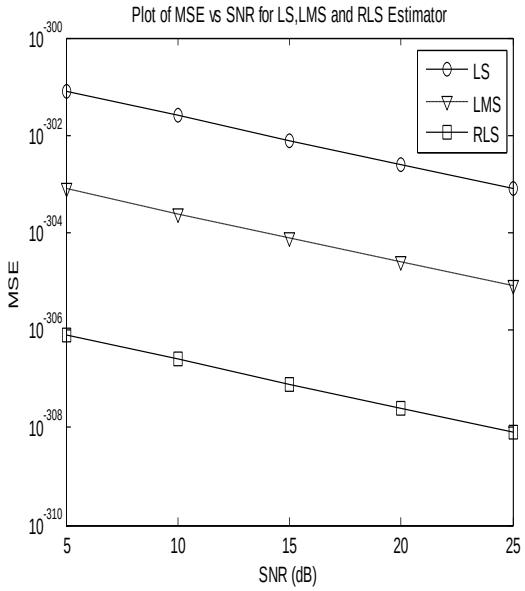

Figure 3.33: MSE v/s SNR for LS, LMS and RLS Estimators

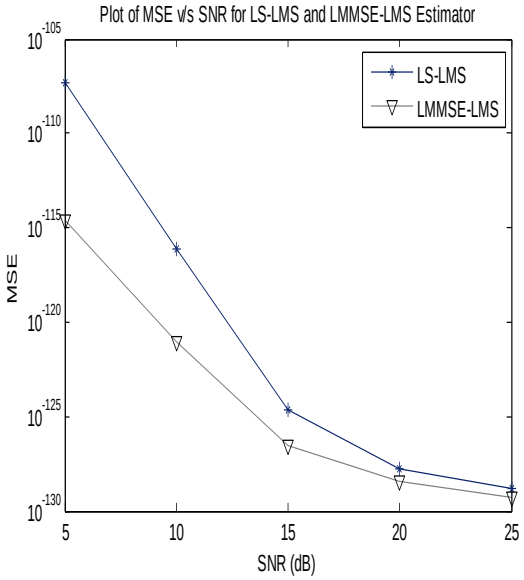

Figure 3.34: MSE v/s SNR for LS-LMS and LMMSE-LMS Estimators

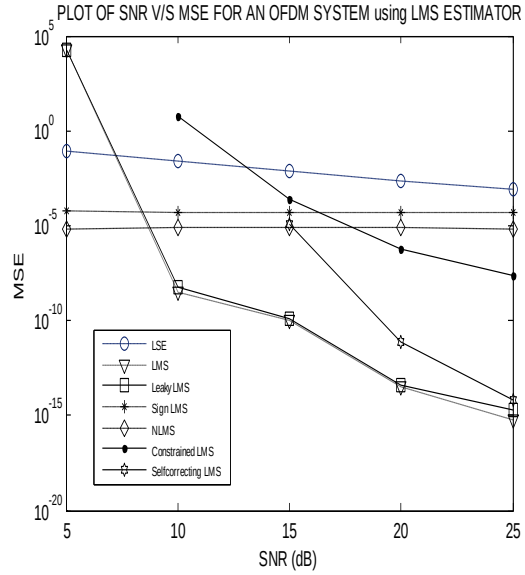

Figure 3.35: MSE v/s SNR for LMS Estimators

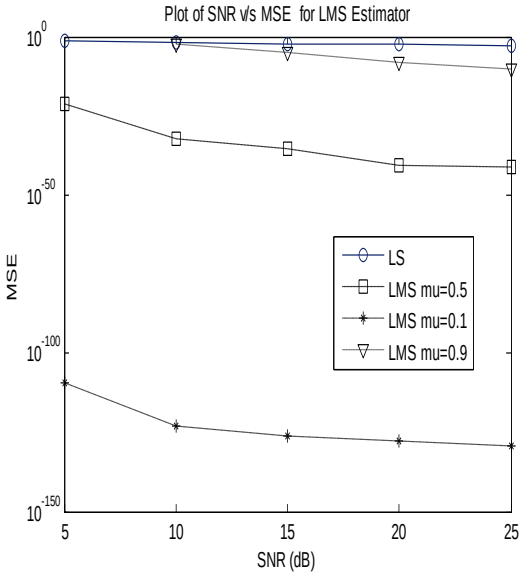

Figure 3.36: MSE v/s SNR for LMS for different Step-Size Values

In LMS, the initial estimated channel can be taken either by LS or LMMSE. Figure 3.34 shows that at low SNR values LMS, utilizing LMMSE as initial estimated channel, demonstrates better performance than LS-LMS while at higher SNR, the performance remains almost same and only complexity increases in case of LMMSE-LMS. MSE comparison between LS, LMS and its different variants is shown in Figure 3.35. LMS and Leaky-LMS show almost same performance for all operating SNR values. At low SNR values, the performance of self-correcting LMS degrades but at high SNR it approaches to LMS but has 15% more complexity. NLMS and $sign$-LMS demonstrates better behavior at low SNR but advantage in case of $sign$-LMS is in form of reduced complexity. No doubt the performance of constrained LMS is degraded but the computational time remains same for all values of the step-size. Table 3.12 shows that the effect of changing step-size is most prominent in case of LMS only and for other techniques the effect is not so much significant.

In Leaky-LMS, $sign$-LMS and self-correcting LMS the complexity reduces when changing step-size from 0.1 to 0.5 while further increase of step-size has no effect on complexity. The effect of different values of step-size for LMS is shown in Figure 3.36. It is clear from Figure 3.36 that there is a wide gap of performance for step-size 0.1 and 0.5 while further increment in step-size does not affect the performance significantly. The computational time for different step-size values is shown in Table 3.12.

TABLE 3.12: COMPUTATIONAL TIME OF LMS FOR DIFFERENT STEP-SIZE VALUES

μ	1000 Simulations (mSec)
0.1	2.6
0.5	2
0.9	1.8

TABLE 3.13: COMPLEXITY COMPARISON OF LMS

		1000 Simulations (mSec)	1 OFDM Symbol (nSec)	1 Bit (nSec)
CIR Samples	2	1.66	25.93	13
	5	2.2	34.37	17.2
	10	2.32	36.25	18.2
	4	1.92	30	15
Channel Taps	10	2.32	36.25	18.2
	20	2.52	40	20

Symbol Error Rate for different LMS techniques is demonstrated in Figure 3.37 and SER for different step-size values is shown in Figure 3.38. MSE of LMS for different channel taps is shown in Figure 3.39. As we go on increasing the number of channel taps, the performance also improves but this comes at high computational complexity as shown in Table 3.13. From Table 3.14 it is clear that by increasing channel taps from 4 to 10, complexity increases approximately 15% and for 20 channel taps, complexity increases 32% for 1000 independent simulations. The performance of LMS for different filter lengths is shown in Figure 3.40. Less channel impulse response samples show better performance because of high energy concentration while greater number of CIR samples not only degrades the performance but also increases the estimator's complexity. Table 3.13 shows that complexity increase 33% by increasing CIR samples from 2 to 5 and 10 CIR samples also results in same increment of computational time.

MSE behavior of Leaky-LMS for different leakage co-efficients is shown in Figure 3.41, which demonstrates that by increasing the leakage co-efficient the performance degrades for low SNR while there is no effect on performance for high SNR values. Figure 3.42 shows the effect of value of constant term $\boldsymbol{\varepsilon}$ added in NLMS. By increasing this small constant to a certain value the performance improves but by increasing further, the performance degrades.

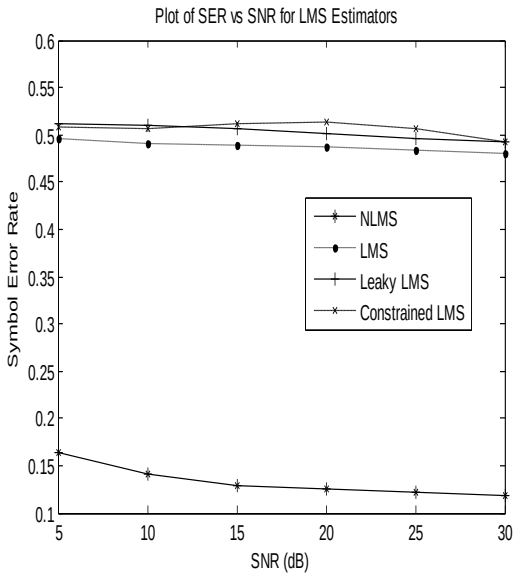

Figure 3.37: SER v/s MSE for different LMS Estimators

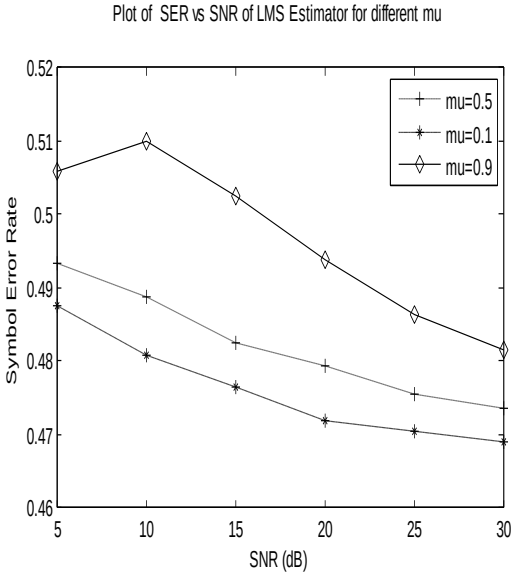

Figure 3.38: SER v/s SNR for LMS for different Step-Size values

TABLE 3.14: COMPLEXITY COMPARISON OF RLS

		1000 Simulations (μSec)	1 OFDM Symbol (pSec)	1 Bit (nSec)
CIR Samples	2	51.78	8.09	4.045
	5	52.78	8.25	4.125
	10	55.65	8.7	4.35
	4	468.97	7320	3660
Channel Taps	10	476.20	7500	3750
	20	538.1	8400	4200

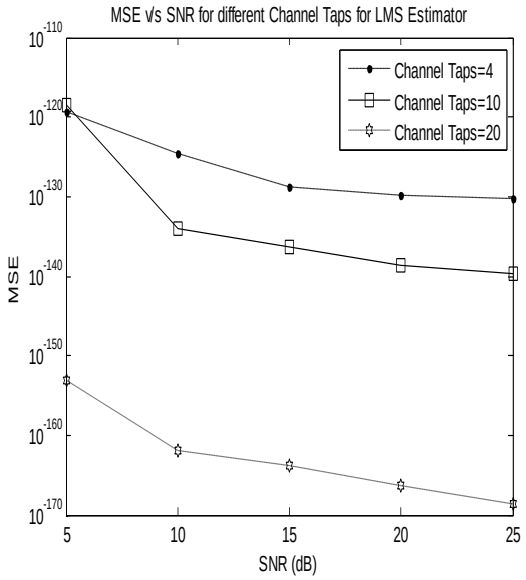

Figure 3.39: MSE v/s SNR for LMS for different Channel Taps

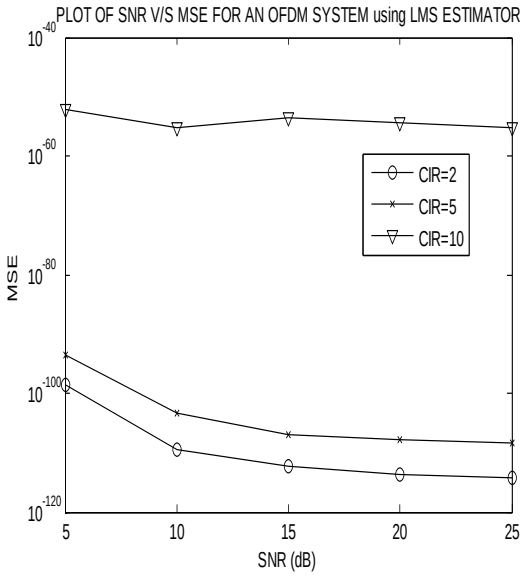

Figure 3.40: MSE v/s SNR for LMS for different CIR Samples

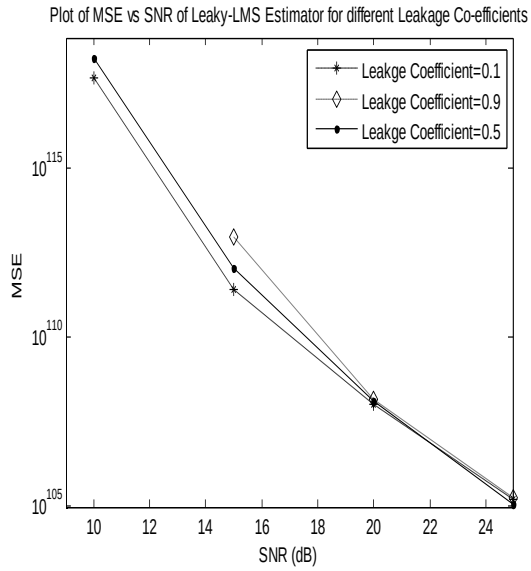

Figure 3.41: MSE v/s SNR for Leaky-LMS for different Leakage Co-efficients

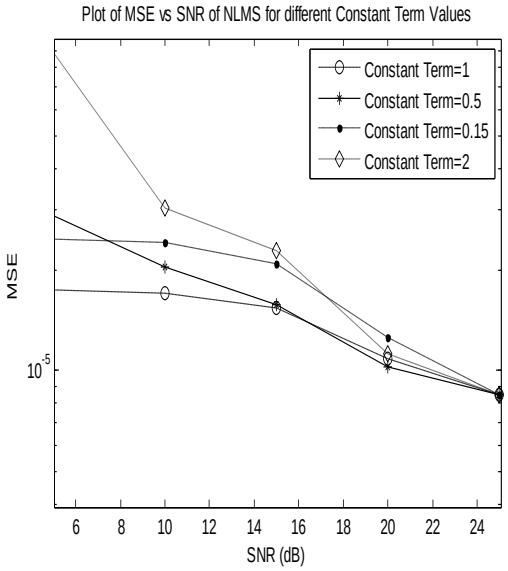

Figure 3.42: MSE v/s SNR for NLMS for ε different values

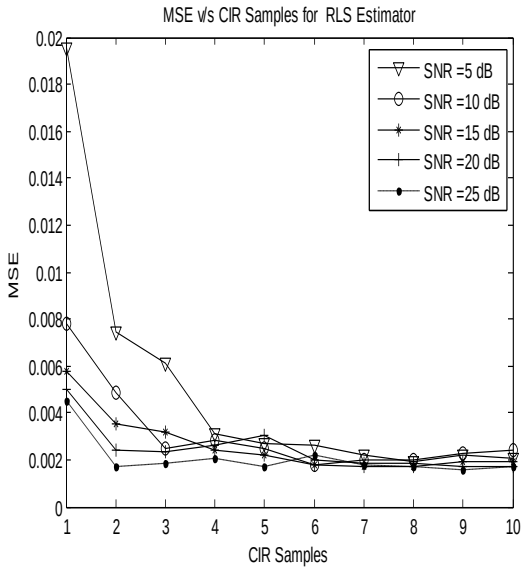

Figure 3.43: MSE v/s CIR Samples for RLS

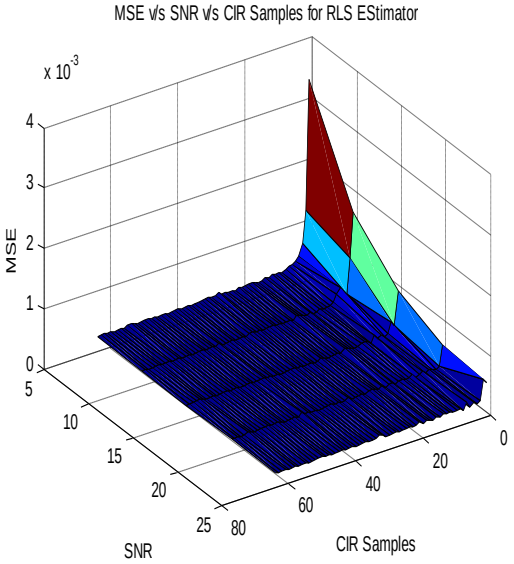

Figure 3.44: MSE v/s SNR v/s CIR Samples for RLS

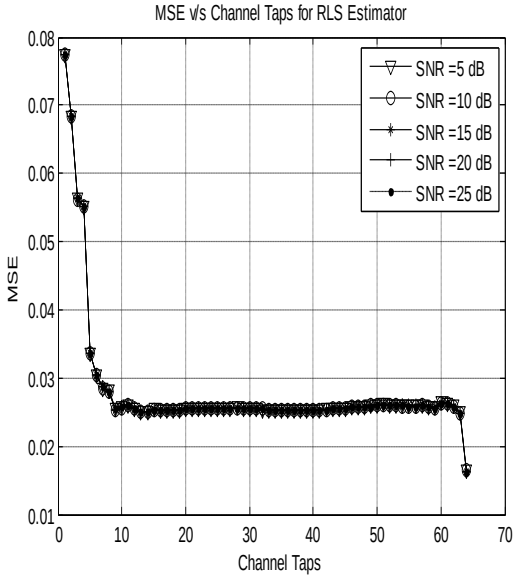

Figure 3.45: MSE v/s Channel Taps for RLS Estimator

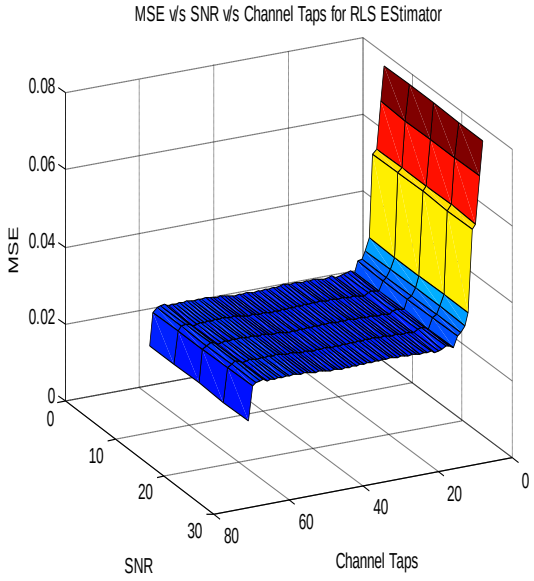

Figure 3.46: MSE v/s SNR v/s Channel Taps for RLS Estimator

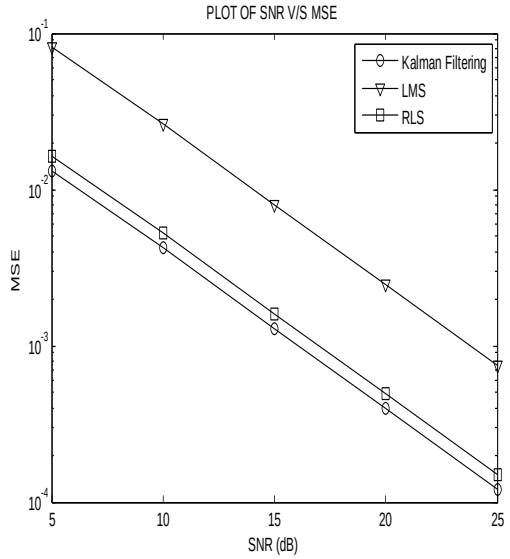

Figure 3.47: MSE vs SNR for LMS, RLS and Kalman-Based CE

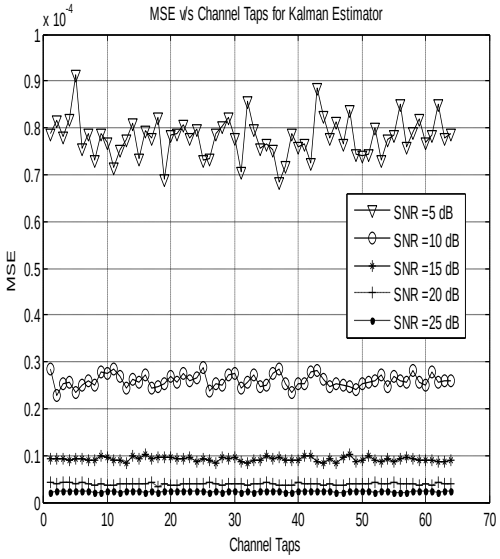

Figure 3.48: MSE vs Channel Taps for Kalman Filtering

For RLS, MSE as a function of CIR samples for different SNR values is shown in Figure 3.43. Performance will be better for less CIR samples and for high SNR values. The effect of CIR samples is dominant only for low SNR values as for high CIR samples, performance remains same for all SNR values while complexity goes on increasing, as shown in Table 3.15. 2% more time is required for 5 CIR samples in place of 2 CIR samples while it becomes 8% for 10 CIR samples. Overall effect of SNR and CIR samples on MSE for RLS is shown in Figure 3.44. In Figure 3.45, it is shown that performance improves significantly for increasing channel taps up-to 10 but further increment does not improve performance and only increases computational time as shown in Table 3.15. The combined effect of SNR and channel taps on MSE for RLS is shown in Figure 3.46. A comparison of Kalman-Based channel estimation with RLS and LMS is shown in Figure 3.47. Kalman Filtering shows better performance than both RLS and LMS at all SNR values. Its performance is significantly better than LMS as compared to RLS. The MSE vs Channel Taps is given in Figure 3.48. For all channel taps, high value of SNR is preferred. And we also observe that for a specific SNR value, there is no effect of changing the number of channel taps on the performance and we have to only pay for more complexity. That is why for Kalman channel estimation, less number of channel taps are preferred. The combined effect of channel taps and SNR on performance is given in Figure 3.49.

The performance of Kalman-Based channel estimation technique for different values of CIR samples is shown in Figure 3.50. The performance remains same for CIR samples more than 4 but at the cost of more complexity. For high SNR values, different values of CIR samples does not affect the performance so for high SNR operating conditions we prefer less number of CIR samples to be considered. The effect of CIR Samples and SNR on MSE for Kalman Filtering is given in Figure 3.51.

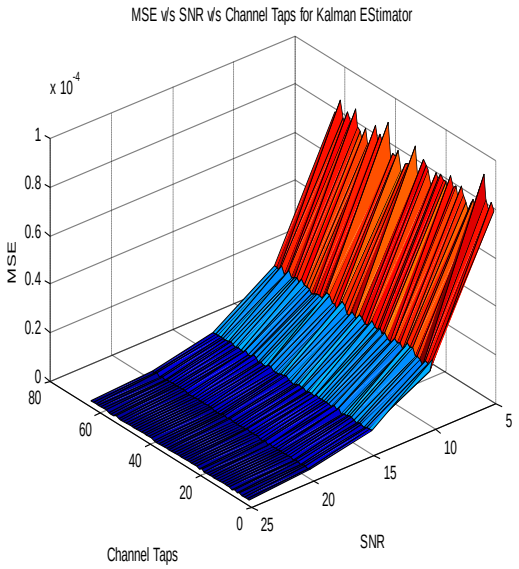

Figure 3.49: MSE vs SNR vs Channel Taps for Kalman Filtering

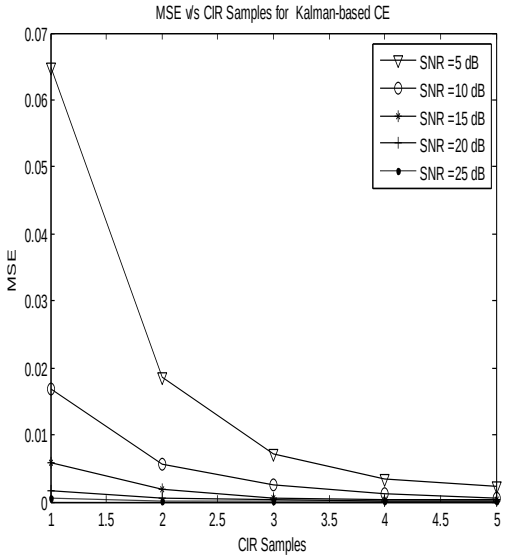

Figure 3.50: MSE vs CIR Samples for Kalman Filtering

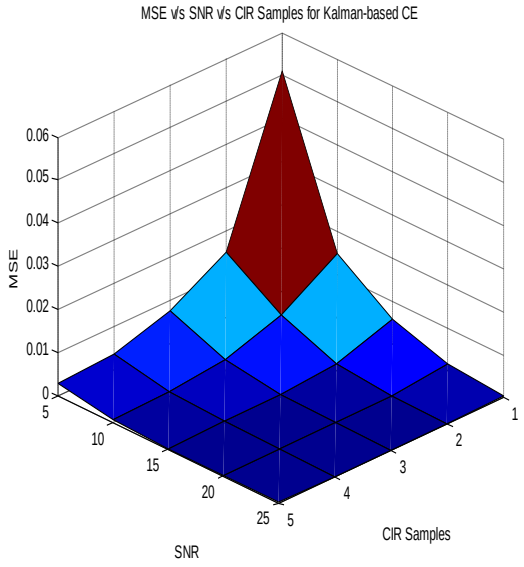

Figure 3.51: MSE vs SNR vs CIR Samples for Kalman Filtering

3.5 Conclusion

In this chapter, LMMSE and LSE channel estimators based on CIR samples and channel taps are presented and their comparison in terms of performance and complexity is evaluated. The performance of LMMSE is better than LSE as it assumes the channel statistics which results in high complexity.The performance can be improved by increasing either CIR samples or channel taps but after a certain limit there is no prominent impact on performance while the complexity goes on increasing. . As we go on increasing CIR samples, after a certain value LSE degrades LMMSE both in performance and copmplexity. It is noticed that the channel taps have no effect on the performance of LSE estimator for different SNR values. So if a channel filter of more length is used then the channel estimator performance can be improved even without having a prior channel information.

The performance and complexity comparison of different transform-based channel estimation techniques is also carried out based on channel filter length and the number of multi-paths. For low SNR, Windowed-DFT approach is proposed due to better performance and its complexity is also not too much high and for DFT and DCT to have better performance a filter of smaller length is preferred. But for high SNR values, filter having larger length is proposed where we have to pay for more complexity. Due to the removal of high frequency component, DCT is applied but it results in more computational time than LSE and DFT-based techniques. At low SNR all techniques show almost same performance but for high SNR, DCT/IDCT gives improved performance than IDCT/DCT and DFT. A channel having a filter length of 2-5 CIR

samples and 5-10 multi-paths is preferred for optimized performance and complexity in wireless channel.

Three adaptive channel estimation algorithms, RLS, LMS and Kalman-Filtering based, are compared in terms of performance, MSE and SER, and complexity. . Among LMS techniques, Leaky-LMS is proposed both for better performance and less complexity, by using small value of leakage co-efficient. We note that the performance of RLS is better than conventional estimators, LS and LMMSE, but its complexity is large due to the requirement of a-prior knowledge of the channel. A compromise between performance and complexity can be achieved by using a channel filter of length 2-3 CIR samples and 1-6 channel taps for RLS but for LMS channel taps should be more, for example 15-20, for better performance. Kalman-Filtering shows better performance as compared to both LMS and RLS. For optimized channel estimator employing Kalman Filtering in wireless communication system, 4-5 CIR samples and any number of channel taps can be used. But for less complexity, channel taps should be less than 10.

Chapter No 4

Channel Estimation of MIMO-OFDM System

4.1 Linear Based Channel Estimation

4.1.1 LMMSE Channel Estimation

If we assume that the channel statistics remains same across all receive antennas, then LMMSE estimation of the channel at r^{th} receive antenna is given by [6]

$$\widehat{H}_{r,t}^{LMMSE} = FR_{g_{r,t}y_r}R^{-1}{}_{y_r y_r}y_r \tag{4.1}$$

Where $R_{g_{r,t}y_r} = E[g_{r,t}y_r^H]$ is cross co-variance matrix of the channel vector $g_{r,t}$ and the received signal y_r. $R_{y_r y_r} = E[y_r y_r^H]$ is auto co-variance matrix of y_r. F is DFT matrix used for conversion to frequency domain channel estimation.

The above Equation can be written in compact form as [9]

$$\widehat{H}_{r,t}^{LMMSE} = FR_{g_{r,t}g_{r,t}}F^H P^{-1}(\sum_{l=1}^{N_{ch}} P_l FR_{g_{r,t}g_{r,t}}F^H P_l + \sigma_r^2 I)^{-1}y_r \tag{4.2}$$

At receiver, the matrix inversion is required which increases the complexity. The pilot sequences used as reference signals are shifted version of each other for all users.

4.1.2 Modified LMMSE Channel Estimation

For large value of N, the complexity of LMMSE increases due to matrix inversion. If we consider only first L taps, with significant energy, then the complexity can be optimized and modified channel estimation becomes [6]

$$\widehat{H}_{r,t}^{Mod,LMMSE} = TR'_{g_{r,t}g_{r,t}}T^H P'^{-1}(\sum_{l=1}^{N_{ch}} P_l{}'TR'_{g_{r,t}g_{r,t}}T^H P_l{}' + \sigma_r^2 I)^{-1}y_r \tag{4.3}$$

Where T is containing first L columns of DFT matrix F and $R'_{g_{r,t}g_{r,t}}$ is upper left corner $L \times L$ matrix of $R_{g_{r,t}g_{r,t}}$.

4.1.3 Low Complex LMMSE Channel Estimation

If we assume that the channel remains constant over all frequencies and the transmitter follow same modulation constellation over one OFDM symbol, then the matrix inversion can be simplified, which results in the following channel estimation [6]

$$\widehat{H}_{r,t}^{Low\ Com,LMMSE} = R_{g_{r,t}g_{r,t}}(R_{g_{r,t}g_{r,t}} + \frac{\beta}{SNR}I)^{-1}X_t y_r \qquad (4.4)$$

Where β is modulation constant and depends upon the constellation diagram.

4.1.4 LSE Channel Estimation

In addition to matrix inversion, the limit of LMMSE is that it also requires a priori knowledge of the channel statistics which is not possible to have, especially in real-time wireless communication. To avoid this probabilistic knowledge, LSE estimation is preferred which has degraded performance than LMMSE but has reduced complexity. LSE estimation is given by [6]

$$\widehat{H}_{r,t}^{LSE} = FQ_{ls}F^H X_t y_r \qquad (4.5)$$

Where

$$Q_{ls} = (F^H {X_t}^H X_t F)^{-1} \qquad (4.6)$$

$\widehat{H}_{r,t}^{LSE}$ can also be written as [6]

$$\widehat{H}_{r,t}^{LSE} = {X_t}^{-1} y_r \qquad (4.7)$$

4.1.5 Down-Sampled Impulse Response LSE Channel Estimation

The complexity due to matrix inversion can be further decreased by discarding some channel taps and setting their values equal to zeros. For example the channel vector can be [6]

$$\bar{g} = (g_0\ \ g_1\ \ 0\ \ g_3\ \ g_4\ \ 0\ \ \ldots\ \ g_{L-1})^T \qquad (4.8)$$

Here 1/3 of the channel taps are discarded.

4.2 Transform Based Channel Estimation

4.2.1 DFT-Based Channel Estimation

DFT approach is used to suppress the time-domain noise. Significant Channel Tap Detector (SCTD) is used to discard less energy CIR samples, but for this method maximum multi-path delay need to be known, which is not possible to be available in real time scenario.

First channel is estimated by using LSE, which is given by

$$\widehat{H}_{r,t}^{LSE} = X_t^{-1} y_r \qquad (4.9)$$

Then this frequency-domain estimated channel is converted into time-domain channel impulse response by performing IDFT operation [7]

$$\widehat{H}_{r,t}^{IDFT} = IDFT\{\widehat{H}_{r,t}^{LSE}\} \qquad (4.10)$$

Next SCTD is applied to select those CIR samples which have significant energy than noise, then values of discarded CIR samples are replaced by zeros.

$$\widehat{H}_{r,t}^{IDFT} = \begin{cases} IDFT\{\widehat{H}_{r,t}^{LSE}\} & 0 \le n \le L-1 \\ 0 & otherwise \end{cases} \qquad (4.11)$$

To lessen the effect of noise, a windowing function e.g. Hamming Window or Hanning Window can also be used instead of SCTD, as proposed in [7].
Before converting the channel impulse response to frequency-domain, zeros are padded to increase the length of channel impulse response, so we have

$$\widehat{H}_{r,t}^{IDFT} = \begin{cases} \widehat{H}_{r,t}^{IDFT} & 0 \le n \le L-1 \\ 0 & otherwise \\ \widehat{H}_{r,t}^{IDFT} & N-L \le n \le N-1 \end{cases} \qquad (4.12)$$

Now this channel impulse response is converted to channel frequency response by performing DFT operation

$$\widehat{H}_{r,t}^{DFT} = DFT\{\widehat{H}_{r,t}^{P,IDFT}\} \qquad (4.13)$$

To improve the performance of DFT-based channel estimator, following conditions must be satisfied: 1- Number of pilots inserted should be greater than the maximum delay spread of the channel; 2- Pilots should be equi-distanced. Second condition is a provision to reduce leakage

effect [8], otherwise null sub-carriers need to be transmitted to avoid discontinuities caused by null spectrum. The complexity of DFT-CE can be reduced by using FFT/IFFT algorithms.

4.2.2 DCT-Based Channel Estimation

The performance of DFT-CE degrades due to the aliasing error when multi-path delays are not integer-multiples of the sampling period. For such situations, DCT approach is preferred instead of DFT, which also reduces the occurrence of high frequency component due to the discontinuity in the edges. In DCT, the discontinuous edge can be removed by making *N*-point data into *2N*-point data using mirror extension.

In DCT-CE, initially channel is also estimated by using LSE and then DCT operation is performed to convert into transformed-domain

$$\widehat{H}_{r,t}^{DCT}(n) = w_k(n) \sum_{m=0}^{N_c-1} \widehat{H}_{r,t}^{LSE}(k) \cos\left[\frac{\pi(2m+1)n}{2N_c}\right] \qquad (4.14)$$

Where N_c shows the number of sub-carriers.

$$w_{N_c} = \frac{1}{\sqrt{N_c}}, \quad n = 0 \qquad w_{N_c} = \sqrt{\frac{2}{N_c}}, \quad n \neq 0$$

Similar to DFT-CE, after performing DCT operation, zeros are padded to increase the channel impulse response length and we get $\widehat{H}_{r,t}^{P,DCT}$.

In next step, extendible IDCT operation is performed to get back the frequency domain [7]

$$\widehat{H}_{r,t}^{IDCT}(k) = \sum_{n=0}^{N-1} w_k(n) \widehat{H}_{r,t}^{P,DCT}(n) \cos\left[\frac{\pi(2k+N/N_c)n}{2N}\right] \qquad (4.15)$$

Where N is length of the original data sequence before mirror extension.

4.2.3 Windowed-DFT Based Channel Estimation

The use of Most Significant Taps (MST) method for suppression of interference and noise, results in the energy leakage, which degrades the performance of direct DFT-based channel estimation technique, especially for non-integer spaced multipath delays [6]. For alleviation of energy leakage effect, two techniques are proposed: Windowed based DFT channel estimation and second approach is the addition of the Virtual Channel Frequency Response (VCFR).

Initially the channel is estimated by Least Square (LS) method, which is given by [4]

$$\widehat{H}_{r,t}^{LSE}[k] = X_t{}^{-1}[k]\, y_r[\mathrm{k}] \qquad (4.16)$$

Hanning Window is applied to this estimated channel to reduce the leakage effect, so

$$\widehat{H}_{r,t}^{Windowed}\ [k] = \widehat{H}_{r,t}^{LSE}[k].\, d(m) \qquad (4.17)$$

Where

$$d(m) = \left(0.5 + 0.5cos\frac{2\pi m}{\Gamma}\right) e^{j\pi\left(\frac{m\Delta}{MT}\right)} \quad , \qquad m = 1,2, \ldots N-1$$

Exponential term shows the phase rotation. Δ is guard interval length of OFDM and $T = \frac{T_{carrier}}{N}$ Where $\frac{1}{T_{carrier}}$ is spacing between OFDM subcarriers.

Now *M*-point IFFT operation is performed to convert the channel frequency to time-domain channel impulse response, after padding zeros. IFFT operation results in

$$\hat{h}_{r,t}^{Windowed}\ [i] = \frac{1}{M}\sum_{m} \widehat{H}_{r,t}^{Windowed}\ [k]\, e^{\frac{j2\pi mi}{M}} \quad , \quad -\frac{M}{2}+1\ \leq i \leq \frac{M}{2} \qquad (4.18)$$

To reduce MSE, a weighting function can also be applied to $\hat{h}_{r,t}^{Windowed}$ as proposed in [9].

In next step, *N*-point FFT operation is applied to get frequency domain channel response

$$\widehat{H}_{r,t}^{Windowed}\ [k] = \frac{1}{M}\sum_{i=-\frac{N}{2}+1}^{\frac{N}{2}} \hat{h}_{r,t}^{Windowed}\ [i]\, e^{-\frac{j2\pi ni}{N}} \qquad (4.19)$$

In last step, windowing effect and phase rotation is removed to get the estimated channel, so

$$\widehat{H}_{r,t}[k] = \frac{\widehat{H}_{r,t}^{Windowed}\ [k]}{d'(m)} \qquad n = -\frac{N}{2}, \ldots, \frac{N}{2} \qquad (4.20)$$

Where

$$d'(m) = \left(0.5 + 0.5\ cos\frac{2\pi n}{\Gamma}\right) e^{j\pi\left(\frac{n\Delta}{NT}\right)} \qquad (4.21)$$

4.3 Adaptive Filtering Based Channel Estimation

4.3.1 RLS-Based Channel Estimation

Due to high convergence rate and fast steady-state adaptation, RLS channel estimator is used for time-varying mobile channels. Due to the poor convergence of LMS-CE, RLS is preferred for highly correlated data but for better performance the disadvantage comes in form of increased complexity.

As compared to Gradient Algorithms, RLS algorithm is used to implement simple LS-CE as adaptive estimator. The cost function for LSE initially estimated channel case is given by

$$J_{RLS}[N] = \sum_{i=1}^{N} \gamma^{N-i}. \left|E_{m,n}[i]\right|^2 + \delta.\gamma^N. \|w[N]\|^2 \qquad (4.22)$$

Where γ is forgetting factor whose exact value is difficult to be estimated and δ is regularization parameter.

The error vector for n^{th} OFDM symbol at m^{th} carrier is given by

$$E_{m,n}[i] = H_{m,n}[i] - w^H \widetilde{H}_{m,n}[i] \qquad (4.23)$$

$\widetilde{H}_{m,n}[i]$ is the estimated channel, which at initialization is determined by LS method.

Channel up-dating is done by the following steps

1- The value of correlation matrix $\widehat{R}_{g_{r,t}g_{r,t}}$ at iteration $\boldsymbol{n}$ is given by

$$\widehat{R}_{g_{r,t}g_{r,t}}[n] = \lambda \widehat{R}_{g_{r,t}g_{r,t}}[n-1] + \widehat{H}_{r,t}^{RLS}[n]\widehat{H}_{r,t}^{H,RLS}[n] \qquad (4.24)$$

2- Gain Matrix is given by

$$\widehat{R}_{g_{r,t}g_{r,t}}[n]k[n] = \widehat{H}_{r,t}^{RLS}[n] \qquad (4.25)$$

3- Error vector is

$$E[n] = \widehat{H}_{r,t}^{LS}[n] - \widehat{W}^{T}[n-1]\widehat{H}_{r,t}^{RLS}[n] \quad (4.26)$$

4- Conversion Factor at iteration $\boldsymbol{n}$ is

$$\alpha[n] = 1 - k[n]\widehat{H}_{r,t}^{RLS}[n] \quad (4.27)$$

5- After which the error is given by

$$\varepsilon[n] = \alpha[n]E[n] \quad (4.28)$$

6- After n^{th} iteration, the up-dated co-efficients are

$$\widehat{W}^{T}[n-1] = \widehat{W}^{T}[n-1] + k[n-1]E^{*}[n] \quad (4.29)$$

Now the estimated channel becomes

$$\widehat{H}_{r,t}^{RLS}[n] = \sum_{m=0}^{M-1} \widehat{W}[m]\,\widehat{H}_{r,t}^{RLS}[n-m] \quad (4.30)$$

The gain vector $k[n]$ is given by

$$k[n] = \frac{\lambda^{-1}\,Q[n-1]\widehat{H}_{r,t}^{RLS}[n]}{1 + \lambda^{-1}\widehat{H}_{r,t}^{RLS}[n]Q[n-1]\widehat{H}_{r,t}^{RLS}[n]} \quad (4.31)$$

and

$$Q[n] = \frac{1}{\lambda}\left(Q[n-1] - k[n]\widehat{H}_{r,t}^{RLS}[n]Q[n-1]\right) \quad (4.32)$$

Initially the parameter values are

$$Q[0] = [\widehat{H}_{r,t}^{RLS}[0].\widehat{H}_{r,t}^{RLS}[0] + \delta I]^{-1} \quad (4.33)$$

and

$$k[0] = Q[0]\widehat{H}_{r,t}^{RLS}[0] = \frac{1}{\left\|\widehat{H}_{r,t}^{RLS}[0]\right\|^{2} + \delta}.\widehat{H}_{r,t}^{RLS}[0] \quad (4.34)$$

4.3.2 LMS Based Channel Estimation

To avoid the matrix inversion, involved in LSE and LMMSE [18], LMS algorithm can be used to solve Wiener-Holf equation, which may or may not require a priori statistical information of the channel and data.

A summary of LMS algorithm is given as follows

1- LSE method is applied to get the initialized, $\widehat{H}_{r,t}^{LS}$, used for first iteration.

2- After finding the filter co-efficients, the channel estimation becomes

$$\widehat{H}_{r,t}^{LMS}[n] = \widehat{W}^{H}[n]\widehat{H}_{r,t}^{LS}[n] \qquad (4.35)$$

Where

$$\widehat{H}_{r,t}^{LS}[n] = [\widehat{H}_{r,t}^{LS}[n]\ \ \widehat{H}_{r,t}^{LS}[n-1] \ldots \widehat{H}_{r,t}^{LS}[n-1+M]]$$

Where LMS filter has length M.

3- At n^{th} iteration, the error is given by

$$E[n] = \widehat{H}_{r,t}^{LS}[n] - \widehat{H}_{r,t}^{LMS}[n][n] \qquad (4.36)$$

4- From this error, co-efficients can be updated by

$$\widehat{w}[n+1] = \widehat{w}[n] + \mu\widehat{H}_{r,t}^{LS}[n]E^{*}[n] \qquad (4.37)$$

Where the value of step-size parameter μ depends on the correlation between the data.

5- After up-dating the co-efficients. The weighted-error is given by

$$\epsilon[n] = w[n] - \widehat{w}[n] \qquad (4.38)$$

4.3.3 Kalman-Filtering Based Channel Estimation

Channel can be estimated by using the following state space vector

$$h_{r,t}[n+1] = Fh_{r,t}[n] + v_{r,t}[n] \quad (4.39)$$

Where $h_{r,t}[n] = (h_{r,t_n}[0]\ h_{r,t_n}[1]\ \dots\ h_{r,t_n}[L-1])^T$, F is $M_T \times N_R$ channel matrix showing the state transition of $h_{r,t}[n]$. $v_{r,t}[n]$ is the complex white Gaussian noise.
At receiver the signal is given by [39]

$$y_{r,t}[n] = {h_{r,t}}^H[n]x_{r,t}[n] + w_{o_{r,t}}[n] \quad (4.40)$$

The following Kalman Filtering equations are performed iteratively to find the estimated channel [40].

$$\hat{h}_{r,t}[n/n-1] = F\hat{h}_{r,t}[n-1/n-1] \quad (4.41)$$

$$e[n/n-1] = y_{r,t}[n] - {\hat{h}_{r,t}}^H[n/n-1]x_{r,t}[n] \quad (4.42)$$

$$q[n] = \sum_{k=0}^{L-1}[R_{h_{r,t}}[0]]_{k,k}\,\sigma^2_{x_{r,t}}[n-k] + N_{o_{r,t}} \quad (4.43)$$

$$k[n] = \frac{P[n/n-1]x_{r,t}[n]}{q[n] + {x_{r,t}}^H[n]P[n/n-1]x_{r,t}[n]} \quad (4.44)$$

$$\hat{h}_{r,t}[n/n] = \hat{h}_{r,t}[n-1/n-1] + k[n]e^*[n/n-1] \quad (4.45)$$

$$P[n+1/n] = F\left(I - k[n]{x_{r,t}}^H[n]\right)P[n/n-1]F^H + Q_{v_{r,t}}[n] \quad (4.46)$$

Initialized parameters are

$$\hat{h}_{r,t}[-1/-1] = \mu_{h_{r,t}} \quad (4.47)$$

$$P[-1/-1] = C_{h_{r,t}} \quad (4.48)$$

$k[n]$ is the gain vector of Kalman filter.
$Q_{v_{r,t}}[n]$ is the covariance matrix of the Gaussian noise $v_{r,t}[n]$ and

$$R_{h_{r,t}}[0] = E\left[\hat{h}_{r,t}[n/n-1]{\hat{h}_{r,t}}^H[n/n-1]\right] + P[n/n-1] \quad (4.49)$$

4.4 Simulation Results

The above discussed channel estimation techniques in this chapter are evaluated and optimized in this section in terms of Mean Square Error (MSE), Symbol Error Rate (SER), Packet Error Rate (PER) and Frame Error Rate (FER) by using MATLAB simulations for MIMO-OFDM system whose parameters are given in Table 4.1.

TABLE 4.1: SYSTEM PARAMETERS FOR MIMO-OFDM CHANNEL ESTIMATION

Parameter	
Number of Packets	100
Frame Length	130 Symbols
Modulation	BPSK, QPSK, 8-PSK,16-PSK
Channel Type	Rayleigh Fading
MIMO	2 x 2
FFT Size	512
CP Length	16

Figure 4.1 shows the MSE comparison between LSE and LMMSE from which it is clear that LMMSE is better technique than LSE which does not utilize the channel statistics. At high SNR values, the performance gap is more than at low SNR. But for improved performance in LMMSE we have to pay for more complexity which results in increased computational time and high implementation cost of hardware to have a priori knowledge of channel behavior.

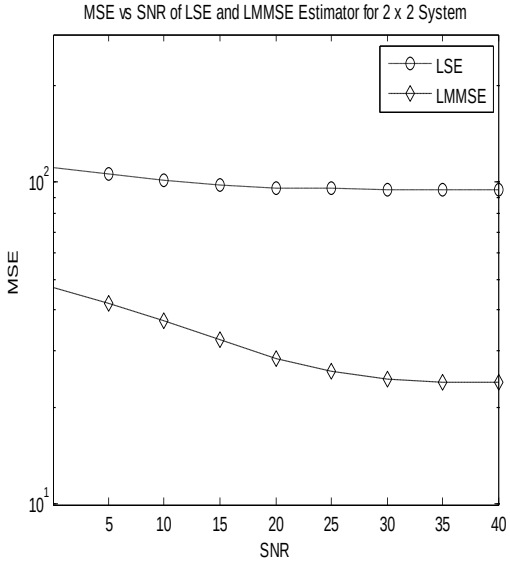

Figure 4.1: Comparison of LSE and LMMSE

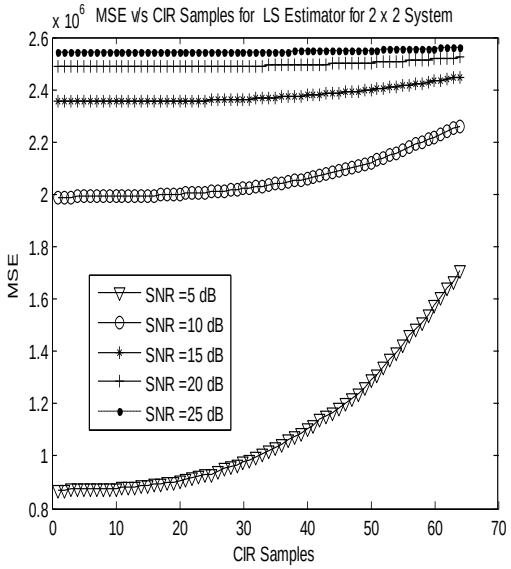

Figure 4.2: Comparison of MSE for different CIR Samples at various SNR Values

The effect of discarding certain CIR samples on performance for LSE is given in Figure 4.2. The performance is better for limited transmitting power communication systems. For low SNR values, as CIR samples are increased the performance goes on degrading. CIR samples less than 20 shows almost same performance while for value greater than 20, not only performance is degraded but also has more complexity. For high SNR values, the value of CIR samples does not have significant effect on performance.

From Figure 4.3, we observe that less CIR samples operating at low SNR are preferred for less MSE. As we increase SNR and CIR Samples, the MSE increases but after certain values, further increment in any parameter does not have affect on the performance and behavior remains almost same.

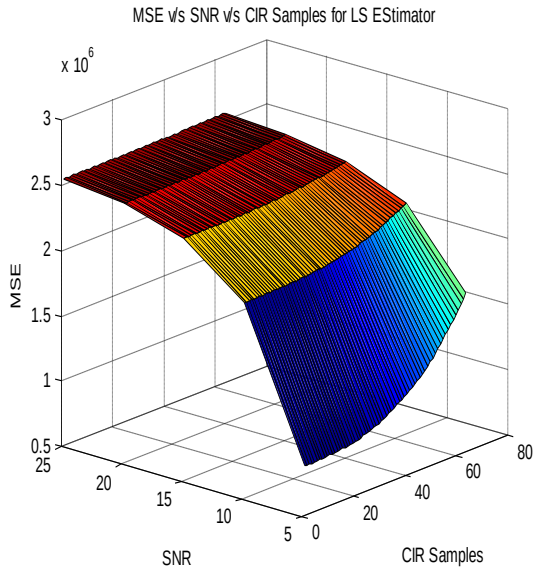

Figure 4.3: MSE vs SNR vs CIR samples for LSE

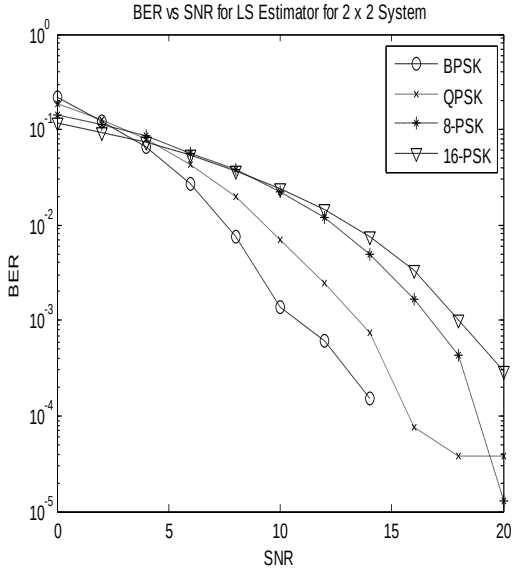

Figure 4.4: BER of different Modulation for 2 x System

Figure 4.4 shows the comparison of different modulations for 2 x 2 system. As expected, BPSK outperforms all other modulations techniques. At low SNR, the performance is same for all modulations but the increasing effect in SNR has clear demonstration of the difference of performance. So for high SNR, we choose modulation according to the system requirement but for low SNR we can choose any one. The same observation is also concluded for SER as shown in Figure 4.5. But here a performance gap is found even for low SNR values. So from Figure 4.5 we can have a better view for modulation choice.

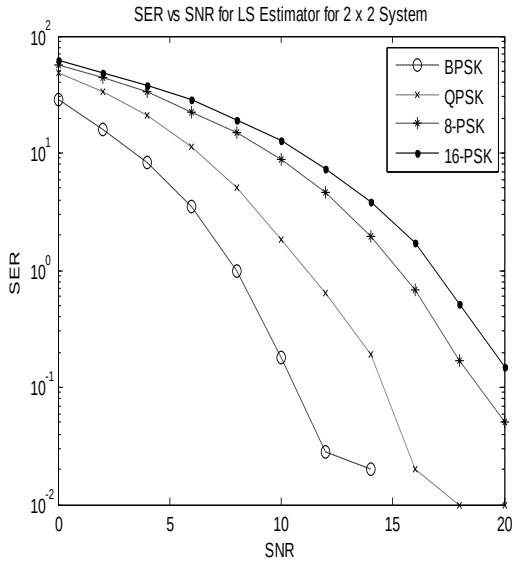

Figure 4.5: SER vs SNR of LSE for different Modulations

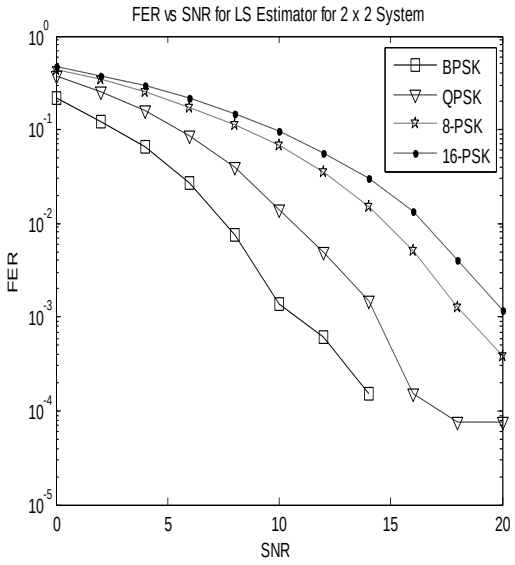

Figure 4.6: FER of LSE for different modulations

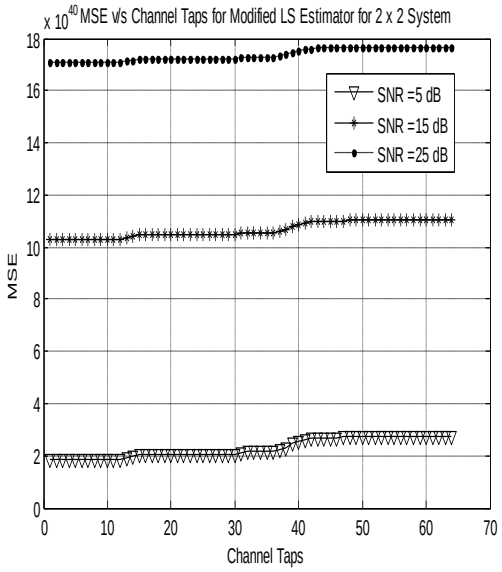

Figure 4.7: MSE for Modified LSE Estimator

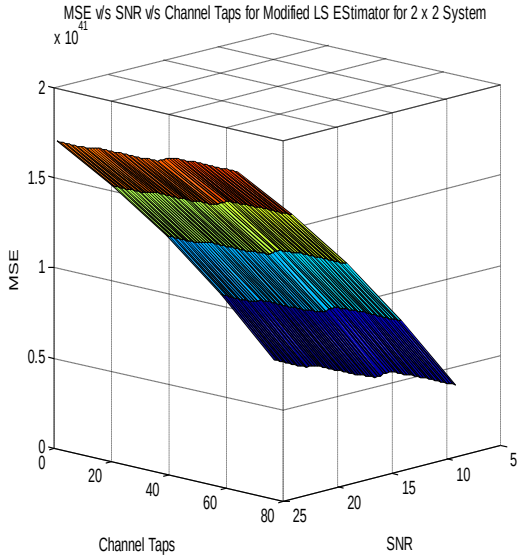

Figure 4.8: MSE vs Channel Taps vs SNR for LS

FER for LSE for different modulations is shown in Figure 4.6. Here again we observe that the performance is almost same for low SNR but by increasing SNR the high-point modulation degrades greatly than the low-point modulation. From Figure 4.4, 4.5, 4.6, we can choose the best one modulation for any wireless communication system for better performance optimization. The comparison of the modified LSE estimators at different SNR values is demonstrated in Figure 4.7. For better performance low SNR operating condition is preferred having less number of channel taps. For more channel taps the performance is also lost in terms of more MSE at the cost of more complexity.

The combined effect of Channel Taps and SNR of performance of LSE is shown in Figure 4.8 from which it is clear that for better performance, low SNR for more number of channel taps are proposed. For different CIR samples, the performance of LMMSE estimator is given in Figure 4.9. Similar to LSE, low SNR is also preferred for LMMSE. But for low SNR, the performance is same almost for initial 35 CIR samples and further increment in value, not only results in degraded performance but also more complexity. For high SNR, CIR samples have not impact on performance, only we have to consider the complexity issue.

The modified LMMSE estimators are optimized according to their performance for different Channel Taps as shown in Figure 4.10. We observe the for low SNR, the performance is better for less than 10 Channel taps but further increment in channel taps degrades the performance not too much only affect is on complexity. As the SNR value is increased, the range of channel taps for better performance also increases, for example, for SNR value of 10, the performance is ideal for up to 30 channel taps and similarly for 25 dB, channel taps can be 60 for accepted performance.

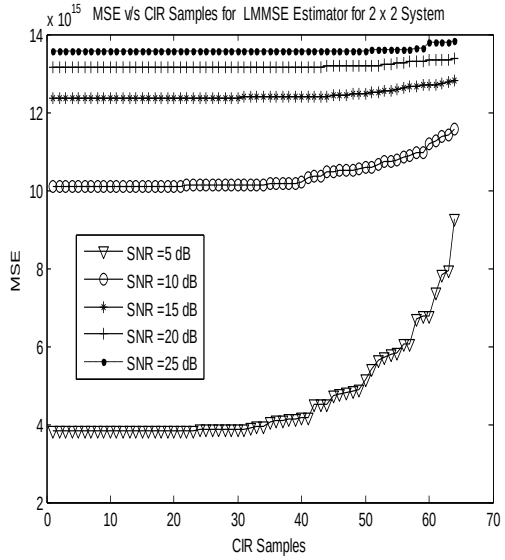

Figure 4.9: MSE vs CIR Samples for LMMSE

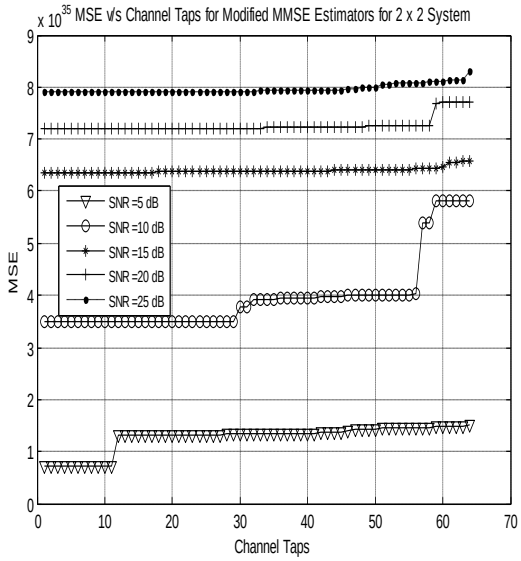

Figure 4.10: Effect of Channel Taps on LMMSE

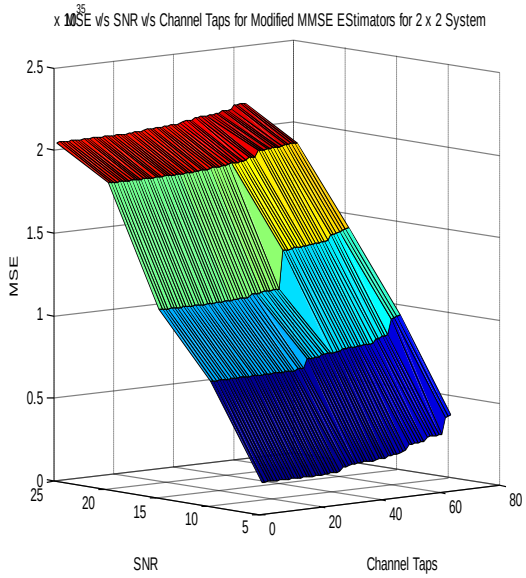

Figure 4.11: MSE vs SNR vs Channel taps for Modified LMMSE

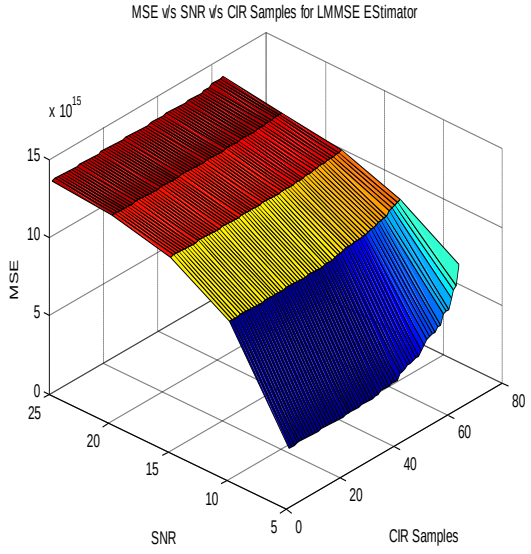

Figure 4.12: Effect of SNR and CIR Samples for LMMSE

Figure 4.11 shows that for better performance, in case of LMMSE, small values of SNR and channel taps are preferred. For specific values of channel taps, the performance lowers down significantly by increasing the SNR value. In Figure 4.12 MSE variation according the varying values of SNR and CIR Samples is demonstrated. Small values of SNR and CIR samples are proposed for better system performance.

MSE as a function of CIR samples for different SNR values is given in Figure 4.13. We observe that by increasing SNR value, the performance goes on degrading for all CIR samples. For low SNR value, the performance degradation occurs only for high number of CIR samples. But as we increase the SNR value, the effect of increasing the CIR samples on performance goes on disappearing. So for all SNR operating conditions, less number of CIR samples due to less complexity are proposed. The performance comparison for different number of channel taps is shown in Figure 4.14. For small number of CIR samples, the performance remains same for any number of channel taps. But as we increase CIR samples, the performance is better for small value of channel taps. The combined effect of channel taps and CIR samples on performance is shown in Figure 4.15.

Less number of channel taps and small length of channel impulse response not only results in better performance but also has reduced complexity and opposite behavior is observed

for high number of channel taps and large channel filter length. Small value of SNR and small channel filter length is used for having small value of Mean Square Error. At low SNR, high channel filter length results in the degraded performance, similar to performance of high channel filter length. Figure 4.16 shows the comparison of performance of DFT-CE and DCT-CE. For less number of CIR samples, the performance of both estimators is same but as we increase the channel filter length, the performance of DFT degrades slightly as compared to DCT-CE. For DCT-CE, DCT and IDCT operations can be exchanged. The comparison between these two options is shown in Figure 4.17.For small value of channel filter length, up to 30 CIR samples, the performance of DCT/IDCT is better than IDCT/DCT but when we take more CIR samples, the gap in performance decreases. To use any method of DCT-CE, less number of CIR samples are considered, not only for better performance but also for reduced complexity.

MSE behavior for DFT and DCT as a function of channel taps is shown in Figure 4.18. We observe that performance of DFT is better than DCT/IDCT method but IDCT/DCT-CE shows better performance than DFT-CE. For any specific channel estimator, the performance remains same for channel taps less than 10, but as we take more channel taps, MSE increases and then again remains constant for some channel taps. So for better performance less number of channel taps are proposed, which also gives reduced complexity. The effect of varying channel taps for certain value of channel filter length is shown in Figure 4.19

.

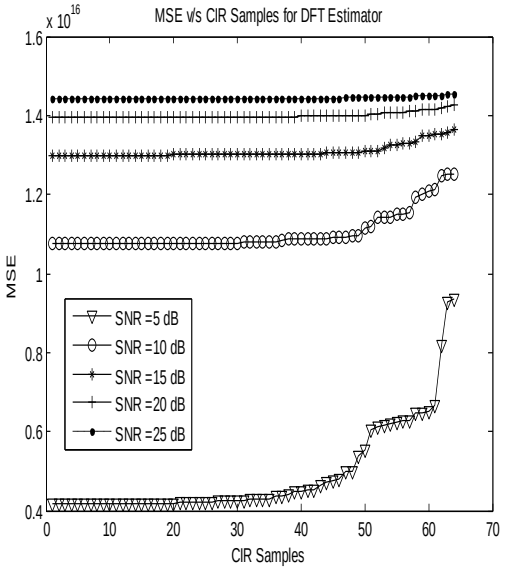

Figure 4.13: MSE vs CIR Samples for DFT-CE

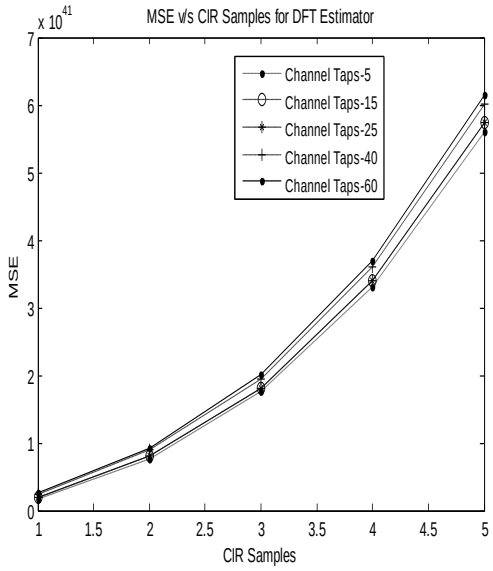

Figure 4.14: MSE vs CIR Samples for different Channel Taps for DFT-CE

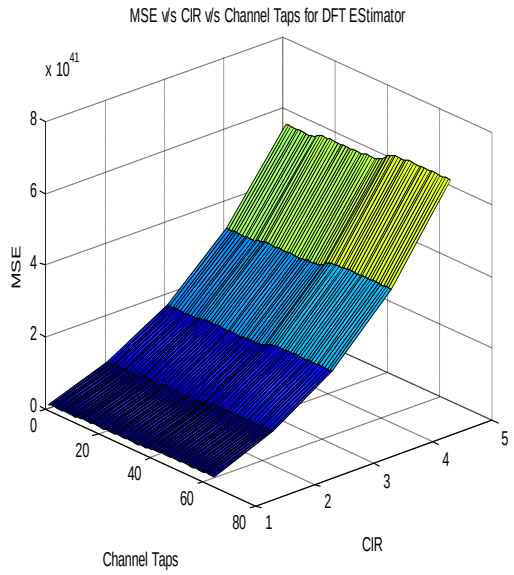

Figure 4.15: MSE vs Channel Taps vs CIR Samples for DFT-CE

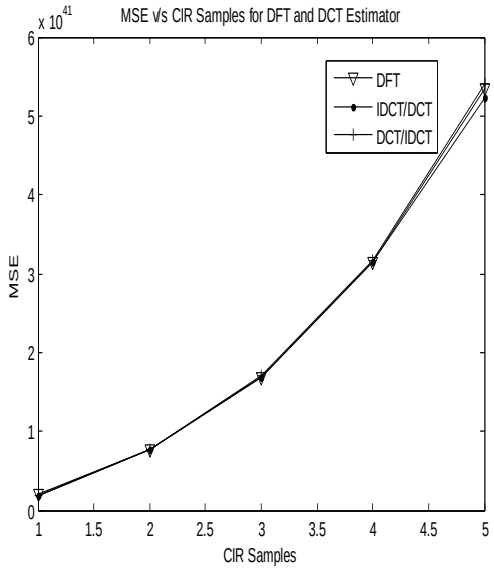

Figure 4.16: MSE vs CIR Samples for Transform-Based Channel Estimators

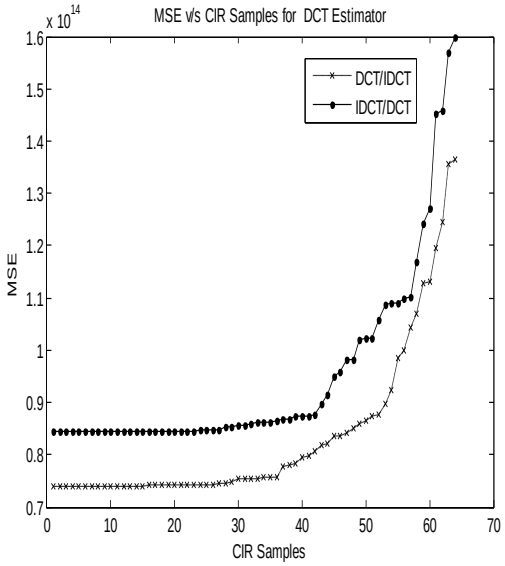

Figure 4.17: MSE vs CIR Samples for DCT-CE

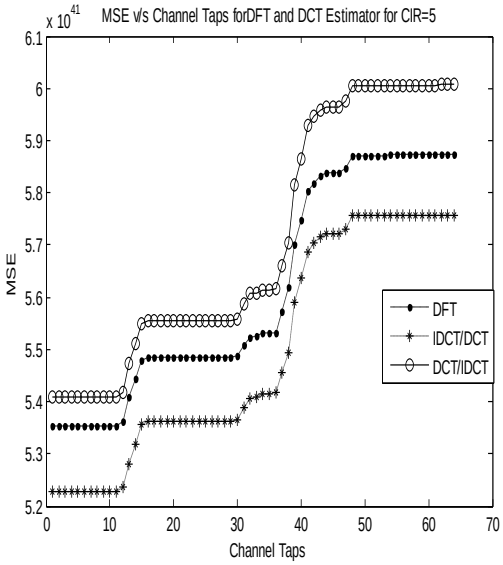

Figure 4.18: MSE vs Channel Taps for DFT-CE and DCT-CE

We observe that for smaller values of CIR samples, there is no effect of changing the channel taps as performance remains same for whole range of channel taps. But as we take larger channel filter length, then as we go in increasing the number of channel taps, the performance also goes on degrading. So we use smaller value of channel filter length with less number of channel taps.

The effect of different channel filter lengths on performance of Windowed-DFT channel estimator is shown in Figure 4.21. According to this figure, we observe that for low SNR, less number of CIR samples are preferred, approximately of length 0-20, and high value of CIR samples not only degrades the performance but also increase the computational time. As we go on increasing the SNR value, a proportional increase on filter length gives acceptable performance. For example for 25dB, performance remains almost same for all CIR samples. For reliable communication, a channel filter of smaller length is used at low SNR values, as shown in Figure 4.21.

For high CIR samples, any SNR value can be used because it gives the same performance. The computational time of Windowed-DFT channel estimator for different CIR samples is given in Table 4.2, as compared to other transform-based channel estimators. For low CIR samples the complexity of Windowed-DFT CE is less than DCT-CE but greater than direct DFT method. 30% increment in filter length increases the computational time by 6.7% while for 100% increment, computational time increases by 30%.

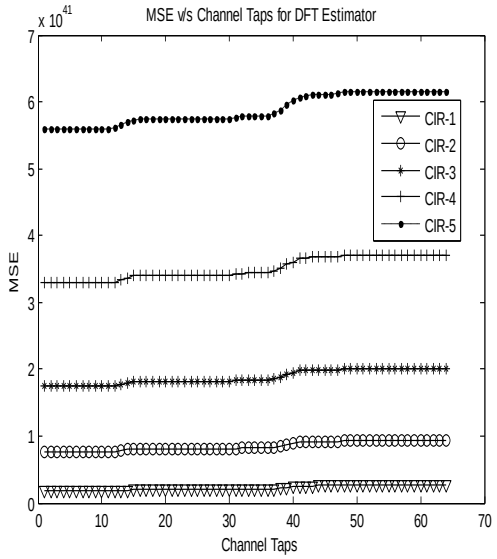

Figure 4.19: MSE vs Channel Taps for different CIR Samples

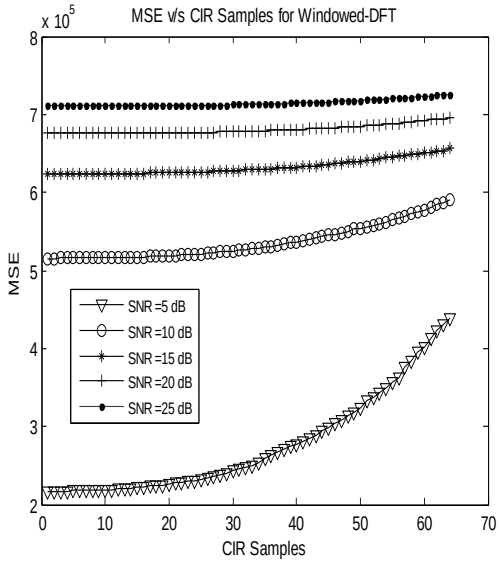

Figure 4.20: MSE v/s CIR Samples for Windowed-DFT CE

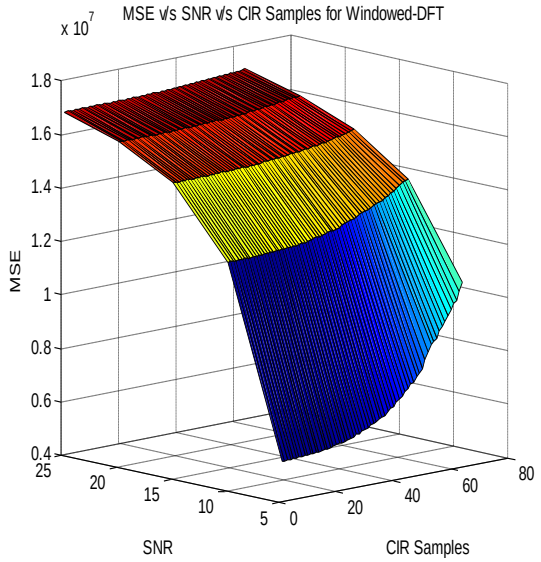

Figure 4.21: MSE as a function of SNR and CIR Samples

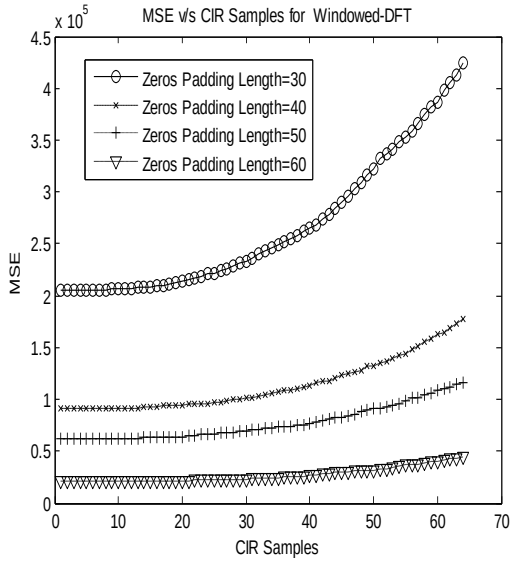

Figure 4.22: MSE for different Zero Padding Lengths

TABLE 4.2: COMPLEXITY COMPARISON

CIR Samples	5	20	40
Windowed-DFT	0.89	0.015	.02
DFT	.0812	.012	.02148
IDCT/DCT	0.998	.01343	.0184
DCT/IDCT	1.1074	.0153	.0179

TABLE 4.3: COMPLEXITY COMPARISON FOR DIFFERENT CHANNEL TAPS

Channel Taps	3	10	20
Windowed-DFT	.0018	.0018	.0021
DFT	.0251	.0016	.0016
IDCT/DCT	.0021	.002	.0023
DCT/IDCT	.002	.0023	.0022

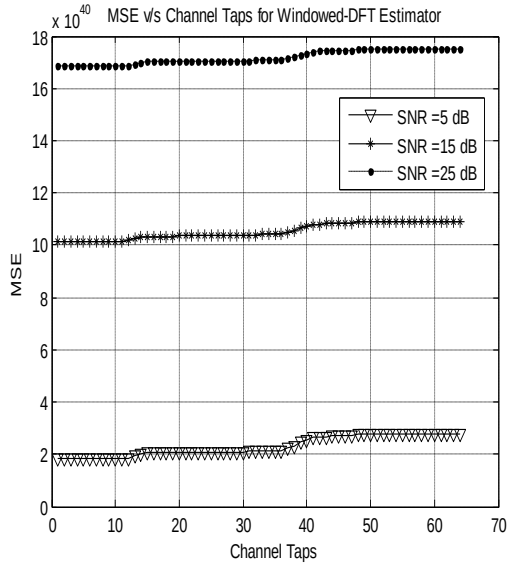

Figure 4.23: MSE as a function of Channel Taps

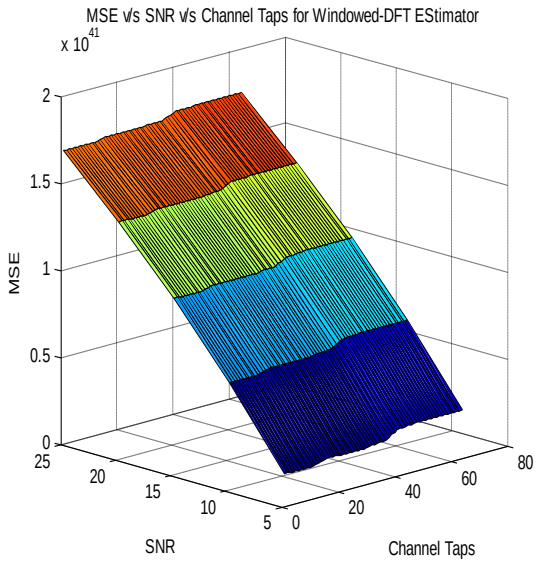

Figure 4.24: MSE vs SNR vs Channel Taps

To make Windowed-DFT approach, less complex than DFT, a filter length containing higher values of CIR samples is used but in such cases, its complexity will increase than DCT approach. The effect of Zero padding lengths for varying CIR samples is shown in Figure 4.22. Performance will be better for case of more zeros as in such situation, we consider only high energy CIR samples and less energy components are discarded to remove the noise effect. As we go on padding less number of zeros, the effect of varying CIR samples also becomes significant. For example for more number of zeros, performance does not change by increasing CIR samples but for less number of zeros, the performance shows same behavior for less CIR samples, but as CIR samples increases, the performance degrades and complexity also increases. The performance as a function of channel taps is shown in Figure 4.23. Performance is better for low SNR for any value of channel taps.

For any specific SNR value, the performance degrades slightly for high number of channel taps. The combined effect of SNR and channel taps is given in Figure 4.24. According to this figure less number of channel taps at low SNR are preferred for better performance. For a specific value of channel taps MSE increase almost linearly by increasing SNR. The comparison of computational time of Windowed-DFT with other methods is given in Table 4.3. According to Table 4.3, Windowed-DFT requires more computational time than DFT-CE but its complexity is less than DCT-CE. The effect of increasing number of channel taps on complexity is not considerable so we can use any number of channel taps, from complexity point of view. The computational time for 5000 simulations and 1 OFDM symbol is shown in Table 4.4. By increasing channel taps from 5 to 20, complexity increases approximately 126%. But further increment of channel taps from 20 to 64, causes 33% more computational time only.

The effect of zero padding lengths on MSE for different channel taps is demonstrated in Figure 4.25. Higher the number of zeros padded to CIR, the better will be performance. For any particular zeros-length, performance remains same for channel taps less than 10, but as we further increase channel taps, the performance degrades but this effect comes into observation after specific interval length so normally, channel taps less than 10 are proposed, irrespective of the zero-length. The performance comparison of Windowed-DFT for different zero-lengths is given in Figure 4.26. We note that for less number of zeros, Windowed-DFT performs better than DFT-CE but as we increase zeros then its performance degrades as compared to DFT so to use Windowed-DFT, we prefer less number of zeros to be padded to channel impulse response. The complexity comparison of Windowed-DFT for different channel taps and for different zero lengths is given in Table 4.5.

TABLE 4.4: COMPUTATIONAL TIME OF WINDOWED-DFT

Channel Taps	5000 Simulations (sec)	1 OFDM Symbol (sec)	1 Bit (sec)
5	3.31	0.051	.025
20	7.5	0.12	.06
64	10	0.15625	.078

TABLE 4.5: COMPUTATIONAL TIME FOR DIFFERENT ZERO-PADDINGS

	Zero-Padding Lengths		
Channel Taps	32	40	50
5	.0021	.0017	.0022
20	.0698	.0015	.0711
64	.098	.0896	.082

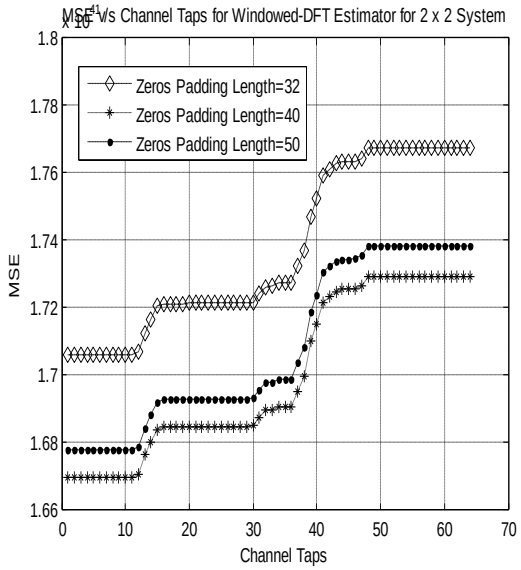

Figure 4.25: MSE as a function of Channel Taps for Windowed-DFT

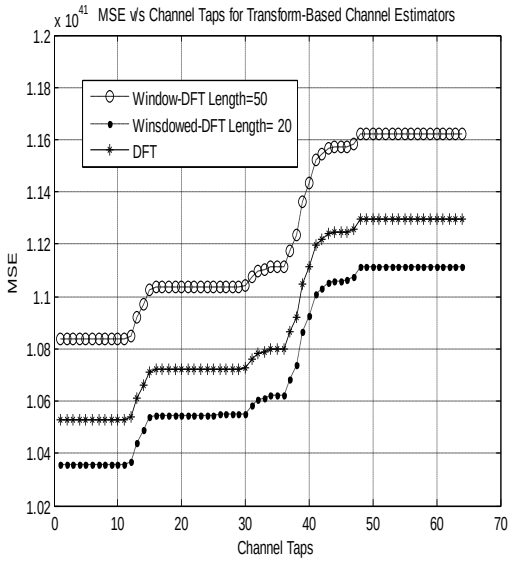

Figure 4.26: MSE vs Channel Taps for different Channel Estimators

The performance comparison of LMS channel estimator as a function of CIR samples for different SNR values is shown in Figure 4.27. From Figure 4.27, it is clear that for any channel length, the performance is better under low SNR operating conditions. As we go on increasing CIR samples, MSE also increases. So for better performance, less number of CIR samples for low SNR values are preferred. The effect of channel filter length on MSE for different LMS estimators is shown in Figure 4.28. We note that performance remains same for LMS and Leaky-LMS estimators for all CIR samples. The complexity of LMS estimator as a function of CIR samples is given in Table 4.6. By increasing CIR samples from 5 to 10, the complexity increases 20%. While further increase of CIR samples to 20, there is 60% increment in complexity. The combined effect of SNR and CIR samples on performance is shown in Figure 4.29. MSE for different MIMO schemes is shown in Figure 4.30. The performance is better for 2×2 system than 3×3 and 4×4 systems. Irrespective of CIR samples, low order MIMO scheme results in better performance. MSE behavior remains same for CIR samples less than 5, after that the performance degrades, almost linearly for increasing CIR samples.

Figure 4.31 shows the performance of LMS for the cases when initially channel estimator is LS and LMMSE. The performance of LMMSE-LMS is better than LS-LMS because in first technique, second order channel statistics are exploited due to which this method results in more complexity as given in Table 4.7. By increasing CIR samples from 5 to 10 in LMMSE-LMS, the complexity increases by 8% while in LS-LMS this increment was 20%. While the increment in complexity is 18.91% when increasing CIR samples from 5 to 20 but in case of LS-LMMSE it was 60%. Table 4.8 also demonstrates that for 5 CIR samples the complexity increases by 167%

in case of LMMSE-LMS as compared to LS-LMS. While for 10 CIR samples, this increment is 140% and this value reduces to 96% for 20 CIR samples. So the larger the number of CIR Samples, the increment will be less for LMMSE-LMS scheme than that of LS-LMS. The computational time for different MIMO systems for both LMMSE-LMS and LS-LMS schemes is shown in Table 4.8. More computational time results for higher order MIMO schemes e.g. 3×3 scheme results in 115% more computational time for both LS-LMS and LMMMSE-LMS cases as compared to 2×2. While for 4×4, the increment is almost 290%. The performance as a function of channel taps for LMS is shown in Figure 4.32.

By increasing the channel taps, the performance also goes on degrading for all SNR values. So for better performance and less complexity, small number of channel taps are proposed, as for large number of channel taps not only the performance degrades but complexity also increases as given in Table 4.9. The increment of channel taps value from 5 to 10 results in 5% more computational time while 20 channel taps gives 26% more complexity. . Performance as a function of SNR and channel taps is shown in Figure 4.33. The performance for different MIMO systems as a function of channel taps is shown in Figure 4.34. The low order MIMO systems give better performance for all channel taps. For less order MIMO scheme, the effect of increasing the channel taps on performance is not so significant as for 2×2 case but as we increase the order of MIMO system, the performance degrades, almost, as a linear function of increasing channel taps.

TABLE 4.6: COMPLEXITY OF LMS ESTIMATOR FOR 2×2 SYSTEM

CIR Samples	Time (μsec)
5	67.66
10	81.4
20	108

TABLE 4.7: COMPLEXITY COMPARISON OF LS-LMS AND LMMSE-LMS ESTIMATOR

CIR Samples	LS-LMS (μsec)	LMMSE-LMS (μsec)
5	67.05	179.2
10	80.4	193.63
20	108.5	213.09

TABLE 4.8: COMPLEXITY COMPARISON OF LMS ESTIMATOR FOR DIFFERENT MIMO SCHEMES

CIR Samples	2×2 (μsec)		3×3 (μsec)		4×4 (μsec)	
	LS-LMS	LMMSE-LMS	LS-LMS	LMMSE-LMS	LS-LMS	LMMSE-LMS
5	68.65	180.6	147	395	260	705.5
10	80.045	178.83	176.6	440.8	453	753
20	106.23	286.16	238	525	470	1100

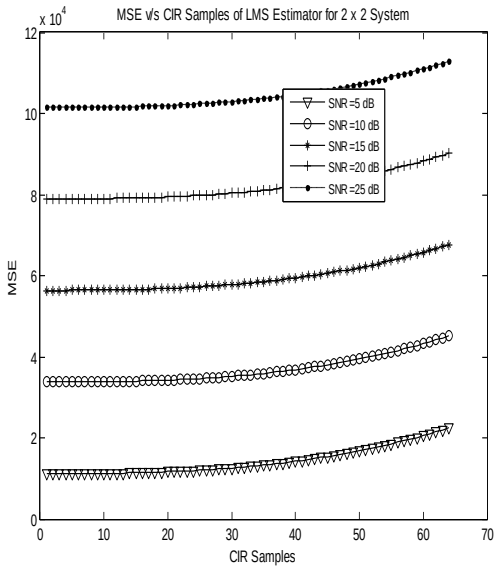

Figure 4.27: MSE vs CIR Samples for LMS Estimator

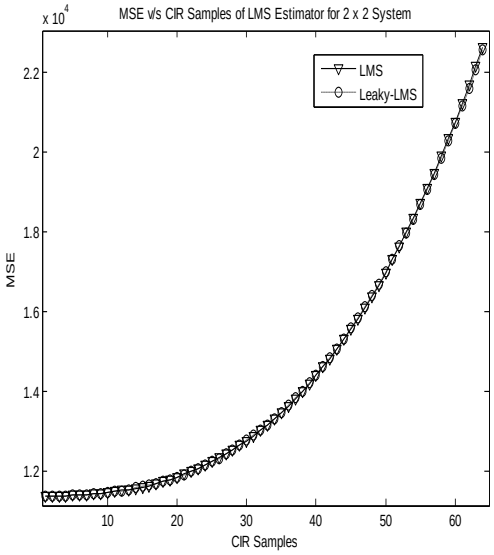

Figure 4.28: MSE vs CIR Samples for different LMS Estimators

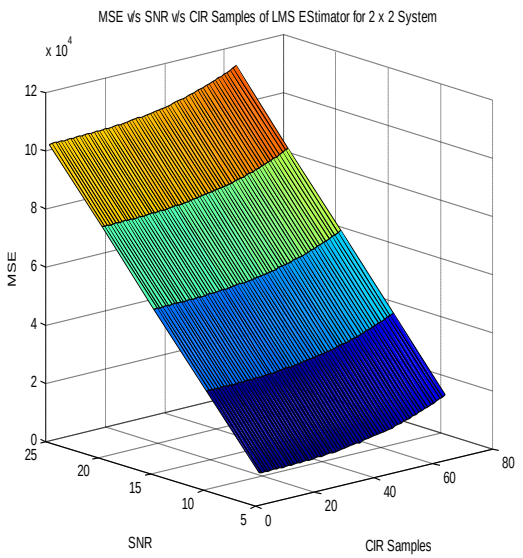

Figure 4.29: MSE vs SNR vs CIR Samples for LMS Estimator

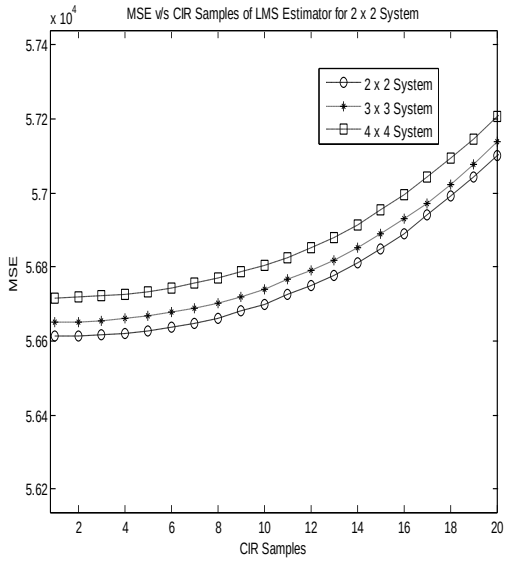

Figure 4.30: MSE vs CIR Samples for different MIMO Schemes

TABLE 4.9: COMPLEXITY OF LMS ESTIMATOR FOR DIFFERENT CHANNEL TAPS FOR 2 × 2 SYSTEM

Channel Taps	Time (μsec)
5	255.2
10	269.6
20	321.4

TABLE 4.10: COMPLEXITY OF LMS ESTIMATOR FOR DIFFERENT MIMO SCHEMES

Channel Taps	2 × 2 (μsec)	3 × 3 (μsec)	4 × 4 (μsec)
5	258	260.6	467
10	291	269	526
20	340	470	565

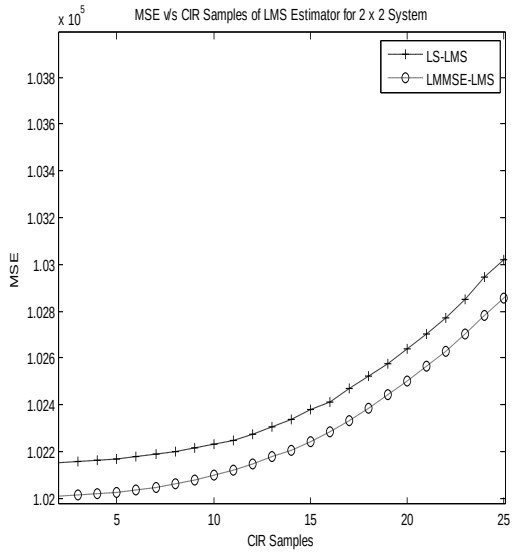

Figure 4.31: MSE vs CIR Samples for LS-LMS and LMMSE-LMS

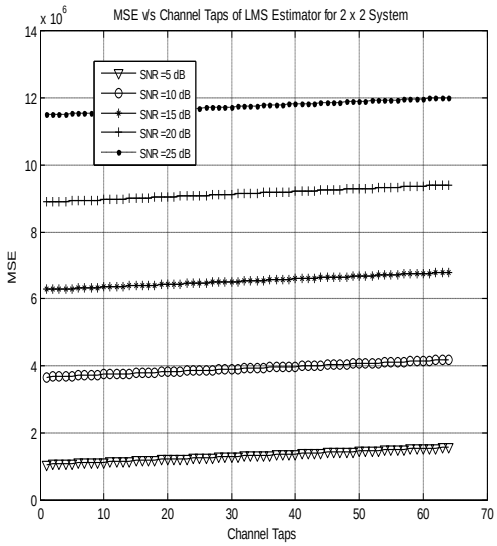

Figure 4.32: MSE vs Channel taps for LMS Estimator

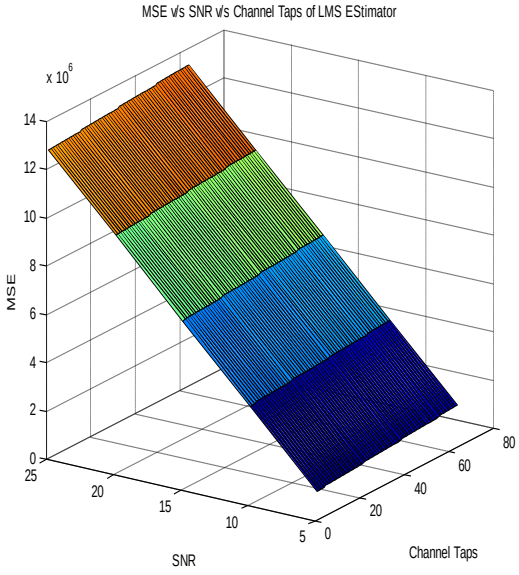

Figure 4.33: MSE vs SNR vs Channel Taps for LMS Estimator

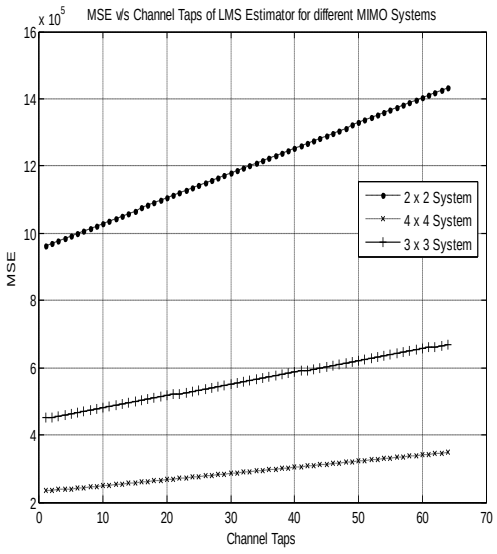

Figure 4.34: MSE vs Channel Taps for different MIMO Schemes

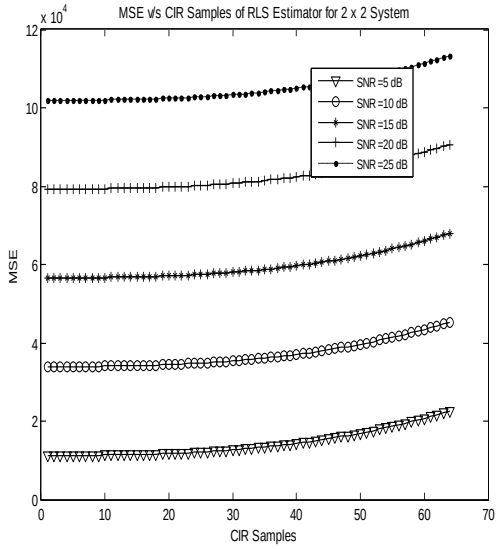

Figure 4.35: MSE vs CIR Samples of RLS Estimator for 2×2 System

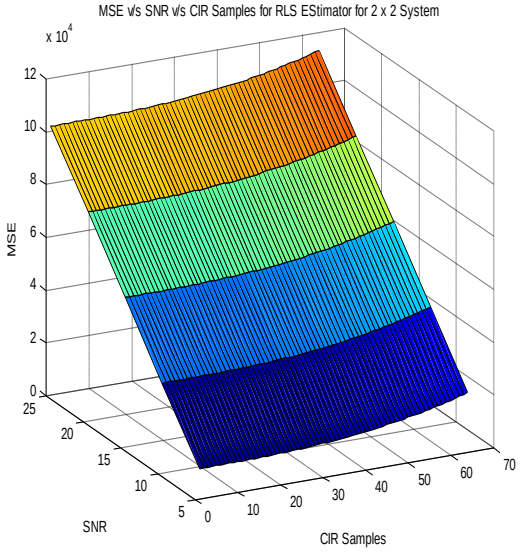

Figure 4.36: MSE vs SNR vs CIR Samples of RLS Estimator

Under different SNR operating conditions, the effect of varying the channel filter length on the performance of RLS estimator is shown in Figure 4.35. As we increase SNR value, the performance degrades for any channel filter length. For a specific SNR value, the performance degrades as larger length of channel filter is considered. So for better performance, less complexity and less power-consumption, less number of CIR samples are taken for low SNR values. The performance of RLS estimator as a function of SNR and CIR Samples is shown in Figure 4.36. The complexity of RLS estimator for different channel filter lengths is given in Table 4.11. By increasing the channel length from 10 CIR samples to 20, the complexity increases by 37%. Further increment of channel filter length to 40 increases the complexity by 93%.

MSE as a function of different channel filter lengths for different MIMO systems is given in Figure 4.37. Up to filter length of 5, the performance remains same for any MIMO system but as we increase the filter length beyond 5 CIR samples, the performance degrades almost as a linear function of increasing the channel filter length. Figure 4.37 also demonstrates that as the order of MIMO system is increased the performance also improves and this improvement is observed for all channel filter lengths under consideration. But higher order system gives better performance at the cost of more computational time. For RLS estimator, the initialized channel

estimator can be either LSE or LMMSE. The performance comparison for both cases is given in Figure 4.38. LMMSE-RLS gives the better performance for all channel filter lengths as it exploits the prior knowledge of the channel statistics that is why it has more complexity as given in Table 4.12. From Table 4.12, we note that for 2×2 MIMO system the complexity of LMMSE-RLS is 113% greater than that of LS-RLS for channel filter length of 10 but as we increase the channel filter length to 40 CIR Samples then this increment is only 77%. For LS-RLS method, the complexity of 3×3 is 71% more than that of 2×2 system while for 4×4 this increment is about 233%. Similarly in case of LMMSE-RLS approach, as compared to 2×2 system the computational time of 3×3 is 151% greater while for 4×4 case this increment becomes 350%.

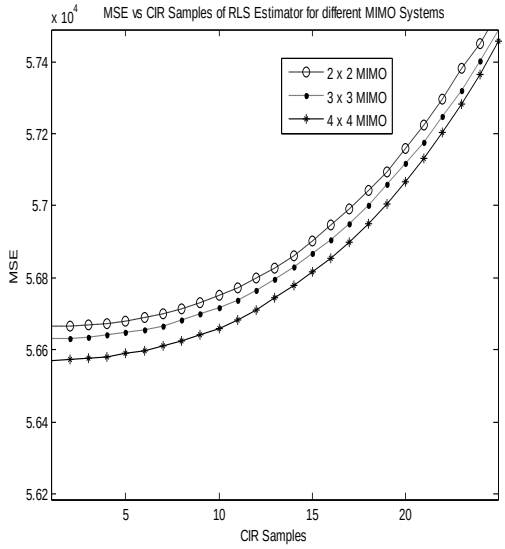

Figure 4.37: MSE vs CIR Samples of RLS Estimator different MIMO Systems

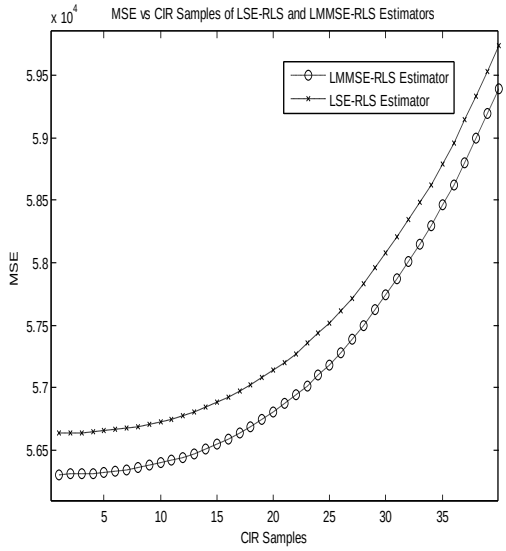

Figure 4.38: MSE vs CIR Samples of LS-RLS and LMMSE- for RLS Estimator

TABLE 4.11: COMPLEXITY OF RLS AS A FUNCTION OF CIR SAMPLES FOR 4×4 MIMO

CIR Samples	Time (μsec)
10	403.2
20	553.15
40	779.34

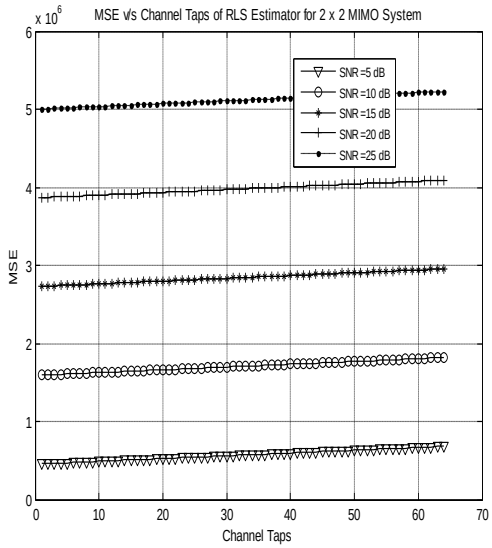

Figure 4.39: MSE vs Channel Taps of RLS Estimator for 2×2 System

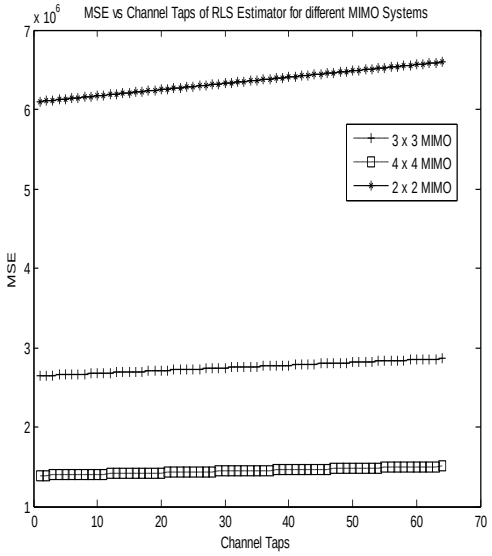

Figure 4.40: MSE vs Channel Taps of RLS Estimator for different MIMO Systems

The performance of RLS estimator in terms of Mean Square Error as a function of Channel Taps at different SNR operating conditions is shown in Figure 4.39. The effect of channel taps is same as that of CIR samples. The performance is better for low SNR values and less number of multi-path channel taps. The effect of channel taps on complexity is shown in Table 4.13. By increasing the channel taps two times, the complexity increases by 14 % but if the channel taps are made four times, then increment in complexity is 28%.

The effect of increasing the channel taps is not so significant in case of high order MIMO e.g. 4×4, but for low order MIMO systems the effect of increasing channel taps results in degraded performance. For better performance under any value of channel taps, higher order MIMO is preferred which gives improved performance at the cost of more computational time. The complexity behavior of both LS-RLS and LMMSE-RLS is given in Table 4.14. For all values of channel taps, LMMSE-RLS takes 6-7 times more computational time than that of LS-RLS method. The performance comparison of LS-RLS and LMMSE-RLS is shown in Figure 4.41. We note that the effect of increasing the channel taps is more significant in case of LSE-RLS than LMMSE-RLS. We also observe that the performance of LSE-RLS for less number of channel taps is same to that of LMMSE-RLS at large number of channel taps. So we can

optimize the complexity by considering appropriate value of channel taps for LMMSE-RLS estimator. The combined effect of SNR and channel taps on performance is shown in Figure 4.42.

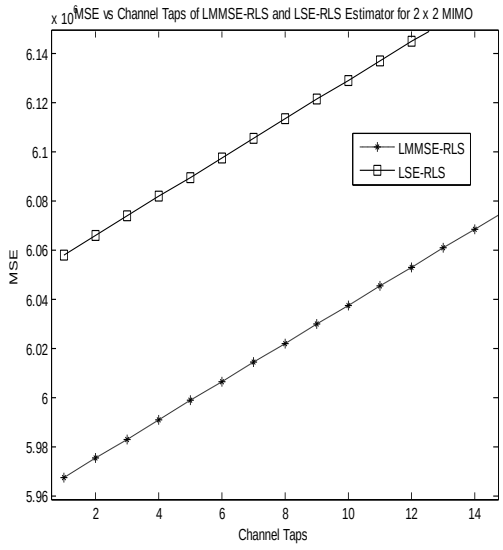

Figure 4.41: MSE vs Channel Taps of LS-RLS and LMMSE-RLS Estimator

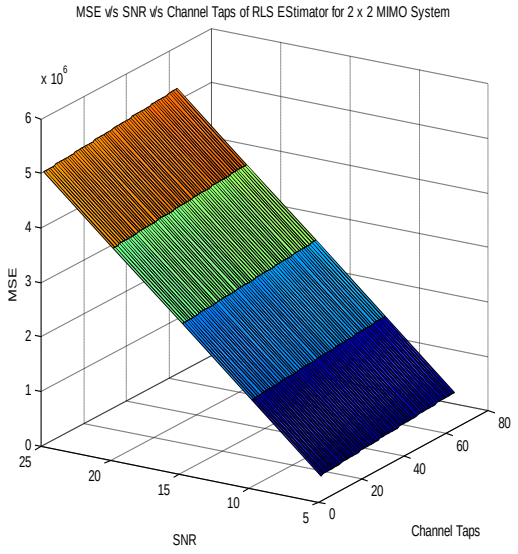

Figure 4.42: MSE vs SNR vs Channel Taps of RLS Estimator

TABLE 4.12: COMPLEXITY OF RLS FOR DIFFERENT MIMO SCHEMES

CIR Samples	$2 \times 2\ (\mu sec)$		$3 \times 3\ (\mu sec)$		$4 \times 4\ (\mu sec)$	
	LS-RLS	LMMSE-RLS	LS-RLS	LMMSE-RLS	LS-RLS	LMMSE-RLS
10	104.33	222.62	178.84	559.85	348.15	1000
20	113.74	252.68	236.3	640.61	464	1200
30	170.73	302.92	356.17	700.44	765.6	1400

TABLE 4.13: COMPLEXITY OF RLS VS CHANNEL TAPS FOR 2×2 SYSTEM

Channel Taps	Time (μsec)
5	252.5
10	850.25
20	323.41

TABLE 4.14: COMPLEXITY OF RLS VS CHANNEL TAPS FOR DIFFERENT MIMO SYSTEMS

Channel Taps	2×2 (μsec)		4×4 (μsec)	
	LS-RLS	LMMSE-RLS	LS-RLS	LMMSE-RLS
5	175.53	1400	328	2900
10	201.9	1400	365.5	3100
20	223.4	1600	394.57	3800

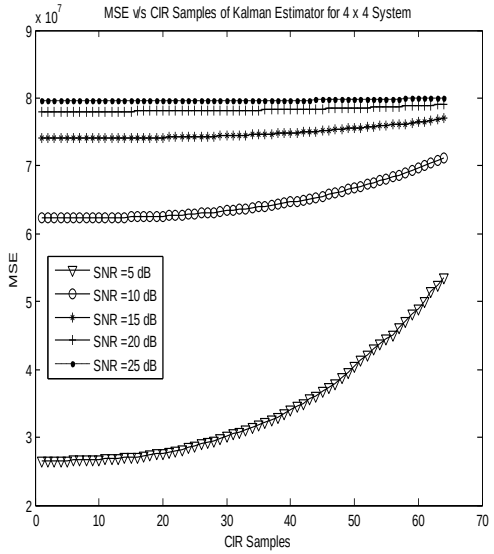

Figure 4.43: MSE vs CIR Samples of Kalman Estimator for 4×4 System

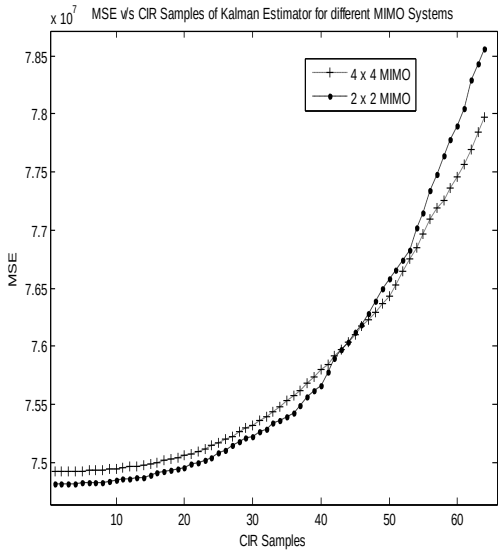

Figure 4.44: MSE vs CIR Samples of Kalman Estimator for different MIMO Systems

The performance of Kalman Filtering based channel estimator is given in Figure 4.43. For low SNR operating conditions, the performance degrades as we increase the channel filter length. Performance remains same for channel length up to 10-15 CIR Samples but after this value the performance goes on degrading. But as we increase SNR value, the effect of CIR samples on performance goes on diminishing and at high SNR value of 25dB, MSE remain almost constant for all channel filter lengths. The performance comparison for different MIMO systems is shown in Figure 4.44. We observe that for channel filter length up to 40-45 CIR samples, 2×2 MIMO system outperforms the 4×4 MIMO system but as we increase the lentgh of channel filter further the 4×4 MIMO system gives better performance behavior. So for larger channel filter lengths higher order MIMO systems are preffered but we have to pay for more computaitonal time for higer order MIMO systems as given in Table 4.15.

For LSE initially estimated channel, the complexity increases by 97% as we go from 2×2 system to 3×3 system and for 4×4 system the complexity increases by 268%. For LMMSE initially estimated channel, the complexity increment is 88% for 3×3 system but it increases to 268% for 4×4 system. For 2×2 system and LSE initially channel estimator, as channel filter length is increased from 5 to 10, the complexity increases by 6% but for 20 CIR samples, there is 18% increment in computational time. For case of LMMSE estimator and 2×2 system, the increment in complexity is 65% by increasing the channel length from 5 to 10 and by further increase to 20 CIR samples the complexity increment is 68%. MSE behavior for LMMSE-Kalman Estimator is given in Figure 4.45. As compared to LSE-Kalman Estimator, the performance remains same for almost 35-40 CIR samples but after that the performacne degradation is significant as compared to LSE-Kalman estimator for further increments in channel lengths. The performance as a function of both SNR and CIR Samples is shown in Figure 4.46.

TABLE 4.15: COMPLEXITY COMPARISON OF KALMAN ESTIMATOR FOR DIFFERENT MIMO SCHEMES

CIR Samples	2×2 (μsec)		3×3 (μsec)		4×4 (μsec)	
	LS-Kalman	LMMSE- Kalman	LS- Kalman	LMMSE- Kalman	LS- Kalman	LMMSE- Kalman
5	213	315	420	594	785	1000
10	227	522	448	784	837	1200
20	253	530	680	928	1100	1600

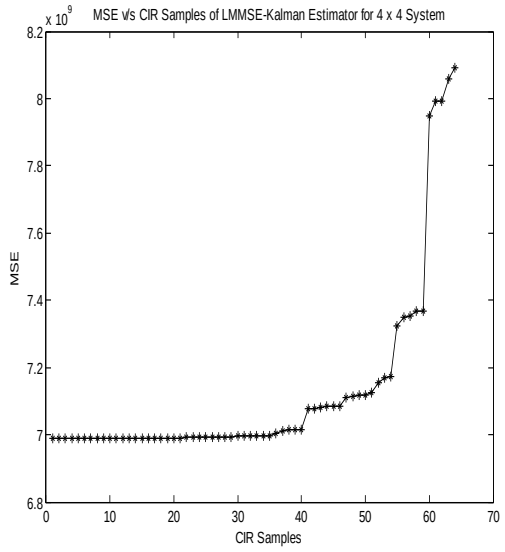

Figure 4.45: MSE vs CIR Samples of LMMSE-Kalman Estimator for 4 × 4 Systems

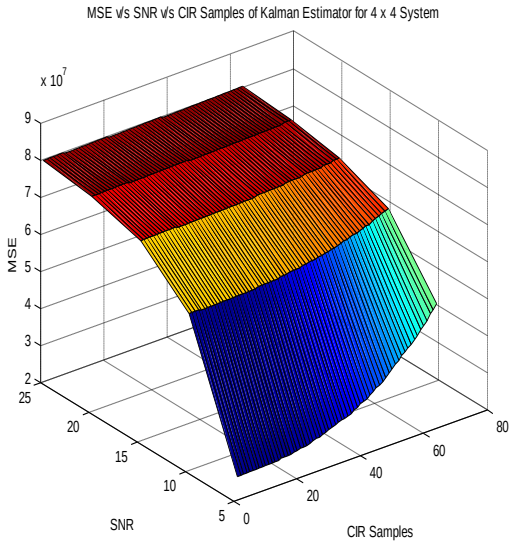

Figure 4.46: MSE vs SNR vs CIR Samples of Kalman Estimator for 4 × 4 System

For different number of multi-path channel taps, the performance of Kalman Estimator is shown in Figure 4.47. The effect of changing the number of multi-paths is most prominent for higher SNR values as compared to low SNR values. By increasing the number of channel taps considered for channel estimation, the performance also goes on degrading as for larger number of channel taps the noise effect is also more severe. The performance of Kalman Estimator for different MIMO systems is shown in Figure 4.48. The performance also improves for higher order MIMO systems but here again this better performance comes at the cost of more complexity. The computational time of both LSE-Kalman and LMMSE-Kalman Estimators for different MIMO systems is shown in Table 4.16. For 2×2 system and LSE-Kalman Estimator, there is 15% more complexity by increasing the channel taps from 5 to 10 and there is 20% more complexity when 20 channel taps are considered. For 5 channel taps and LSE-Kalman Estimator, the complexity increases by 15% when taking 3×3 system and 38% when taking 4×4 MIMO system as compared to 2×2 system. But for LMMSE-Kalman Estimator, 19 % more complexity is observed for 3×3 system and for 4×4 MIMO this becomes 61%. The combined effect of SNR and channel taps on MSE is shown in Figure 4.49.

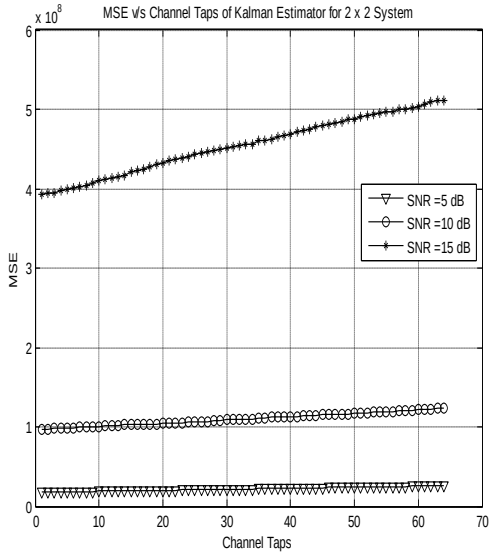

Figure 4.47: MSE vs Channel Taps of Kalman Estimator for 2 × 2 System

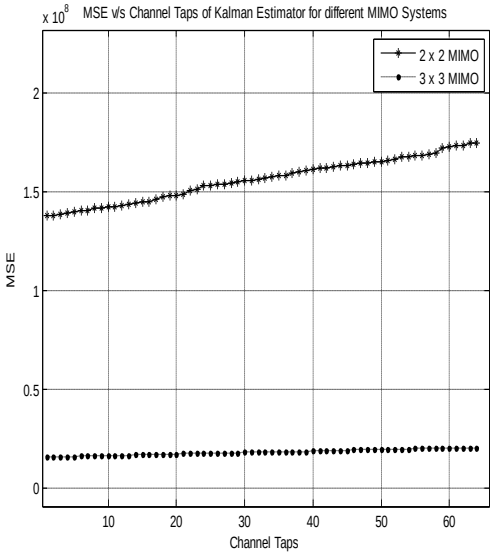

Figure 4.48: MSE vs Channel Taps of Kalman Estimator for different MIMO Systems

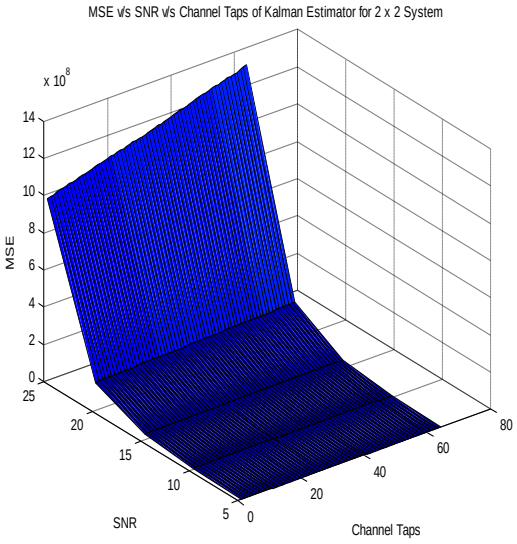

Figure 4.49: MSE vs SNR vs Channel Taps of Kalman Estimator for 2 × 2 System

TABLE 4.16: COMPLEXITY COMPARISON OF KALMAN ESTIMATOR FOR DIFFERENT MIMO SCHEMES

Channel Taps	$2 \times 2\ (sec)$		$3 \times 3\ (sec)$		$4 \times 4\ (sec)$	
	LS- Kalman	LMMSE- Kalman	LS- Kalman	LMMSE- Kalman	LS- Kalman	LMMSE-LMS
5	0.0026	0.0028	0.0030	0.0031	0.0036	0.0042
10	0.0030	0.0032	0.0031	0.0035	0.0037	0.0050
20	0.0032	0.0040	0.0041	0.0045	0.0043	0.0060

Chapter No 5

Conclusion and Future Work

In Chapter 5, the performance and complexity of channel estimation algorithms are compared. The performance of LMMSE is better than LSE because it depends on the channel and noise statistics, which is not possible to have in wireless communication and further it also increases the complexity of the transceiver. For LSE, small number of CIR samples and channel taps are preferred for low SNR conditions. And same system parameters are also proposed for LMMSE approach. For LSE, generally CIR samples less than 30 and channel taps approximately 40 are used and for LMMSE, only 10 channel taps are used for better performance.

For DFT-CE, under any SNR operating condition, a small length of channel filter is proposed for better performance and for less computational time. Similarly a multi-path channel with less number of channel taps with small channel filter length is used. For less CIR samples, both DFT-CE and DCT-CE have same performance but for high channel filter length, DCT-CE is better to use. Among DCT estimators, DCT operation is preferred to be performed before IDCT, irrespective of number of CIR samples. From point of view of channel taps, IDCT/DCT-CE is better to use than DFT and DCT/IDCT. For an MIMO-OFDM system, usually a channel with small number of channel taps and of small channel filter length is proposed under low SNR operating conditions.

Windowing Function is applied to remove the effect of noise from channel impulse response. For reliable and spectrally efficient transmission, a linear proportional relationship is required between the operating SNR and channel filter length. If channel filter has high length, then any SNR value can be used for that communication system and in such situation another advantage comes in form of reduced complexity than DFT-CE. To make performance more efficient and independent of CIR samples, more zeros are padded to channel impulse response. For low SNR, less number of channel taps are preferred for improved performance and reduced complexity. But the disadvantage of more zeros is only that performance of Windowed-DFT degrades than that of DFT.

Small length of channel filter is preferred not only for better performance but also for less complexity for low SNR values and for low order MIMO systems. If complexity can be compromised then performance can be made even better by taking the initially estimated channel

using LMMSE method. Similar to channel filter length, less number of channel taps not only gives better performance but also less complexity. To achieve the data rate targets of a wireless communication system through channel feedback, LMS channel estimator is optimized for a system with channel filter length of 5-10 CIR Samples and channel taps less than 10 for both optimized performance and complexity.

To make power-efficient communication with better performance less number of CIR samples are used under low SNR values. When the initialized channel estimation is by LMMSE, then RLS gives better performance but with high complexity as LMMSE exploits the second order channel statistics. Higher the order of MIMO system, better will be performance and for any MIMO system, channel filter length of 5 CIR samples is preferred for optimized performance and complexity. Similar behavior is also observed for channel taps as that of channel filter length. For higher order MIMO system, the effect of varying channel taps on performance goes on diminishing so for reduced computational time less number of channel taps are preferred.

In this thesis, only one dimension channel estimation techniques are discussed. Either time-domain or frequency-domain channel estimation algorithms are optimized for channel filter lengths and channel taps. Channel can be estimated simultaneously in both time and frequency domains. Performance can be further improved by estimating the channel in two dimensions.

References

[1]3GPP, TS 36.211 V0.1.2. (2006-11), " *Physical Channels and Modulation(Release 8)*". Available: www.3gpp.org

[2]3GPP, TR 36.814 V9.0.0. (2010-03), " *E-UTRA, Further advancements for E-UTRA Physical Layer Aspects (Release 9)*" .Available: www.3gpp.org

[3]3GPP, TS 36.912 V9.2.0 (2010-03), " *Feasibility Study for Further Advancements for E-UTRA (LTE-Advanced)(Release 9)*".Available: www.3gpp.org

[4]3GPP, TS 36.913 V9.0.0. (2009-12), "*Requirements for further advancements for E-UTRA (LTE-Advanced) (Release 9)*".Available: www.3gpp.org

[5]G. Andrews, Jeffrey. *Fundamentals of WiMAX, Understanding Broadband Wireless Networking*, Prentice Hall.

[6]A.Goldsmith, *Wireless Communication*, Cambridge University Press, 2005 Oppenheim, Alan V. *Discrete Time signal Processing*, Second Edition, Prentice Hall

[7]*Selected MIMO Techniques and Their Performance,* IST-2001-32125 Flows, Deliverable No: D14, 31st December, 2003

[8]Hebbar, Anil Madhava, *Empirical Approach for Rate Selection in MIMO-OFDM.* Master Thesis, Blacksburg Virginia, 17th December 2004

[9]Kala Parveen Bagadi, "MIMO-OFDM Channel Estimation using Pilot Carries", International Journal of Computer Application, Vol.2, No.3, May 2010

[10]F.Delestre, Y.Sun, "Pilot Aided Channel Estimation for MIMO-OFDM Systems", London Communication Symposium 2009

[11]Peter Hoeher, Stefan Kaiser, Patrick Robertson, " Two-Dimensional Pilot-Symbol-Aided Channel Estimation by Weiner Filtering", ISSn: 0-8186-7919-0/97 @ 1997 IEEE

[12]Eric Pierre Simon, Laurent Ros, Hussein Hijazi, Jin Fang, Davy Paul Gaillot, Marion Berbineau, "Joint Carrier Frequency Offset and Fast Time-varying Channel Estimation for MIMO-OFDM System", IEEE

[13]Jari Ylioinas, "Iterative Detection, Decoding and Channel Estimation in MIMO-OFDM ", PhD Dissertation, Faculty of Technology, Department of Electrical and Information Engineering, University of Oulu

[14]Daniel R.Fuhrmann, "On Adaptive Sensing of Complex Communication Channels", ISSn: 978-1-4244-1714-8/07 @ 2007 IEEE

[15]Eitel, Emna. Speidel ,Joachim," Enhanced Decision Directed Channel Estimation of Time Varying Flat MIMO Channels",PIMRC'07

[16]Saqib Saleem, Qamar-ul-Islam, "Optimization of LSE and LMMSE Channel Estimation Algorithms based on CIR Samples and Channel Taps", IJCSI International Journal of Computer Science Issues Vol. 8 Issue.1,pp.437-443, January 2011

[17]Jongsoo Choi, Martin Bouchard and Ter Hin Yeap,"Adaptive Filtering-Based Iterative Channel Estimation for MIMO Wireless Communication", 0-7803-8834-8, IEEE 2005

[18]Saqib Saleem, Qamar-ul-Islam, "Performance and Complexity Comparison of Channel Estimation Algorithms for OFDM System", IJECS International Journal of Electrical and Computer Sciences, Vol. 11 , No.02, pp.6-12, April 2011

[19]Yongming Liang, Hanwen Luo, Jianguo Huan,"Adaptive RLS Channel Estimation in MIMO OFDM Systems", 0-7803-9538, IEEE 2005

[20]J.J. van der Beek, O. Edfors, M. Sandell, S.K. Wilson, and P. O.Borgesson, "On channel estimation in OFDM systems," Proc. VTC'95, pp. 815-819.

[21]Du ,Zheng, Song ,Xuegui,"Maximum Likelihood BasedChannel Estimation for Macrocellular OFDM Uplinks in Dispersive Time-Varying Channels", IEEE Transactions On Wireless Communications, Vol. 10, No. 1, January 2011

[22]Edfors, M. Sandell, J. J. van der Beek, S. K. Wilson, and P. O.Borgesson, "OFDM channel estimation by singular value decomposition,"IEEE Trans. Comm., vol. 46, no.7, pp. 931-939, July 1998.

[23]Srivastava, C. K. Ho, P. H. W. Fung, and S. Sun, "Robust mmse channel estimation in ofdm systems with practical timing synchronization," in Wireless Communications and Networking Conference, 2004. WCNC.2004 IEEE, vol. 2, pp.711–716 Vol.2, 2004.

[24]Y. Li, L. J. Cimini, Jr., and N. R. Sollenberger, "Robust channel estimation for OFDM systems with rapid dispersive fading channels,"IEEE Trans. Comm., vol.46, no. 7, pp. 902-915, July 1998.

[25]Dimitris G. Manolakis, Vinay K. Ingle. Statistical and Adaptive Signal Processing,Spectral Estimation, Signal Modeling, Adaptive Filtering and Array Processing,Artech House, Boston London

[26]Ancora. A, Bona. C, Slock, D.T.M," Down sampled impulse response LS channel estimation for LTE OFDMA", IEEE International Conference on Acoustics, Speech and Signal Processing, 2007.ICASSP 2007.Vol.3, pp.293-296, 2007

[27]Jun-Hee Jang, Se-Bin Im, Jeong-soon Park, Hyung-Jin Choi," DFT-based decision directed channel estimation for OFDM systems in very large delay spread channels", 14th Asia-Pacific Conference on Communications, 2008. APCC 2008.

[28] Kwak, K, Lee, S, Hong, D, Jihyung Kim," A new DFT-based Channel estimation approach for OFDM with virtual subcarriers by leakage estimation", IEEE Transactions on Wireless Communications,Volume: 7, Issue:6, pp.2004-2008,June 2008

[29]Y. Baoguo, K. B. Letaief, R. S. Cheng, and C. Zhigang, Windowed DFT based pilot-symbol-aided channel estimation for OFDM systems in multipath fading channels," in Vehicular Technology Conference Proceedings, 2000. VTC 2000-Spring Tokyo. 2000 IEEE 51st, 2000, pp.1480-1484 vol.2

[30]Jie Ma, Hua Yu, Shouyin Liu," The MMSE Channel Estimation Based on DFT for OFDM System", 5th International Conference on Wireless Communications, Networking and Mobile Computing,2009. WiCom '09.2009

[31]Y. H. Yeh and S. G. Chen, "DCT-based channel estimation for OFDM systems, "Communications,2004 IEEE International Conference, vol. 4,pp.2442-2446, June 2004.

[32] Y. H. Yeh and S. G. Chen, "Efficient channel estimation based on discrete cosine transform," IEEE ICASSP'03, vol. 4, pp.IV_676-IV_679.

[33]Saqib Saleem, Qamar-ul-Islam, "LMS and RLS Channel Estimation Algorithms for LTE-Advanced", Journal of Computing, Vol.3, Issue.4, pp.155-163, April 2011.

[34]M.A.Mohammadi,M.Ardabilipour,"Performance Comparison of RLS and LMS Channel Estimation Techniques with Optimum Training Sequences for MIMO-OFDM Systems", 978-1-4244-1980-7, IEEE 2008

[35]Yongming Liang,Hanwen Luo,"Adaptive RLS Channel Estimation in MIMO-OFDM Systems", Proceedings of ISCIT, 2005

[36]Dieter Schafhuber,Markus Rupp,"Adaptive Identification and Tracking of Doubly Selective Fading Channels for Wireless MIMO-OFDM Systems", 4th IEEE Worshop on Signal Processing Advances in Wireless Communications, 2003

[37]Alexandar D.Poularikas, "Adaptive Filtering Primer with MATLAB" Taylor & Francis.

[38]Valery Ramon, Cedric Herzet, Xavier Wautelet and Luc vandendrope,"Soft Estimation of time-varying frequency selective channels using Kalman smoothing", IEEE ,1-4244-0353-7

[39]Hala mahmoud, Allam Mousa, Rashid Saleem, " Kalman Filter Channel Estimation Based on Comb-Type Pilots for OFDM System in Time and Frequency-Selective Fading Environments", IEEE MIC-CCA 2008

[40]Seongwook Song, Andrew C.Singer and Koeng-Mo Sung,"Soft Input Channel Estimation for Turbo Equalization", IEEE Transaction on Signal Processing, Vol.52, No.10,October 2004